CONSTRUCTION AND IMPLEMENTATION OF A LiDAR BASED ESP8266 ENABLED REAL-TIME REMOTE GROUNDWATER MONITORING DEVICE

BY

MICHAEL OBOROGHENETARE ATENAGA

B.Sc (EKPOMA), M.Sc (BENIN).

PG/PSC1917728

DEPARTMENT OF PHYSICS

FACULTY OF PHYSICAL SCIENCES

UNIVERSITY OF BENIN

BENIN CITY, NIGERIA

JUNE 2026

CONSTRUCTION AND IMPLEMENTATION OF A LiDAR BASED ESP8266 ENABLED REAL-TIME REMOTE GROUNDWATER MONITORING DEVICE

BY

MICHAEL OBOROGHENETARE ATENAGA

B.Sc (EKPOMA), M.Sc (BENIN).

PG/PSC1917728

A THESIS WRITTEN IN THE DEPARTMENT OF PHYSICS AND SUBMITTED TO THE SCHOOL OF POST GRADUATE STUDIES, AS PART OF THE REQUIREMENTS FOR THE AWARD OF A DOCTOR OF PHILISOPHY DEGREE (PhD) IN ELECTRONICS, UNIVERSITY OF BENIN, BENIN CITY, NIGERIA

JUNE 2026

CERTIFICATION

This is to certify that this Doctorate degree (PhD) thesis was written **by Michael Oboroghenetare ATENAGA (PG/PSC1917728)** in the Department of Physics, Faculty of Physical Sciences, University of Benin, Benin City, Nigeria, Under the Supervision of Prof S. O. Azi.

Prof S.O. Azi **(Supervisor)**	**Date**
Dr T.E. Okuonghae **(Co-Supervisor)**	**Date**
Prof. C.O. Aigbogun **(Head of Department)**	**Date**

DECLARATION

UNIVERSITY OF BENIN

SCHOOL OF POST GRADUATE STUDIES

CONSTRUCTION AND IMPLEMENTATION OF A LiDAR BASED ESP8266 ENABLED REAL-TIME REMOTE GROUNDWATER MONITORING DEVICE

BY

MICHAEL OBOROGHENETARE ATENAGA

B.Sc (EKPOMA), M.Sc (BENIN).

PG/PSC1917728

The Board of Examiners Declares as Follows

That this is the original work of the candidate

That the thesis is accepted in partial fulfilment of the requirement for the award of the degree of Doctor of Philosophy (PhD) in Electronics

NAME	SIGNATURE	DATE
SUPERVISOR: Prof S.O. Azi	…………………	…………………
CO-SUPERVISOR: Dr T.E. Okuonghae	…………………	…………………
HEAD OF DEPT: Prof. C.O. Aigbogun	…………………	…………………

DEDICATION

I dedicate this work to God Almighty whose steadfast love and mercies ensured my progress.

Also, to my supportive wife Mrs Uyimwen Tracy Atenaga, my adorable children - Oghenetega Emmanuel Atenaga & Oghenetejiri Jasmine Atenaga.

CERTIFICATION OF THESIS/DISSERTATION ON PLAGIARISM

We the undersigned attest and declare that the thesis of Mr **MICHAEL OBOROGHENETARE ATENAGA** titled: **DESIGN AND CONSTRUCTION OF A LiDAR BASED ESP8266 ENABLED REAL-TIME REMOTE GROUNDWATER MONITORING DEVICE,** has successfully passed the antiplagiarism test and does not violate any copyright regulation

____

Name of Chief Supervisor/ Sign & Date

____

Name of Co-Supervisor/ Sign & Date

____

Name of HOD/ Sign & Date

ACKNOWLEDGEMENT

Firstly, my deepest gratitude goes to God Almighty, who in His infinite love showed me mercy and granted me grace; without which I would not achieve any success.

I deeply appreciate to Prof. S.O. Azi, for his patience, tolerance, understating fatherly and professional guidance all through the journey of this research. His critical, incisive and meticulous corrections, have been of immense benefit to the actualization of this work. May God bless your labour of love sir.

I deeply appreciate the Head of Physics Department Prof. C. O. Aigbogun for his firm support and assistance. Special thanks to Prof O. D. Osahon for assisting me obtain very useful data from the Nigerian Hydrological Service Agency (Nihsa). I express heartfelt gratitude to Prof Ben E. Iyorzor, Prof Samuel Okunzuwa, Dr T.E Okuonghae (my Co-supervisor), Dr Shedrack Onwusinkwue, Dr J. Airen, Prof O.M. Alile, Dr M.I. Babalola, Mr E.J.K. Oni for his technical assistance, Dr Onuora. M. Awodu, Dr O. Ebomwonyi and the entire staff of the Department of Physics, University of Benin. Many thanks to my fellow Ph.D students-Mr Popoola Adegoke, Mr Ademola Olanegan for their encouragement.

Special thanks to Dr E.Ighodaro for his assistance with Nisah. I appreciate Mrs Aisha Tani Ibrahim, former Director, Nisah and Mr Taiwo Bamgbose, IT department Nisah for the effort in ensuring approval for my request for data.

Finally, I very specially appreciate my loving wife Mrs Uyimwen Tracy Atenaga for her patience, endurance, encouragement, understanding, sacrifice and genuine love. Her support throughout this voyage is immensurable. May God satisfy the deep concerns of your heart my queen.

God bless you all.

TABLE OF CONTENT

LIST OF FIGURES

LIST OF PLATES

LIST OF TABLES

ABSTRACT

Expanding noncontact techniques for monitoring groundwater level variations to include laser based devices has been limited in the past by the low reflectivity of water to laser light The advances made in the realization of highly sensitive receivers has greatly enabled Laser devices with the prospect for effective noncontact monitoring of groundwater levels. In this work a real-time groundwater level monitoring devices was implemented using a LiDAR-lite v3HP laser-based sensor, an Arduino Uno rev 3 microcontroller, and an ESP8266 Wi-Fi module.

Hardware implementation involved interfacing the microcontroller with the LiDAR-lite, the Wi-Fi module, a 16 x 2 liquid crystal display and other necessary basic electronic components. The software implementation involved writing, editing, compiling and uploading codes through the Arduino ide unto the microcontroller. The implemented prototype was powered by a 20,000mAH, 5V power bank and deployed on two artesian wells to collect depth to water surface data which were uploaded automatically to ThingSpeak platform. Measurements at various times taken with the device were compared with manual measurements from a calibrated tape. A correction factor was applied to correct measurement residuals.

Results of the validation showed that measured values were uploaded to the ThingSpeak platform an average of 33 seconds which could be reconfigured to longer timeframes. The results were remotely accessed on the platform. A correlation graph of measurement before and after applying the correction revealed a near perfect correlation coefficient of 0.99995 for the LiDAR readings for both pre-correction and post correction measurements; confirming a strong linear relationship with tape measurements. The coefficient of variation, root mean square error and limits of agreement from the Bland Altman's plots all ascertained the improvement in post-correction measurements.

CHAPTER ONE

1.1 INTRODUCTION

Groundwater refers to the part of subsurface water that occupies the pore spaces and fractures of soil and rock formations below the water table. It accumulates in geological formations known as aquifers from which it can be extracted in usable quantities (Todd and Mays, 2005). Unlike surface water bodies such as rivers and lakes, groundwater is often invisible and consequently underappreciated, despite constituting one of the most significant freshwater reserves on Earth (Re and van der Gun, 2016). The importance of groundwater to human existence and ecological systems cannot be overemphasized. It is estimated to supply almost fifty percent of all drinking water withdrawn globally and approximately two-fifth of water used for irrigated agriculture, making it indispensable to food security and public health (Bierkens and Wada, 2025). Beyond direct human consumption, groundwater serves as a natural buffer against the climate change induced rainfall variability (Re and van der Gun, 2016).

Despite its critical importance, groundwater resources face a range of escalating global pressures. Decades of unsustainable exploitation have led to acute degradation of groundwater quantity and quality, creating pressing challenges that society must address if viable access to this crucial resource is to be maintained for future generations (Bierkens and Wada, 2025). Among the foremost of these pressures is over-abstraction, whereby the rate of groundwater withdrawal for agricultural, industrial, and domestic purposes exceeds the natural rate of aquifer recharge, resulting in progressive depletion of water tables (Famiglietti, 2014).

The global pattern of groundwater stress is similar, and in several respects intensified, within Nigeria. Nigeria possesses substantial groundwater which serves as a reliable and accessible source of safe drinking water for millions of its inhabitance distributed across the country's thirty-six states and the Federal Capital Territory (Fashae and Obateru, 2024). In Nigeria, 75% of rural dwellers and 85% of urban population rely on groundwater (Kalu, 2018). In Lagos, Nigeria's rapidly growing coastal megacity, declining recharge combined with over-abstraction threatens to deplete aquifer storage, trigger land subsidence, and exacerbate water scarcity issues already evident in comparably stressed cities elsewhere in the world (Olabode and Comte, 2025). Sustainable Development Goal 6 of the United Nations is targeted at ensuring availability and sustainability in the management of water by 2030 (Cobbing *et al*.,2021)

Groundwater constitutes a huge part-over 95% of all the fresh liquid water available globally (Mary, 2018). Figure 1.1 shows the distribution of global water (Gleick, 1993).

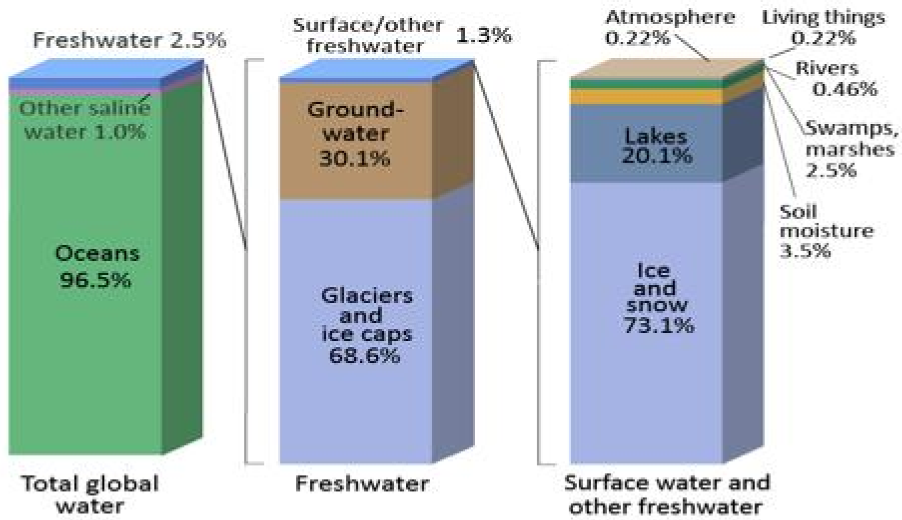

Figure 1.1: Percentage distribution of total global water (culled from Gleick, 1993)

Monitoring groundwater levels provides useful information for quantifying depletion of groundwater and evaluating the environmental effect. The importance of monitoring groundwater levels cannot be overemphasized. It provides an avenue through which potential changes in flow direction and velocity can be identified (Nielsen and Nielsen,2007). It is a source of data through which migration of contaminants can be determined (Taylor and Alley, 2001). Monitoring provides data with which groundwater storage and recharge rates are estimated (Healy and Cook ,2002). It can serve as a veritable tool for monitoring the effect of climate variability (Green *et al*.,2011). Hence it is obvious that proper attention must be paid to effectively and efficiently manage groundwater resources; as poorly managed schemes can induce stress on groundwater resources, thereby negatively impacting regional socio-economic development (Chen *et al*, 2016). Managing groundwater effectively depends a lot on understanding how both its levels and storage capacity are changing. On-site groundwater level monitoring provides groundwater users, policy-makers and other stakeholders with information for an effective water management plan (Calderwood *et al*, 2020). Monitoring groundwater variations is of utmost importance in determining the constituents of terrestrial water storage (Masood, 2022).

In other to improve accessibility to groundwater information globally, the Global Groundwater Monitoring Network (GGMN) programme was established in 2012 (IGRAC, 2020). A 2020 review by the International Groundwater Resources Assessment Center-IGRAC, listed Nigeria as one of the countries with a groundwater monitoring programme. According to the review, groundwater monitoring networks can be divided into three – National, regional and project-based. While the national programme is a network that spans an entire country and are managed by a central body, the regional or local monitoring programme comprises of several networks that are managed by different bodies. The project-based monitoring network is one that is set up as a result of a specific funded project; 75% of African countries with monitoring programmes, have a centralized monitoring network (IGRAC, 2020).

Techniques for measuring groundwater level can be broadly classified into two categories on the basis of whether the sensing element makes physical contact with the water being measured: contact (in-water or submersible) methods and non-contact (above-water or remote) methods. (Tanko et al, 2024). Contact methods require the sensing element to be submerged in, or to physically touch, the water column whose level is being measured. Steel tapes, E-tapes/dippers submersible pressure transducers and airline/bubbler are examples of the contact techniques. Non-contact methods, by contrast, determine water level from a position above the water surface, without any part of the sensing apparatus touching the liquid. Conventional automatic, non-contact water level gauges principally include ultrasonic and radar (microwave) sensors, both of which operate on the time-of-flight (ToF) principle, whereby a signal is emitted toward the water surface, reflects back to the sensor, and the elapsed travel time is converted into a distance measurement (Wu et al., 2023). Quite recently, laser-based ranging techniques have attracted the attention of some researchers to carry out river stage measurement, water level measurement in turbid reservoirs (Tamara et al., 2016), laser-based designs that employed the use of a floating target to enhance reflections during deployment, and the application of other low-cost LiDAR modules (Chooruang *et al*.,2023; Dementria et al.,2023). While these efforts reasonably established the proof of concept that water level could be measured and monitored using laser based devices, it is extension to groundwater environment is yet to be sufficiently verified and validated.

When weighed against one another, non-contact methods offer several systemic advantages over contact-based instrumentation that justify their increased deployment in groundwater monitoring networks, particularly in resource-constrained settings such as Nigeria. First, because non-contact sensors are not immersed in the monitored water, they are immune to the corrosion, sediment abrasion, and biofouling that necessitate frequent maintenance, recalibration, and eventual replacement of submersible instruments (Wu et al., 2023); this translates directly into lower lifecycle costs and reduced field-visit frequency, both of which are significant considerations in the typically under-resourced groundwater monitoring infrastructure of developing regions (Egbueri et al., 2025). Secondly, non-contact sensors eliminate the risk of cross-contamination between wells that arises when a single submersible probe is reused across multiple monitoring points without rigorous decontamination, a risk of particular concern where groundwater quality is already compromised by industrial, agricultural, or domestic pollution (Tanko *et al.*, 2024). Thirdly, non-contact installation is mechanically simpler, generally requiring only that the sensor be mounted above the wellhead or borehole opening, which reduces installation complexity and makes such systems more readily deployable across the dispersed and often inaccessible well networks characteristic of rural Nigerian communities.

As already mentioned, Nigeria has a National Groundwater Level Monitoring Programme. Almost 75% (32 out of 43) of the monitoring points in the programme are equipped with pressure-based water level logger systems that take measurement daily or twice in a day (Kalu, 2018; IGRAC, 2020). This temporal resolution cannot capture rapid events such as flash floods, pumping-induced decline in groundwater level, or recharge pulses. Although contact methods- chief amongst which are the pressure-based sensing system, have been used extensively, there are certain concerns that limit the functionality of such system. Firstly, pressure-based sensing systems that are designed to measure water levels are prone to corrosion and biological fouling after prolonged use (Boon, Heitsenrether and Hensley, 2012). This can be as a result of rusting of metal part of the device-having been in continuous contact with water. Secondly, the advancement in electronics has brought about affordable and very functional sensors that can now be readily integrated with the versatility that the IOT offers in facilitating real-time monitoring, hence expanding the monitoring network and increasing frequency of monitoring via an affordable and effective technique become very attractive. Increased monitoring frequency combined with IOT storage capabilities would further serve to provide machine learning tools with the data-driven demands that these models need for accurate prediction (Igwebuike, *et al*.,2025**)**; as accurate forecasts of the fluctuations in groundwater level can contribute to understanding its availability and distribution (Feng, Ghorbani and Radwan, 2024).

Hence the need for a more frequent and continuous monitoring approach that will guarantee the availability of sufficient data to marshal regional action for the sustainable development and use of groundwater resources (Jijingi, *et al*.,2019), as uncoordinated water resources development by state and federal has been identified as one of the reasons for the poor implementation of the National water resources master plan in Nigeria (Njoku, 2022)**.**

Among the available non-contact techniques, LiDAR (Light Detection and Ranging)-based ranging offers a distinct combination of advantages that justifies its preferential adoption over ultrasonic, and radar alternatives for groundwater level monitoring applications. Unlike ultrasonic sensors, which depend on the propagation of sound through air and are consequently vulnerable to errors introduced by temperature gradients, humidity, and turbulent or vapour-laden atmospheres within a borehole (Pokcenser, 2025), LiDAR systems use coherent or pulsed light, whose propagation velocity in air is effectively constant and largely insensitive to the modest temperature and humidity variations encountered within a typical well or borehole environment. This affords LiDAR a fundamental precision advantage, particularly the narrow beam divergence achievable with laser sources permits highly localized, well-defined spot illumination of the water surface, in contrast to the comparatively wide beam cones of many ultrasonic transducers, which can lead to spurious reflections from borehole walls and casings in confined geometries.

While microwave radar sensors offer notable resilience to atmospheric interference, enabling reliable all-weather water level measurement (Wu et al., 2023), their practical deployment in confined hydrogeological settings remains constrained by inherent hardware and electromagnetic design limitations. Contemporary radar systems typically require bulky transceiver assemblies and directional antennas whose physical dimensions are governed by operational frequency, making miniaturization for standard-diameter groundwater monitoring boreholes technically challenging and cost-prohibitive (Klotzsche et al., 2018; Rodrigues and Li, 2021). These spatial and economic constraints limit the scalability of radar-based solutions for dense, low-cost monitoring networks. In contrast, time-of-flight LiDAR sensors provide a compact, low-power alternative with decent precision and simplified optical alignment, making them highly suitable for integration with microcontroller-driven IoT architectures.

Critically, the integration of a LiDAR ranging module with an Arduino uno microcontroller and providing an internet ability through an ESP8266 Wifi module, allows these optical advantages to be combined with the remote connectivity, low cost, and scalability that characterizes the contemporary Internet of Things based (IoT-based) approach to environmental monitoring (Okafor et al, 2024). This approach revolutionizes water resource management practice by enabling continuous, real-time data acquisition, remote accessibility, and timely, informed decision-making without reliance on labor-intensive manual field visits (Sowndharya and Duraisamy, 2024). Calderwood et al. (2020) demonstrated the feasibility of a low-cost open-source wireless sensor network for groundwater monitoring, using open hardware and software to reduce costs by over 70% relative to existing commercial solutions. Open-source IoT frameworks such as ThingSpeak provide free accessible platform for logging data visualization and analytical tools, hence facilitating overall deployment (Kondapuram et al., 2024).

Within the Nigerian context, where the absence of comprehensive groundwater monitoring infrastructure has been directly identified as a contributing factor to unchecked aquifer depletion (Egbueri, 2025), the deployment of a low-cost, low-maintenance, non-contact, real-time LiDAR-based monitoring device of the kind implemented in this study represents a technically appropriate and economically viable pathway toward closing the prevailing groundwater data deficit evident both globally and, more acutely, within the Nigerian context.

This present work is designed to extend the study by Dementria et al., (2023) which tested the LiDAR-lite v3hp on water cased in a polyvinyl chloride(pvc) pipe, by deploying a modified version of their device in an artesian wells and validating its operation. The thesis is organized as follows: chapter one is the introductory chapter that serves as a preamble to the entire work; where the problem statement the study seeks to address is clearly stated, justification for the work is asserted, the aim and objectives, the scope of study are all spelt out. Chapter two covers literature review. A theoretical review of some related optical concepts are dealt with, followed by a literature survey of past related studies. Chapter three deals with the methodology employed in the work. A description of the component's selection justification is outlined; the circuit diagram and programming codes are presented. Chapter four covers testing, validation, results and discussions. The fifth and final chapter contains summary of the findings, contributions to knowledge, conclusion and recommendations for future studies.

1.2 STATEMENT OF PROBLEM

Underground water is an important resource to mankind. Its variation can indicate the onset of an environmental event. One way of physically confirming its variation is by checking it level. While this has been traditionally achieved by several manual procedures or techniques, the need to access the data rather quickly has challenged designers to utilize the tools presented by an ever evolving and adaptive field of scientific designs, to implement real-time measuring systems. While the developed world may have quite easily taken advantage and successfully obtained these systems, developing (third world countries) have more or less been at best just consumers. In addition, Current monitoring frequency is not short enough to capture variations in a smaller timescale, which may slow down early detection of the onset of an environmental event like flooding or drought. Data obtained from Nigeria Hydrological Service Agency (NIHSA) reveal that present monitoring is on a twice a day basis (12 hourly measurements). Plate 1.1 shows a snapshot of groundwater level data obtained from NIHSA. This frequency may not capture variations on a shorter time scale that may hold potential information of interest.

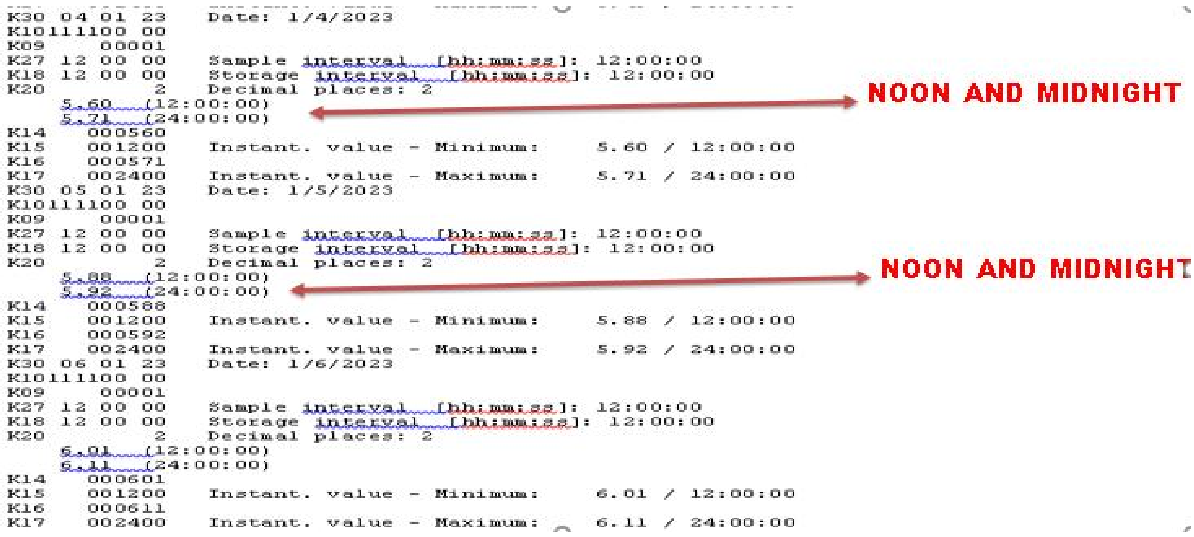
```
K30 04 01 23    Date: 1/4/2023
K10111100 00
K09      00001
K27 12 00 00    Sample interval [hh:mm:ss]: 12:00:00
K18 12 00 00    Storage interval [hh:mm:ss]: 12:00:00
K20          2  Decimal places: 2
    5.60  (12:00:00)
    5.71  (24:00:00)
K14    000560
K15    001200   Instant. value - Minimum:    5.60 / 12:00:00
K16    000571
K17    002400   Instant. value - Maximum:    5.71 / 24:00:00
K30 05 01 23    Date: 1/5/2023
K10111100 00
K09      00001
K27 12 00 00    Sample interval [hh:mm:ss]: 12:00:00
K18 12 00 00    Storage interval [hh:mm:ss]: 12:00:00
K20          2  Decimal places: 2
    5.88  (12:00:00)
    5.92  (24:00:00)
K14    000588
K15    001200   Instant. value - Minimum:    5.88 / 12:00:00
K16    000592
K17    002400   Instant. value - Maximum:    5.92 / 24:00:00
K30 06 01 23    Date: 1/6/2023
K10111100 00
K09      00001
K27 12 00 00    Sample interval [hh:mm:ss]: 12:00:00
K18 12 00 00    Storage interval [hh:mm:ss]: 12:00:00
K20          2  Decimal places: 2
    6.01  (12:00:00)
    6.11  (24:00:00)
K14    000601
K15    001200   Instant. value - Minimum:    6.01 / 12:00:00
K16    000611
K17    002400   Instant. value - Maximum:    6.11 / 24:00:00
```


Plate 1.1: Groundwater level measurement data from NIHSA showing 12 hourly measurements

Finally, there is also the unavailability of data at the local and state government level, as data collected by many African countries are stored in a central database- in Nigeria, NIHSA in Abuja the nation's capital, is in custody of such data (Kalu, 2018; IGRAC, 2020). Ease of obtaining such data can be limited by logistics and bureaucratic constraints. The result of this research seeks to address these important concerns.

1.3 JUSTIFICATION OF STUDY

Real-time monitoring is the continuous observation of data as the occur. It is the automatic acquisition, processing, transmission, and visualisation of sensor-obtained data with latency sufficiently low to support time-critical decision-making, where the interval between physical measurement and data availability is negligible relative to the temporal dynamics of the monitored phenomenon (Hampton et al., 2013). A real-time monitoring device can reduce cost of monitoring as number of scheduled onsite visitation (to retrieve data or otherwise) is reduced. Also, the design is crafted to improve frequency of monitoring, ensure availability of current data that will strengthen and make more effective, existing groundwater management system capable of capturing short term trends of interest centred on current data.

Lastly, Utilizing the opportunity that a free IOT platform (like Thingspeak) offers will helps to automate analytics, simplify analysis and encourage integration with machine learning models. Machine learning is an important technological advancement whose potentials has been extended to groundwater monitoring (Ali *et al.*, 2024; Igwebuike, et al.,2025). It is data-driven, requiring large dataset which are processed to extract inherent patterns that eventually aid prediction accuracy. A groundwater level monitoring device that is designed to output sub-minute level data could serve as a large pool of data needed by machine learning or artificial intelligence tools to predict groundwater level data accurately.

1.4 AIM AND OBJECTIVES

The aim of this work was to implement a laser based real-time groundwater level monitoring system. The objectives are:

1. integrating a LiDAR-lite v3hp sensor with an Arduino Uno microcontroller.
2. implementing a Wi-Fi-based data transmission system using an ESP8266 module and establish a connection to the IOT platform.

3. obtaining manual measurement using steel tape and determine possible offsets with respect to the LiDAR measurements.
4. to evaluate the accuracy and reliability of the prototype by comparing with the manual measurements.
5. to optimizing the design so as to minimize cost and ensure a low-cost characterization of the device

1.5 SCOPE OF STUDY

The project sought to validate the operational capability of a laser based level device to correctly measure and monitor groundwater level. The prototype was implemented on a breadboard and subsequently on a Vero board. A printed circuit board implementation was not considered. The device was deployed and tested on two real life artesian wells located at Oghara, Delta state. Readings were compared with manual measurements taken from measuring tape. A permanent power unit was not incorporated in the design as a separate power bank was used to power the device during testing.

CHAPTER TWO

LITERATURE REVIEW

2.1 INTRODUCTION

Water level measurements can be broadly divided into two approaches- manual and automatic/automated water level measurement (Wu et al., 2023). Manual methods include the use of steel tapes, airlines, electrical methods and piezometers. On the other hand, automatic measuring techniques include pressure transducers, Ultrasonic sensors, Radar and laser based technique (LiDAR).

2.1.1. MANUAL MEASUREMENT

2.1.1.1 Steel Tapes

This is the oldest technique for measuring groundwater level (Masood *et al*, 2022). The steel tape with a weight attached to the end going into the well, is slowly lowered into the monitoring well. Chalk is applied to the lower end of the tape so that a wetted chalk mark will indicate the part of the tape that was submerged in the groundwater. To aid ease of reading, the tape has to be quickly retrieved from the well before the wet section dries out. The measurement is noted after adjustments that took into account the wetted chalk mark and the measuring point above the land surface datum have been effected (Cunningham and Schalk,2011).

2.1.1.2 Air-line Submergence method

According to Nielsen and Nielsen (2007), the instrument consists of a small diameter tube of known length made of plastic, copper or steel. The tube is attached to a pressure gauge which measures pressure as air is pumped into the airtight tube/line from an air source (compressor or hand operated pump), The airline is pressurized by slowly allowing air into its tube to force out any water in it; after which pumping is halted and the air source is removed. The gauge pressure which was hitherto increasing while the pumping was on, begins to gradually reduce until it stabilizes at a particular value. This final steady reading on the gauge is the height of the water in feet above the top of the pump. If the gauge is calibrated in psi, multiplying the measured value by 2.31 converts it to feet of water. The actual water level is then obtained by subtracting this value from the known length of the line. While some advantages of this method include its capability to be used even while well is being pumped, its robust results in the presence of bends or spirals in the airline; disadvantages include its reduced accuracy in comparison to other manual methods like wetted chalk tape and electronic methods, and the fact that its procedure requires careful computation (Cunningham and Schalk,2011).

2.1.1.3 Electrical Methods

This includes electronic tapes that have been modified to incorporate electronic sounding devices at their lower end. Some variants also have light indicators accompanying the acoustic components (Masood *et al*, 2022). These types rely on the fact that a circuit is complete when two electrodes (or probes) come in contact with the water surface; other variants of electrical method utilize difference in electrical properties such as resistance, capacitance or self-potential to generate a signal that informs the user (via indicators such as Light or sounding devices) to take note of the measurement on the attached tape (Nielsen and Nielsen ,2007).Some merits of this method are that it provides faster multiple measurement than the steel tape and wetted steel tape techniques, it also offers more reliable results in conditions where condensation and splashing occur in the well (Cunningham and Schalk,2011). A disadvantage of this method is that adequate electrical contact of the probe with the water surface, necessary for the proper working of the method can be impeded by the presence of considerable quantity of nonconductive materials such as oil on the water surface. Also, the method is prone to errors arising from changes in the dimensions (length and diameter) of the cable due to regular use; increased depth, and temperature (Nielsen and Nielsen ,2007).

2.1.1.4 Piezometers:

This is generally an open ended tube deployed in an observation or monitoring well to measure pore water pressure and groundwater level. It is also known as a cased well. Surrounding water is allowed to flow in until equilibrium level is attained. The height of the water column inside this cased well corresponds to the pressure and water table level at that point. Measurement of the water level can be manual or automatic. For the manual measurement, a graduated steel or electronic tape is used to detect the depth to the water level. The automatic measurement involves the use of transducers in form of a diaphragm or vibrating wire, that will deflect or vibrate respectively due to changes in pressure. The detected pressure change is then used to compute the water level/depth (Cain *et al*., 2004).

2.1.2 AUTOMATIC MEASUREMENT

2.1.2.1 PRESSURE TRANSDUCERS/SUBMERSIBLE PRESSURE SENSOR

A pressure sensor has a diaphragm which is vented to the atmospheric pressure on one side (the vent helps to compensate for atmospheric pressure), but is in contact with the liquid on the other side. The part of the diaphragm in contact with the liquid measures the static pressure of the liquid column above the sensor. This pressure which is due to the weight of the liquid above the sensor's transmitter, is then utilized in the computation of the liquid level. The sensor is able to detect small changes in the static pressure resulting from increase or decrease of the liquid level above the sensor.

The static pressure is due to the weight of the fluid column. Hence the hydrostatic pressure is measured as the height dependent weight force of a column of fluid. As pressure varies with temperature in accordance to Gay-Lussac's law, an error is introduced into the water level computation. The error in the height/level computation introduced due to the pressure-temperature relation can be compensated for by adding or subtracting a correction value (Mary *et al.,* 2018).

For smooth operation, the measured water level need to be stored for future or real-time access, hence these systems are usually equipped with a data/level logger. Data-loggers automates the retrieval of measured data. when connected to a transducer, they provide ready access to and processing of the measured data (Nielsen and Nielsen ,2007).

2.1.2.2 ULTRASONIC METHOD

Ultrasonic water-level sensors measure the distance from the sensor to the water surface by emitting short acoustic pulses and recording the time-of-flight (TOF) of the echo returned from the surface. The one-way distance is computed from the round-trip travel time and the speed of sound in air which depends on temperature, humidity, and pressure. This non-contact principle has become increasingly popular for monitoring groundwater, stream stage, and reservoirs, particularly in situations where immersion of equipment is undesirable due to fouling, corrosion, or access limitations (Panagopoulos *et al*., 2021; Pereira *et al*., 2022). Operationally, an ultrasonic transducer emits a burst of acoustic energy in the ultrasonic frequency range (typically 20–200 kHz). When this pulse encounters the water surface, part

of the energy is reflected back and detected by the same transducer. The elapsed time is converted to distance by applying the known speed of sound in air (approximately 343 m/s at 20°C). Corrections are required for ambient air temperature and humidity, which influence the velocity of sound (Gao *et al*., 2021). For groundwater applications, ultrasonic sensors are often mounted at the wellhead, pointing downward through a vented borehole cap or installed in stilling wells that provide a smooth reflective surface.
Overall, ultrasonic groundwater and surface water level sensors provide a robust and increasingly popular option for non-contact monitoring. Their primary advantages are portability, immunity to fouling, low maintenance, and declining cost, especially with the rise of open-source microcontroller platforms. Limitations include sensitivity to environmental noise, temperature dependency, and limited range. Inaccuracies can arise from the use of this technique if obstacles or other sonic targets are inside the monitoring wells; when wells are crooked or below a minimum diameter- usually given in the manufacturer's manual ; and also when condensation is present on the screen of the sensor (Drage and Kennedy, 2020). In groundwater monitoring, they are best suited for relatively shallow wells and those whose walls have smooth reflective conditions. Based on the fact that the beam shape of the the ultrasonic pulses are progressively cone-shaped, the range of measurement can be limited by the well bore due to the divergence of the ultrasonic beam.

2.1.2.3 RADAR METHOD

Radar-based water level measurement devices operate with the principle of time of flight in which the time delay between the transmitted radio wave (microwaves) and the reflected echo is used to compute the vertical distance between the sensing unit and the target water surface, in accordance with the Equation 2.1 (Wu *et al*., 2023):

$$R = \frac{ct}{2} \qquad (2.1)$$

Where R is the distance between the radar system and the target, c is the speed of light , and t is the round trip time for the radar signal to travel to the target and be reflected back to the radar sensing unit. The water level is obtained by taking the distance between the sensor and the water surface, away from the known elevation of the radar sensor. They are mainly used for surface water due to their size and problem of reflection from the walls of monitoring wells; research is however ongoing on the development of variants that will be suited for groundwater level monitoring applying guided wave principle (ACSAD and BGR, 2003). Like other acoustic techniques, temperature, humidity, and an obstruction in the beam path all impact on the accuracy of the water-level measurement (Ross, 2001).

In comparison with the Ultrasonic method, the radar method is more resilient to meteorological conditions such as rain, fog, and darkness, as these have a reduced impact on the accuracy. Also radar ranging systems have a longer effective range than acoustic systems as microwave signals suffer less attenuation because they are less prone to the influence of air temperature and humidity. In addition, they have the ability to measure continuously irrespective of weather (Wu et al., 2023).

2.1.2.4 LASER METHOD

Laser based prototypes have shown promising outcomes that prompt more research on the use of laser based devices to measure water levels (Nielsen and Nielsen ,2007). According to Ross (2001), the technique promises greater accuracy of ± 0.01 for ranges of up to 304 m. Due to its high operational frequency , laser pulses are quite resilient to humidity and temperature variations. Some of the demerits are: the path of the beam must be devoid of any obstruction i.e. line of sight to the target surface should be clear to the beam. Also, turbulence-induced scattering can direct the reflected beam away from the detector, thereby impeding successful measurement. In addition, the incident beam may be completely refracted into the water without any portion being reflected by the water surface (Ross, 2001).

2.2 LITERATURE SURVEY OF RELATED STUDIES

Hinging on the advantages of Time of Flight (TOF) LiDAR which include high speed of measurement, potential to function in turbulent condition and remote installation capability, Tamara and Guerrero-Meza, (2016) presented a proof of concept to show that the first evidence that water stage could be monitored during a flash flood by an inclined TOF LiDAR installed on the bank of a river. according to the researchers, unlike traditional methods which involved contact with the water, the proposed system would not be exposed to drifting away by the flood. Hence If successful, such systems could complement or replace traditional sensors in hazardous flood conditions. Measurements were taken as a flash flood passed and LiDAR distances were compared against reference stage measurements from pressure sensors or manual gauges.

The results showed that during the flash flood event, TOF LiDAR successfully detected the water surface. Hence after calibration, stage estimates were in agreement with reference data having high statistical confidence and low maximum error values

The fast response of the system was evident as it reacted in real time during rapidly fluctuating (rising or falling) flood stages, hence the system displayed measurement consistency during dynamic conditions. Even as the system achieved successful measurements, the results cannot be generalized because the test was limited to a single event and location hence long-term deployment reliability could not be ascertained. The system was not evaluated or assessed under clear-water or low-turbidity conditions. Despite these gaps, the work was able to successfully demonstrate the possibility of a non-intrusive, remotely-mounted LiDAR for rapid-response river stage measurement. It also opened new possibilities for LiDAR-based flood monitoring, clear water level (surface and ground water) measurement and potential velocity sensing via Doppler detection.

Recognizing that turbid reservoirs (where Secchi depth < ~1 m) interfered with optical and pressure sensors, Tamari *et al*., (2016) sought to turn this seeming disadvantage to an advantage by exploiting turbidity to monitor reservoir water level. The researchers investigated the performance of a Near Infrared (NIR) LiDAR for monitoring the change in the stage of a reservoir. The LiDAR was installed in an inclined orientation and the monitored reservoir was turbid. The team sought to determine the following: whether other commercial simple LiDAR sensors can replicate earlier results; what is the orientation and configuration of the instrument that will optimally detect suspended particles; the maximum achievable detection depth; the turbidity threshold beyond which detection fails and the practical viability of the long term use of the technique in real reservoir settings. Data was collected from two turbid reservoirs over a two-year period in Mexico. Erratic measurements were filtered out via a signal processing scheme that utilized intensity to reject such readings. The inclined LiDAR unit could not detect subsurface scatterers at Secchi depth greater than approximately 1 m- in deeper water and when turbidity was below a threshold. The work contributed to knowledge in the following ways: It was the first long term field validation of this technique in operational reservoirs. It demonstrated that low-cost terrestrial NIR LiDAR when mounted at steep angles could be used to estimate reservoir stage in turbid water with acceptable uncertainty (±0.08 m, 95%). The study established a turbidity threshold (Secchi depth ~1 m) below which detection can be reliable. The research also showed that by filtering returns based on signal intensity, useful and meaningful stage data can be extracted while erratic readings are filtered off. The investigation opened the possibility of extending the method to monitor other hydrological related phenomena such as sub surface flow velocity estimation via doppler detection of moving particles and coastal flood events.

The study however has the following gaps: The technique was not tested in different environment conditions. This is required to validate the performance of the technique in various conditions as it is suspected that seasonal variability may affect the reliability. Also, performance across broader sensor types remains unexplored as only a rather small set of commercial LiDAR units were tested. Lastly, a cost-benefit comparison with other remotes sensing techniques is necessary to access the economic viability of the method.

A related work done by an expanded team of researchers by Tamari *et al*., (2016), investigated in more details the performances of the technique for monitoring the stage in turbid reservoirs. The work proved that a reservoir stage data could be estimated with decent accuracy using measurements from an inexpensive terrestrial LiDAR. The report also suggested extending the application of the technique to the determination of sub-surface velocity in others similar water entities. Largely the results, contributions, and gaps in this study was very similar to their earlier work (Tamari and Guerrero-Meza, 2016).

Benjamin and Kaplan, (2017) used Leica DISTO E7100i laser distance meter and a raspberry Pi microcontroller to developed a laser-based water level sensor (LB-WLS) capable of measuring sub-centimeter water-level changes in both surface and groundwater systems. This was to address the inability of total pressure based sensors to give such fine scale measurement; thereby not able to track small daily variations in groundwater level which are required for more precise evapotranspiration computations. The device utilized the phase shift method to measure distance from the sensor to the water surface using the relation given in Equation (2.2):

$$D = \frac{c\Delta}{2f} . \frac{\Delta\varphi}{2\pi} \qquad (2.2)$$

where c is the speed of light, f is the modulation frequency, and $\Delta\varphi$ is the phase shift between the measurement signal and the reference signal (Nejad and Olyaee, 2006). The laser distance meter sent data to the acquisition unit via Bluetooth, with time-stamped readings stored for analysis. Field tests successfully tracked and measured diurnal fluctuations in natural surface/groundwater bodies. The design utilized a floating target to take water level measurements due to the need to provide a stable non-cooperative target that would ensure signal returns from the water surface. The design demonstrated significantly lower residual noise compared to pressure transducers. The average Root Square Error of the device was 0.05 ± 0.04 cm, as against 0.19 ± 0.16 cm for Total Pressure Transducer based sensors. Hence the work proved effective in both lab and remote field settings, with superior precision.

There were several gaps in the work despite its success. Firstly, the design did not utilize reflections directly from the water surface. It utilized a non-cooperating floating target. This leaves open the opportunity to explore other recent and more sensitive laser ranging units and designs that could compute distance from reflections directly from water surface. Also, the effect of variation in temperature, relative humidity and other atmospheric interferences on the performance of the device was not evaluated. Evaluating the systems performance in a more diverse environmental conditions need to be explored.

Paul *et al*., (2020**)** realised a water level measurement system that explored the use of a near-infrared (905 nm) LiDAR sensor for hydrometric application. Despite the rather poor reflectivity of a NIR laser beam by water surface, the designed system was able to take measurements under varying conditions which evaluated/assessed the following- effect of sample size, effect of distance of sensor from water surface, effect of water turbidity, effect of sensor inclination, effect of ambient temperature, and effect of water surface rugosity. The prototype had a maximum detectable range of 30- 35 meters. The various test on the system revealed that as regards assessing the effect of sample size on the systems performance, a built in receiver bias correction mode capability of the sensor ensured that fewer measurements are reliably used during operation. With respect to effect of sensor's distance from water surface it was reported that accuracy of the system reduced with increased in measured distance. In other words, measurement bias increased with increase in distance measured. The study could not determine the impact of turbidity on the design's performance due to the apparent high sensitivity of the receiver which ensured that measurements were obtained even in situations where reflectance was low. Hence for a higher reflectance condition, no improvement in the reading was noticed. Lastly, it was revealed that an increase in the rugosity or water surface roughness, led to an improvement in readings. This was apparent because the variance decreased with increased water surface roughness.

In spite of the success achieved, the work pointed out following gaps that could be further investigated; other lasers of different wavelengths, power, and pulse width should be tested to ascertain the generalizability of results. Other effects such as rainfall, debris, or seasonal changes should also be evaluated. More investigation is required to address the thermal compensation issue that was identified. It could be helpful to compare the systems performance with alternative noncontact methods.

Garcia-lopez *et al.* (2023), detailed an innovative non-contact method of measuring the ground water level and mapping the piezometric surface using a drone-mounted LiDAR DJI Zenmuse L1 sensor operating at a wavelength of 905 nm in the near infrared region. The sensor had a maximum detection range of 190m and 450m at 10 % and 80% reflectivity respectively. Measurements were obtained from large diameter wells remotely and validated against readings manually obtained using a Nordmeyer water level meter. A DJI TERRA software was used in processing the downloaded LiDAR data. The piezometric level measured by the LiDAR were derived after refining and averaging points that correlated to the surface of the water. The result obtained showed that the difference between manual and LiDAR measurements ranged from -8.7 cm and +7.9 cm, with a root mean square error of about 5 cm. In terms of accuracy, the LiDAR values were 3 times better than that from official Digital Terrain Models –DTM. The result represents a remarkable step forward in expanding the non-contact method of measuring groundwater level to include the use of laser-based devices. However, the technique may need to be extended to other hydrogeological locations, boreholes and narrower wells for the results to be truly generalizable. Increasing the frequency of monitoring by reducing the time between successive measurements could enhance studying and understanding transient changes. Also, equipping the system with real-time capability could aid easier access to valuable data.

In their 2023 study, Chooruang *et al*. employed the use of a TF lunar LiDAR sensor with a measurement range of 0.2 m to 8 m and an accuracy of 0.06 m to develop a LiDAR based IoT underground water level monitoring device. A SIM800L GSM/GPRS module equipped with an ESP 32 microcontroller was used to provide wireless alternatives and cellular services. A web application was configured with an algorithm to acquire the measured data from the microcontroller, automatically uploading unto the cloud, a Google App script. When applied under actual field conditions, the low-cost sensor performed reasonably well despite environmental factors that impacted its accuracy. The performance of the low-cost sensor was comparable to that of a high-end sensor, exhibiting similar accuracy and higher precision. The designed system was reported to have performed well when compared with a top-tier sensor, mirroring equivalent accuracy and superior precision. Possible research on how environmental factors such as dust, fog and precipitation, affect the performance of such a LiDAR-based device thereby compromising its measurement accuracy is necessary. Also, the design was not tested in different agricultural settings or under other environmental conditions like groundwater or aquifer monitoring.

Suemori *et al*., (2023), developed a laser based liquid level measuring device. The system used the difference in the intensities between the reflected light at the glass-liquid and glass-air interfaces to measure liquid level. The system consisted of a prism to which sixteen photodiodes were attached. The prism was connected to the glass window of the viewport. A red laser having a wavelength and intensity of 635nm and 1mW respectively was employed.

Above the liquid level the laser light was reflected at the glass-air interface. Below the liquid level, most of the laser light passed the glass-liquid interface. However, reflection that occurred at the liquid-air interface was received at the photodiode array. The curvature of the surface at which reflection occurred at the liquid-air interface caused the reflected laser light to spread so that intensity suddenly dropped. The liquid level was measured by taking note of the height at which the laser's intensity suddenly changes. The height of the photodiode which detected the sudden change in intensity of reflected laser light, corresponded to, and was measured as the height of the liquid level. The effect of surface tension of the water surface and beam spreading of the reflected light was also addressed in this work.

In an effort to improve the accuracy of machine learning models to predict water level under various conditions (tilt angle, turbidity and distance between sensor and water surface), Ranieri *et al*. (2024) implemented and tested a design that combined data from a LiDAR sensor, an ultrasonic sensor, and an inertial measurement unit (IMU) using different machine learning models so as to minimize error in prediction. The data from the sensors were collected under controlled (laboratory) conditions. The performance of this combined model was compared to models based on individual sensor measurement. The result showed the combined machine learning approach consistently outperformed individual sensor-based predictions across all turbidity and tilt angles evaluated; error metrics (mean absolute error-MAE and root mean square error- RMSE) for the combined models was significantly reduced while coefficient of determination (R^2) improved. It was reported that in some scenarios (low turbidity and higher incidence angles), the ultrasonic sensor on its own performed comparably or even slightly better than LiDAR, but differences were not statistically significant in most other scenarios. The study highlighted LiDAR as a promising method of water level monitoring due to its lower sensitivity to weather disturbances. The effort of the researchers, however needs to be furthered with a real-world deployment and validation as laboratory results may not be precisely replicated in the field. Other models of LiDAR and ultrasonic sensors could also be tested to confirm the technique's generalizability.

Dementria et al. (2023) used a vertical PVC pipe to simulate underground water well scenario. The designed solar powered LiDAR based telemetry device was made to monitor water level in real-time. Measured data was uploaded unto the ThingSpeak IoT platform for visualization. The system comprised of an Arduino Uno, a LiDAR-lite v3hp, a SIM800C GSM/GPRS module, solar panels, a DFRobot DFR0559 5V Solar Power Manager, and Li-Ion battery pack. The system was configured to take 100 continuous LiDAR samples and then utilize the median value so as to mitigate against outliers. The energy system was tested to evaluate the solar panel efficiency, battery capacity, idle and run-time performances. Data from a measuring tape and a submersible pressure sensor was compared with those obtained from the constructed device. The result revealed that the accuracy of the design increased with repeated sampling and stabilized after about 15 readings or 16 minutes. The discrepancy in the initial measurements was attributed to the need for further calibration and adjustment to enhance performance. The system however successfully transmitted data to the ThingSpeak platform every minute, although signal interruptions occurred occasionally. The pressure sensor was reported to be more consistent, although it required higher power demands. The solar panels Li-Ion battery ensured continuous operation, with estimated battery life of over seven and half hours during transmission and approximately twelve and half hours in idle mode. Further research on the work is expected to test the prototype in real monitoring wells whose water level would fluctuate naturally; and access the impact of environmental variables on the design's performance. In addition, the design needs to be further optimized to stabilize the delay in correct LiDAR readings.

2.3 Theoretical Foundation of LiDAR Reflection

Reflection describes the change in direction of a wavefront at an interface between two different media such that the wavefront returns into the medium from which it originated. Light Detection and Ranging (LIDAR) systems operate on the fundamental principle of electromagnetic wave reflection, where laser pulses are transmitted toward targets and the reflected signals are analyzed to derive desired information (Born and Wolf, 2019).

2.3.1 Specular and Diffuse Reflection

LiDAR reflection occurs when incident electromagnetic radiation interacts with target surfaces, following the fundamental laws of optics. The reflection process can be categorized into specular and diffuse components, with most natural surfaces exhibiting a combination of both (Weitkamp, 2005). For specular reflection light is reflected in a single direction. It occurs when light strikes a microscopically smooth surface whose roughness is significantly smaller than the wavelength of the incident light (Nejad and Mirsaeidi, 2005). A perfectly still water surface acts as an ideal specular reflector, obeying the Law of Reflection, where the angle of incidence equals the angle of reflection. In a LiDAR based water level monitoring system, the LiDAR unit will be normally placed directly above the water surface. Ideally, for a calm water surface, the reflected pulse will return along the incident path, so that the receiver senses maximum returned pulses. However, deviations from normal incidence condition or surface disturbances due to ripples or waves, can cause the specular reflection to deviate from the receiver's field of view, thereby reducing received signal strength (Henley *et al*. 2025). Specular reflection is dominant when water surface is smooth (when laser wavelength is much greater than the water wave's height); when the incidence angle is small (< 30° from normal) and when water turbidity is low-when water is relatively clean/clear. In general, the Law of Reflection dictates the behaviour of the specular reflection.

For diffuse reflection light is scattered in all directions. Diffuse reflection is caused by the interaction of light with a rough surface. When light strikes a rough surface, it is scattered in all directions because the surface is not smooth enough to reflect the light in a single direction (Nejad and Mirsaeidi, 2005), it is often approximated by the Lambertian model (Tatoglu and Pochiraju, 2012) and is valid when the surface roughness is comparable to or larger than the laser wavelength (Mobley *et al.*, 2003).

2.3.2 Lambert's cosine law

A Lambertian surface is an idealized diffuse reflector. For ideal diffuse reflectors, the intensity of the radiant energy is constant irrespective of the angle of view. Lambert's cosine law states that the radiant intensity (I) observed from a point on such a surface is directly proportional to the cosine of the angle θ_r between the direction of observation and the surface normal (Tondal, 2020). It is also known as the cosine emission law. Mathematically the Lambert cosine law is represented by Equation (2.3) (Nicodemus, 1970):

$$I(\theta_r) = I(0)cos\theta_r \tag{2.3}$$

Where:

$I(\theta_r)$ is the intensity of light emitted by the surface in the direction of viewing and, $I(0)$ is the intensity observed when θ_r is zero, this is the intensity emitted in the direction perpendicular to the surface. θ_r is the angle between the normal to the surface and the viewing direction.

2.3.3 Fresnel Reflection Coefficients

The Fresnel equations describe the amplitude and intensity of reflected and transmitted electromagnetic waves at a planar interface between two media with different refractive indices (Born and Wolf, 2019). These are fundamental for predicting LiDAR signal strength from water surfaces.

2.3.4 Fresnel Equations for Intensity Reflectance

Fresnel reflectance determines how much of the LiDAR's pulse is reflected directly at the air–water boundary in comparison with that transmitted. For s-polarized light- when electric field is perpendicular to the plane of incidence, this reflectance is given by Equation (2.4) (Hecht, 2017; Born and Wolf, 2019) as:

$$R_S = \left|\frac{n_1 cos\theta_i - n_2 cos\theta_t}{n_1 cos\theta_i + n_2 cos\theta_t}\right|^2 \tag{2.4}$$

Similarly, when the electric field is parallel to the plane of incidence the reflected plane-polarized light is given by Equation (2.5)

$$R_p = \left|\frac{n_2 cos\theta_i - n_1 cos\theta_t}{n_2 cos\theta_i + n_1 cos\theta_t}\right|^2 \tag{2.5}$$

where θ_t is related to θ_i by Snell's law, as seen in Equation (2.6):

$$sin\theta_t = \frac{n_1}{n_2} sin\theta_i \tag{2.6}$$

For the special case when $\theta_i = 0°$, that is at normal incidence, the reflection coefficient can be written as presented in Equation (2.7);

$$R = \left(\frac{n_1 - n_2}{n_1 + n_2}\right)^2 \tag{2.7}$$

When the interacting interface is for air-water ($n_1 = 1$, $n_2 = 1.333$):

$$R = \left(\frac{1 - 1.333}{1 + 1.333}\right)^2 = 0.0204 \approx 2\%$$

That means that at normal incidence, only ~2% of incident laser power would reflects from a clean water surface. This low reflectance necessitates high-power lasers (mW to W range) requirement, sensitive detectors (avalanche photo diode-APD or single photon avalanche diode-SPAD) and narrow spectral filtering to reject background noise (Mobley, 1994). Figure 2.1 shows the spectral behaviour of the clear still water as function of wavelength; from the figure it is seen that the reflectance of water at 905 nm is very low (Paul *et al.*,2020).

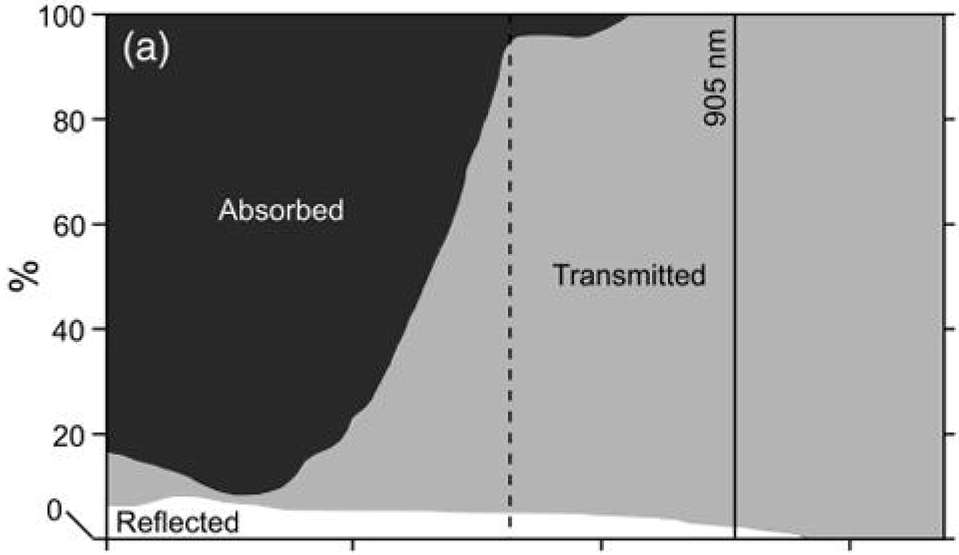

Figure 2.1: Reflectance curve for clear water as a function of laser light wavelength (Paul *et al.*,2020)

Reflectance depends strongly on incidence angle; near normal incidence water has low reflectance (a few percent) but reflectance increases toward grazing incidence. At near-normal incidence the surface reflectance is small (resulting in low return intensity) and subsurface backscatter from suspended particles may dominate; at grazing incidence surface reflectivity increases considerably and can create strong specular returns. Also, polarization of the LiDAR (many laser modules are partially polarized) affects return strength: s-polarized component reflects more strongly at many angles than p-polarized near Brewster's angle.

2.3.5 LiDAR Radar Equation

The LiDAR equation forms the cornerstone of LiDAR system design and performance prediction. It an equation that quantifies the received optical power as a function of system parameters, target properties, and environmental conditions. There are different forms of this equation, each derived to suit specific application (Mobley, 2021).

The derivation of the LiDAR equation is presented here following the approach of Weitkamp, 2005; Kashani *et al.*,2015; Mobley, 2021; and Ma *et al.*, 2022.

Given the peak power of the transmitted laser P_t, subjected to an optical transmission coefficient of the transmitter η_t. The propagating pulse is attenuated as it travels to the target through the atmosphere with an atmospheric transmission coefficient η_{atm}. For a two-way journey this is η_{atm}^2 .

The total power reaching the target P_T is given by Equation (2.8.) as

$$P_T = P_t.\eta_t.\eta_{atm} \tag{2.8.}$$

The reflected pulse can be modelled using the Lambertian approximation, hence the reflected radiance L in the direction of the sensor is represented by Equation (2.9) as

$$L = \frac{P_T.\rho.cos\theta}{\pi.A_{ill}} \tag{2.9}$$

Where ρ is the target reflectance, A_{ill} is the area of the target illuminated by the laser, θ is the angle of incidence between the beam and the normal to the target surface.

The part of the reflected pulse that reaches the sensor detector of area A_r, can be described in terms of the solid angle Ω subtended by the detector at a distance R from the target, as seen in Equation (2.10) thus:

$$\Omega = \frac{A_r}{R^2} \tag{2.10}$$

The power captured by the aperture of the detector P_{ap}, is a product of the radiance (equation 2.8.2), the illuminated area, and the solid angle; represented by Equation (2.8.4 a) and Equation (2.8.4 b):

$$P_{ap} = L.A_{ill}.\Omega \tag{2.11a}$$

$$P_{ap} = \frac{P_T.\rho.cos\theta}{\pi.A_{ill}} \quad .A_{ill}\frac{A_r}{R^2} \tag{2.11b}$$

Travelling back through the atmosphere, the pulse is again attenuated by η_{atm} and the receiver optics having an optical reception efficiency η_r . hence the received power at a distance R is given as obtained in Equation (2.12) as

$$P_r(R) = \frac{P_t\eta_t\eta_{atm}^2\rho A_r cos\theta}{\pi R^2} \tag{2.12}$$

where ρ represents the reflectance (dimensionless), P_t represents the transmitted pulse power (in Joules per pulse duration -J/S), η_{atm} is the transmission coefficient of the atmosphere; and η_t represent the dimensionless optical transmission efficiency, A_r is taken as the area of the receptor(in square meters), θ is the incidence angle of the sensor (in degrees or radians) and R represents how far the sensor is from the surface of the water

From Equation (2.12), it is seen that the maximum detectable range is attained when the power detected at the receiver is at its lowest value, implying that the higher the minimum detectable power the closer will be the maximum range (Kashani et al.,2015; Paul *et al.*,2020; and Ma *et al.*, 2022). According to Paul *et al.* (2020), reflectance at 905nm- the operational wavelength of the LiDAR-lite v3hp, is below 10% (see figure 2.1) and increases with turbidity.

2.4 Description of Hardware Components

A description of some of the main hardware component of a LiDAR based system is given in the subsection that follow;

2.4.1 Arduino Uno

The Arduino Uno is an open-source microcontroller development board designed for rapid prototyping of embedded systems. It is based on the ATmega328P, an 8-bit RISC (Reduced Instruction Set Controller) microcontroller that executes programs uploaded via USB, making it widely accessible for environmental monitoring and automation research (Hernández-Rodríguez *et al*., 2023). It has 32 kB of flash memory, 2 kB of SRAM, and 1 kB of EEPROM, and operates at a clock frequency of 16 MHz, driven by a quartz oscillator for precise timing in sampling and communication tasks (Rudavskyi *et al*., 2024). The board can be powered either through USB or through the barrel jack that can take in 7–12 V external DC voltage). The on-board voltage regulators supply stable 5 V and 3.3 V outputs for sensors and peripherals (Arduino.cc,2023).

The Uno provides 14 digital I/O pins, six of which support Pulse Width Modulation (PWM), and six analog input channels connected to a 10-bit analog-to-digital converter **(**ADC). These allow integration with a wide range of sensors and actuators, enabling environmental data acquisition (Hong *et al*., 2021). Communication is supported through UART, I^2C, and SPI, while a dedicated ATmega16U2 chip functions as a USB-to-serial converter, facilitating programming and computer interfacing (Jan *et al*.,2022).

The Arduino uno is a good starting point for building a real-time groundwater level monitoring systems with LiDAR sensors. Its affordability and straightforward integration with other components make it a practical alternative to more expensive, proprietary data loggers (Baker, 2014). The open-source nature of the Arduino platform demonstrates its value in environmental data collection, enabling the long-term deployment of accurate, low-cost monitoring devices for various field applications like soil moisture, microclimate, and water quality, as long as proper calibration procedures are followed (Mühlbauer *et al*., 2023; Hong *et al*., 2021). In the context of a LiDAR-based real-time water-level sensing, the Uno is quite advantageous for proof-of-concept and prototype stages. It supports I²C and UART communication protocols, making integration with commercial time-of-flight (ToF) LiDAR modules quite straightforward (Rudavskyi *et al*., 2024). Additionally, it can execute basic real-time processing tasks such as moving average filters and threshold detection, which are sufficient for early system validation. Its low power consumption is convenient for solar-powered or battery-operated field applications, which is a critical factor for remote groundwater monitoring (Bulusu *et al*., 2024).

In spite of these functionalities, the Uno has some limitations. it has only 2 kB SRAM and 32 kB flash, constraining data buffering, advanced filtering, and local storage. Studies on low-cost environmental sensing stress the demand for rigorous calibration and, often, more capable controllers for scaling beyond pilot deployments (Hernández-Rodríguez *et al*., 2023; Ding *et al*., 2024). Therefore, while the Uno is ideal for initial development, a more advanced microcontrollers or system-on-chip (SoC) boards (e.g., Raspberry Pi or STM32) is required for improved functionality. Plate 2.1 shows the Arduino Uno microcontroller.

Plate 2.1 Arduino Uno (Arduino, 2023)

2.4.2 LiDAR-lite v3hp

The acronym LIDAR means Light Detection and Ranging. It's a distance measuring technique that uses travel time of laser pulses to measure distance to a target. Time of flight is an important sensing technique that is used by many LiDAR applications (Padmanabhan *et al.*,2019). The LiDAR-lite v3hp sensor uses LiDAR's concept of time of flight (tof) to measure distances. In this technique, the time taken for a signal to get to a target surface from the LiDAR's transmitter after it is reflected and then return to the unit's receiver, is used to calculate the distance between the LiDAR and the reflecting surface. According to Garmin, (2018)**,** the sensor sends out very short pulses of near infrared laser light (905 nm) towards the target. Some of the laser lights are reflected upon hitting the surface of the object. The sensors receiver listens for these reflections which are usually very weak and noisy. So instead of relying on just one, the sensor repeats the pulse several times and adds them together in memory. As these reflections are added, a clear peak is formed in the sensor's record at the exact delay time that matches how long the light took to return. Background noise from say sunlight, electronics or random reflection exists in the system. Hence the sensor differentiates these background noise from the real reflection signal by comparing the peaks with the background noise. If the peak is above a valid signal threshold and higher/ stronger than the calculated noise floor, the measurement is accepted and the distance is calculated; if the peak is below the signal threshold, the sensor rejects the measurement and reports a default value of "1cm". The time delay is used with the known speed of light c, to directly compute the distance according to the Equation (2.13):

$$Distance = \frac{Time\ delay \times c}{2} \tag{2.13}$$

The LiDAR-lite 3vhp has a nominal voltage of 5V but operates between a voltage range of 4.75 – 5.5 V. It uses a 905 nm edge-emitting laser with peak power around 1.3 W. When idle, its current consumption is 65 mA, while it is 85 mA during an acquisition. Beam divergence is about 8 milliradians (approximately 0.5 degrees). It has an effective distance range of approximately 1m to 40 m (at 70% reflectivity) with nonlinearity present below 1 m.The unit has a resolution of 1cm and accuracy: ± 2.5 cm for targets at distance equal to or greater than 2 m. for distance less than 2 m, accuracy degrades to ±5 cm. (Garmin,2018; Driverless Global,2018; Ott *et al*.,2019). The specification of LiDAR-lite v3hp are listed in Table 2.1.

Table 2.1: Specification for LiDAR-lite v3hp (Garmin, 2018).

Specification	Measurement
Wavelength	905 nm (nominal)
Total laser power (peak)	1.3 W
Pulse width	0.5 µs (50% duty cycle)
Pulse train repetition frequency	10-20 kHz nominal
Energy per pulse	<280 nJ
Beam diameter at laser aperture	12 × 2 mm (0.47 × 0.08 in.)
Divergence	8 mRad

The LiDAR-lite v3hp can be connected in either of two configuration or connection modes- (Inter-Integrated Circuit (I^2C) and Pulse Width Modulation (PWM). The I^2C interface connection can be regarded as a two wire communication between the microcontroller (in this case Arduino Uno) acting as a "master" and the LiDAR sensor acting as the "slave". The master sends a command for 'measurement to start' and the sensor does the measurement. The master then reads the result (distance, status etc.) from the sensor's internal register. The I^2C configuration is preferable when digital accuracy and access to extra information is desired. On the other hand, in the PWM configuration, a timed signal is used to encode the distance. The LiDAR unit is triggered to measure when a pin is pulled low. The sensor then sends out a pulse on its PWM output pin. The width of this pulse is equal to the distance measured. The PWM connection only needs one signal wire to read distance.

In terms of complexity, I^2C is more complex than PWM as registers are needed for it to read distance; while PWM's simpler configuration just measures pulse duration (Garmin,2018). In this work, the I^2C configuration is used.

The unit has six wires of different colours- Black, red, blue, green, yellow and orange. For the I^2C configuration four of these are utilized- Black, red, blue and green are used while the PWM configuration used three- Black, red and yellow. Plate 3.2 is a snapshot of the LiDAR-lite 3vhp sensor.

Plate 2.2 LiDAR-lite v3hp sensor (SparkFun Electronics, n.d.)

2.4.3 ESP8266 WI-FI Module and Adapter

The ESP8266 Wi-Fi module functions as a communication interface between the Arduino and the IOT platform-ThingSpeak. It essentially provides the Arduino with internet connectivity by operating as a Wi-Fi modem that receives serial commands from the Uno and transmits the groundwater level data to ThingSpeak. The module operates at 3.3 V, providing multiple general-purpose input/output (GPIO) lines, a single 10-bit analog-to-digital converter (ADC), and support for serial communication protocols (UART, SPI, I^2C). It can be used as a standalone IoT device or as a Wi-Fi modem for an Arduino. For the former, the unit's 32- bit RISC microcontroller will be put to use. However, connecting it with an Arduino separates the task of control from that of communication, thereby simplifying debugging and firmware development. In addition, incorporating the Arduino Uno into the design helps to ease integration with the LiDAR-lite module due to the existence of supportive library available for the Arduino; hence the greater flexibility is also introduced into the system.

The ESP8266's small form factor, low cost, and open-source support makes it an attractive choice for use in Internet of Things (IoT) applications where remote sensing and cloud integration are required (Mesquita *et al*., 2018; Shahrul *et al*., 2021).

The ESP8266 provides connection for the Arduino Uno serially via UART-Universal Asynchronous Receiver Transmitter. The UART pins of the Uno- the Tx and Rx pins, are connected to the Rx and Tx pins of the Wi-Fi module respectively. The Arduino sends AT commands or structured data packets over serial communication (ie the TX/RX pins). In summary, the Arduino collects and formats data from the LiDAR module, and sends it serially through UART to the ESP8266 which receives the data via its RX pin, processes the AT commands or raw data and sends the formatted sensor data via HTTP (e.g. a GET request) or MQTT to the dedicated ThingSpeak channel for storage and visualization (Parida *et al*., 2019; Miry and Aramice, 2020).

An Esp-01 Wi-Fi adapter is used to ease interfacing and optimize the power available to the ESP8266 Wi-Fi module. This adapter has an operational voltage of between 5V – 12V and supplies a regulated 3.3V which the on-board regulator on an Uno is unable to effectively provide at the designated terminal. It has a current consumption of about 170mA. The Esp-01 Wi-Fi adapter has four pins-GND, VCC, Tx and Rx (Nerdshed. n.d). Plate 2.3a, and Plate2.3b show snapshots of the ESP8266 Wi-Fi module and the ESP-01 adapter respectively; while Plate 2.3c shows the Wi-Fi module mounted on the adapter.

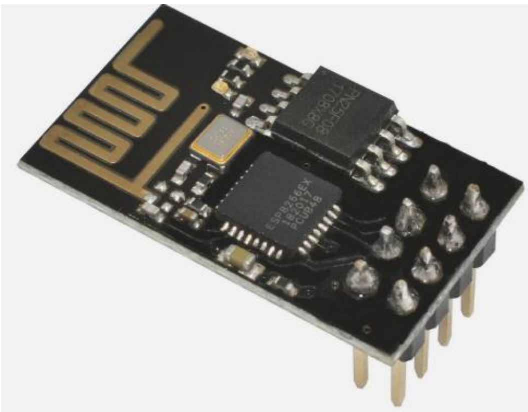

(a)

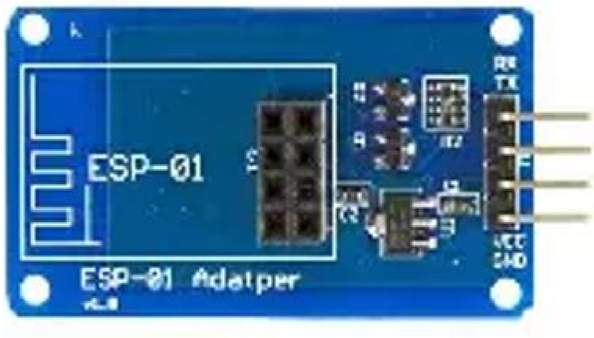

(b)

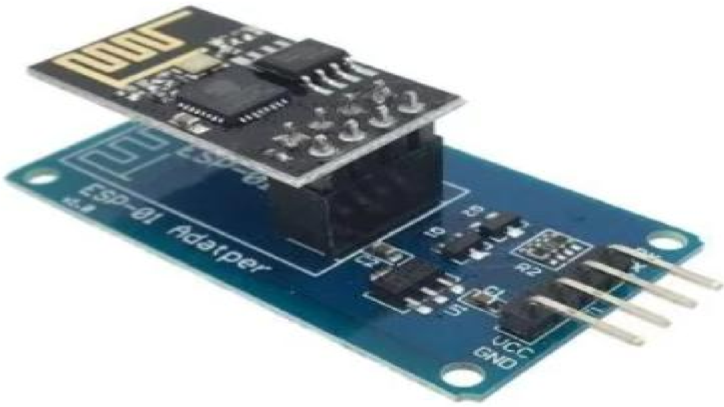

(c)

Plate 2.3 (a) Esp8266 Wifi Module (b) Esp -01 Adapter (c) Esp8266 Module mounted on Adapter **(Nerdshed. n.d)**

2.4.4 16 x 2 Liquid crystal display

A liquid crystal display-LCD, can be described as a simplified computer monitor that provides a means for visual feedback for users. A 16×2-character LCD (commonly driven by an HD44780-compatible controller) is a low-cost, low-power alphanumeric display that shows two rows of 16 characters each. The operating voltage of this unit is 4.7V – 5.3V. The current consumption when the backlight is not in use is 1mA. The pin configuration is composed of 16 pinouts (pin 1 to pin 16) which are briefly describe below (Hitachi,n.d.) :

Pin1 (VDD): This is used to connect the GND terminal of the microcontroller unit or power source.

Pin2 (VSS): This is the voltage supply pin of the unit. It is denoted as VCC in some models It connects the supply pin of the power source.

Pin3 (V0): Some models designate this as VEE. This pin is used to adjust the contrast of the display, used to connect a changeable potentiometer that can supply 0 to 5V.

Pin4 (Register Select-RS/Control Pin): This pin toggles between the data mode and the command mode, after determining whether the input is a command or data

Pin5 (Read/Write-RW/Control Pin): This pin switches the display between the read or writes operation, and it is connected to a microcontroller unit pin to get either 0 or 1 (0 = Write Operation, and 1 = Read Operation).

Pin 6 (Enable/Control Pin): This pin usually designated as “E”, is held high for it to execute Read/Write operations.

Pins 7-14 (D0 –D7): These pins are used to send data to the display. They are called data pins. They can be connected in either 4-wire mode or 8-wire mode. In 4-wire mode. For each wire mode, four and eight pins respectively (D0 to D3, or D0 to D7) are connected to the microcontroller unit.

Pin15 and Pin 16 (positive pin and negative pin of the LED): Labelled as A+ and K- (or Led+ and Led-), these pin provides connection to a +5V supply and ground respectively that feed the backlight of the LCD. The A+ pin is connected to the positive voltage supply through a resistor (220 ohms). Plate 2.4 shows snapshots of 16 x 2 liquid crystal display.

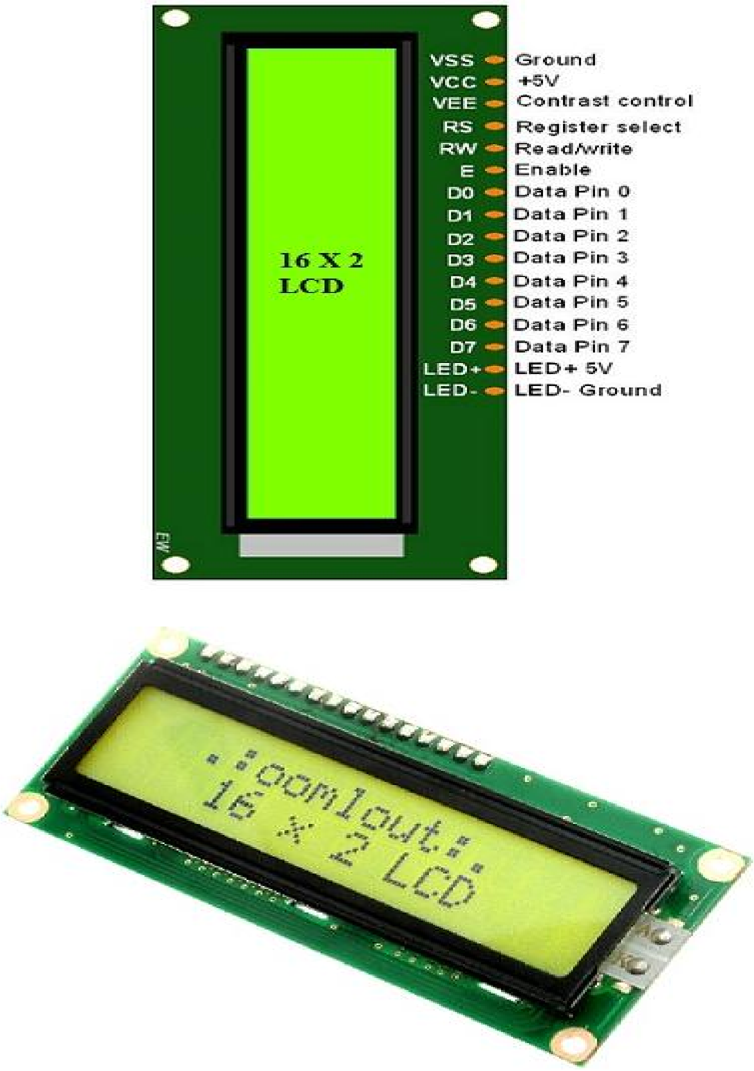

Plate 2.4 :LCD 16 x 2 display (culled from ELPROCUS https://www.elprocus.com/lcd-16x2-pin-configuration-and-its-working/)

It is widely used in embedded and IoT field instruments that need local visual readable feedback such as sensor status, recent measurements etc (Hitachi, n.d.; Vishay Intertechnology, n.d.). The principle of operation of the LCD is hinged on the alteration of the polarization of the molecules of the liquid crystal in response to an electric field. When an electric field is applied across the liquid crystal layer, the molecules align to either block or transmit light in varying degrees from a backlight or reflective surface. This controlled modulation of light creates the visible characters on the pixels (Ceccarini, 2022). The LCD maintain a stable output by continuously refreshing the crystal alignment; achieving this with low power consumption, hence making it attractive for embedded sensor systems requiring real-time local feedback (Saputri et al., 2025).

2.5 The Software Implementation

The Arduino Integrated Development (IDE) software was downloaded from www.arduino.cc , a ThingSpeak account was registered on www.thingspeak.mathworks.com . The account had a single channel and was configured for public viewing. On the channel, real-time groundwater levels could be observed by anyone with the web link.

2.5.1 Arduino IDE

The Arduino Integrated Development Environment (IDE) is a software application for Arduino and other compatible microcontrollers. It enables writing, compiling and upload of programs unto such microcontrollers. It is an open-source application that can be downloaded and installed for free from the official website of Arduino. It helps to accelerate rapid prototyping and simplifies iterative testing. The IDE is composed of two main parts- the editor, which is used for writing the code and the compiler which is used to compile and upload the sketch to microcontroller. The IDE supports C and C++ programming language; has a large library and wide community support (Kondaveeti *et al*., 2021). The Arduino IDE library eases integration of many sensors (like the LiDAR module), interfaces other software applications (like ThingSpeak) and provides a source of control of electronic components and wireless communication modules on IOT projects. Code written in the Arduino environment can handle sensor sampling, interfacing, and periodic data publishing to servers (Espinoza Ortiz *et al*., 2023; Drage and Kennedy, 2020). The complete software code for this work can be found in the Appendix A.

2.5.2 ThingSpeak

ThingSpeak is an open source Internet of Things (IoT) cloud based data acquisition and visualization platform, it is an essential bridge between embedded system components and remote management and analysis of data. It acts as a secure repository for data streamed from devices connected in a network. The architecture provides up to eight fields for storing sensor data, alongside a three fields for location -latitude, longitude, and elevation (Viegas et al., 2021), which is particularly helpful in tracking deployed monitoring units and one field for status. ThingSpeak supports application programming interfaces (APIs) and plugins that allow for easy integration with other web services, social networks, and other APIs (Kondaveeti *et al*., 2021). For this study, the platform's ability to communicate via HTTP protocol simplifies the process of securely posting data from the Arduino microcontroller, which sends data using a HTTP POST or GET request that includes the unique Write API Key. Data is transmitted to a channel via the provided Write API Key**.** Data transmission from the Arduino to the ThingSpeak channel utilizes a standard uniform resource identifier (URI) structure appended with the unique API key and the sensor values as query string parameters. This method of data transfer is very efficient, being light weight and having a key-based authentication; it is thus suitable for resources constrained nature of an Arduino-based monitoring device. ThingSpeak offers capabilities that make it highly compatible with low-cost, real-time environmental monitoring systems

CHAPTER THREE

MATERIALS AND METHODS

3.1 Introduction

Effective groundwater management in data-scarce regions demands monitoring systems that are accurate, affordable, and operationally sustainable. While commercial solutions exist, their high cost and technical complexity exclude many developing nations from establishing adequate observation networks. This chapter presents the systematic methodology employed to design, construct, calibrate, and validate a low-cost, non-contact groundwater level monitoring device. The approach integrates laser based time-of-flight sensing with open-source microcontroller platforms and cloud-based telemetry to achieve real-time data acquisition and remote accessibility.

The methodology is organized into six interconnected phases:

i. system requirements analysis and component selection;
ii. hardware architecture and circuit implementation;
iii. firmware development and control logic;
iv. calibration protocol with uncertainty quantification;
v. field deployment and measurement acquisition; and
vi. statistical validation framework.

Each phase adheres to metrological best practices and is documented to ensure reproducibility. The chapter concludes with explicit acknowledgment of scope boundaries and limitations that bound the validity of the findings.

3.2 System Requirements and Design Specifications

3.2.1 Functional Requirements

The monitoring system was designed to satisfy the following functional requirements listed in Table 3.1, derived from analysis of existing monitoring gaps (Chapter 1) and stakeholder needs assessment:

Table 3.1: Summary of system's functional requirements

Requirement ID	Specification	Rationale
R1	Non-contact distance measurement to water surface	Eliminate sensor corrosion, biofouling, and maintenance associated with submerged instruments
R2	Measurement range: 1.0–40.0 m	Accommodate typical artesian well depths in the Niger Delta region (field survey: mean = 11 m, n = 2 wells)
R3	Accuracy: ±5 cm post-correction	Sufficient for operational water resource management; comparable to manual tape measurement uncertainty
R4	Temporal resolution: ≤1 minute	Enable detection of sub-hourly hydrological transients (pumping, recharge events)
R5	Real-time telemetry with cloud storage	Eliminate site visitation for data retrieval; enable immediate stakeholder access
R6	Local display for field verification	Support technician confidence during installation and troubleshooting
R7	Total hardware cost: <USD 250(N350,000)	Ensure affordability for network-scale deployment in resource-constrained settings
R8	Indigenous	Use components available in Nigerian

	constructability	markets; enable local repair and maintenance

3.2.2 Design Constraints and Trade-offs

The requirements impose inherent trade-offs that guided component selection:

- **Accuracy vs. cost**: Sub-centimeter accuracy (±0.5 cm) requires a higher end Lidar costing more than ten times the cost of a Lidar-lite v3hp ; ±5 cm is achievable with time-of-flight architectures at target price point (Benjamin and Kaplan ,2017; Paul et al.,2020)
- **Power vs. connectivity**: Wi-Fi offers lower power consumption and zero recurring cost versus GSM, but requires hotspot infrastructure; GSM provides universal coverage at higher power and subscription cost
- **Range vs. beam divergence**: The LiDAR-lite v3hp has a maximum range of 40m and a beam divergence of 8mrad (0.5°). A Narrower beam divergence will reduce well-wall interference but requires more precise alignment. At maximum distance beam diameter is 40cm (beam diameter = distance/100). 0.5° was accepted as good compromise.

3.3 Component Selection and Characterization

3.3.1 Selection Rationale and Comparative Evaluation

Prospective components to be used were evaluated against quantitative criteria using an analytic hierarchy process -AHP, (Saaty,2008; Silva and Jardim-Gonçalves,2017) with weights derived from requirement priorities (R1–R8). Six criteria were identified and assigned weight to define their importance based on how critical each are for the specific application. Table 3.2 presents the evaluation matrix for distance sensors; similar matrices guided microcontroller and communication module selection.

Table 3.2: Comparative Evaluation of range Sensing Technologies for Groundwater Monitoring

Criterion (Weight)	**Ultrasonic (HC-SR04)**	**Lidar (Lidar-Lite v3HP)**	**Lidar (TF-Luna)**
Non-contact (0.15)	1.0	1.0	1.0
Range 1–10 m (0.15)	0.4 (2–400 cm)	1.0 (1–40 m)	0.6 (0.2–8 m)
Accuracy ±5 cm (0.20)	0.3 (±3 cm, temperature-sensitive)	0.9 (±2.5 cm)	0.7 (±6 cm)
Beam divergence <1° (0.15)	0.0 (15° cone)	1.0 (0.5°)	0.8 (≈2°)
Immunity to humidity (0.15)	0.2 (condensation affects)	0.9	0.9
Cost <N206,000 (0.10)	1.0 (~N8,000)	0.8 (~N204,000)	1.0 (~N62,000)
Weighted Score	**0.42**	**0.91**	**0.76**

The LiDAR-lite v3hp was chosen as others failed because they were rather great at one thing but terrible at others. The HC-SR04 is cheap but its range is quite short, has a large beam divergence and performs poorly in a humid well (Panagopoulos et al., 2021). The TF-Luna is cheap but can't reach 10 meters reliably. The criteria and assigned weight are;

Non-contact (weight: 15%)

Range 1–40 meters (weight: 15%)

Accuracy ±5 cm (weight: 20%)

Beam divergence <1° (weight: 15%)

Immunity to humidity (weight: 15%)

Cost <N206,000 (USD150) (weight: 10%)

Lidar-Lite v3HP was selected based on highest weighted score.

3.3.2 Component Specifications

3.3.2.1 Distance Sensor: Garmin Lidar-Lite v3HP

The Lidar-Lite v3HP is a single-point time-of-flight laser rangefinder operating at 905 nm wavelength with the specifications detailed in Table 3.3.

Table 3.3 Manufacturer Specifications for Lidar-Lite v3HP (Garmin, 2018)

Parameter	**Specification**	**Test Condition**
Operating principle	Pulsed time-of-flight	—
Wavelength	905 nm (near-infrared)	—
Laser class	Class 1 (eye-safe)	IEC 60825-1:2014
Peak optical power	~1.3 W	Pulse duration <10 ns
Beam divergence	0.5° (8. mrad)	Full angle, $1/e^2$

Range	1–40 m	70% reflective target, indoor
Resolution	1 cm	—
Accuracy	±2.5 cm (≥2 m); ±5 cm (<2 m)	70% reflective target, stable temperature
Update rate	>500 Hz (internal accumulation)	—
Output rate	Configurable: 1–500 Hz	I²C or PWM mode
Interface	I²C (400 kHz) or PWM	Selectable via wiring
Supply voltage	4.75–5.5 V DC	—
Current consumption	65 mA (idle); 85 mA (acquisition)	—
Dimensions	20 × 48 × 40 mm	Without mounting bracket

Signal Processing Architecture. The v3HP employs coherent signal accumulation to overcome low-return scenarios (Garmin, 2018). The transmitter emits a burst of laser pulses (typically 100–1000 pulses per measurement). Returned photons are converted to electrical signals, time-delayed according to target distance, and accumulated in a digital correlator. Coherent addition at the true delay produces a peak; incoherent noise averages toward zero. The peak-to-noise ratio determines measurement validity; if below threshold, the sensor returns a default value (1 cm) indicating invalid measurement.

This architecture is critical for groundwater applications: at 905 nm, water reflectance at normal incidence is approximately 2% (Hecht, 2017; Born and Wolf, 2019), yielding returned signal power far below the manufacturer's 70% reflectance test condition. Signal processing gain compensates for reduced optical return.

3.3.2.2 Microcontroller: Arduino Uno Rev 3

The Arduino Uno Rev 3 specifications is listed in Table 3.4. This microcontroller was selected for its affordability, extensive community support, comprehensive sensor libraries, and established reliability in environmental monitoring applications (Hernández-Rodríguez et al., 2023; Mühlbauer et al., 2023).

Table 3.4 Arduino Uno Rev 3 Technical Specifications

Parameter	Specification
Microcontroller	ATmega328P (8-bit RISC)
Clock speed	16 MHz (quartz oscillator)
Flash memory	32 kB (0.5 kB bootloader)
SRAM	2 kB
EEPROM	1 kB
Operating voltage	5 V DC
Input voltage (recommended)	7–12 V DC
Digital I/O pins	14 (6 PWM-capable)
Analog input pins	6 (10-bit ADC, 0–5 V)
I²C pins	SDA (A4), SCL (A5)
UART	1 hardware serial (pins 0, 1)
SoftwareSerial	Multiple instances possible (pins 3, 4, 5, 6, 7, 8, 9, 10, 11, 12)

The 2 kB SRAM constrains data buffering (Martinez et al., 2024). The 16 MHz clock provides adequate timing for the control loop but limits computational complexity (Khan et al., 2021). These constraints were acceptable for the proof-of-concept scope but would necessitate upgrade for commercial production and deployments.

3.3.2.3 Communication Module: ESP8266 ESP-01 with Adapter

The ESP8266 ESP-01 (Table 3.5) provides IEEE 802.11 b/g/n Wi-Fi connectivity at minimal cost and power consumption. (Basford et al., 2019). Table 3.5 displays the technical details of the module.

Table 3.5 ESP8266 ESP-01 Technical Specifications

Parameter	**Specification**
Processor	Tensilica L106 32-bit RISC
Clock speed	80 MHz (default), 160 MHz (optional)
Wi-Fi standard	802.11 b/g/n
Frequency	2.4 GHz
TX power	802.11b: +20 dBm; 802.11n: +14 dBm
RX sensitivity	–91 dBm (802.11b, 1 Mbps)
Operating voltage	3.0–3.6 V (strict requirement)
Current consumption	≈80 mA average; ≈70 mA peak (TX)
Interfaces	UART (default), SPI, I²C (GPIO-limited)
Flash memory	512 kB–4 MB (variant-dependent)

Critical design consideration: Voltage regulation. The ESP8266 requires 3.3 V; 5 V exposure causes immediate damage. The Arduino Uno's onboard 3.3 V regulator (LP2985-33DBVR) provides maximum 150 mA, insufficient for ESP8266 peak transmission current (~170 mA). The ESP-01 adapter board incorporates an AMS1117-3.3 voltage regulator with

1 A capacity, accepting 5–12 V input and providing stable 3.3 V output. This ensures reliable operation during high-current RF transmission events (Shahrul *et al*., 2021)

Communication protocol. The Arduino communicates with the ESP8266 via AT commands over SoftwareSerial at 115200 baud. The command set includes:

- AT — Module responsiveness test
- AT+CWMODE=1 ; Set station mode (Wi-Fi client)
- AT+CWJAP="SSID","PASSWORD" ; Connect to access point
- AT+CIPSTART="TCP","host",port ; Establish TCP connection
- AT+CIPSEND=length ; Initiate data transmission
- AT+CIPCLOSE ; Close connection

3.4 Hardware Architecture and Circuit Implementation

3.4.1 System Architecture and Block diagram

The implementation process started with a painstaking search and selection of reliable electronics components with which to achieve the aim of the research. The construction entailed interfacing Garmin's LiDAR-lite v3hp sensor, an ESP8266 WIFI module with an Arduino Uno microcontroller. The components were selected to meet the requirements of Institute of Electrical and Electronics Engineering (IEEE) and World Health Organization. The cost of components ensured that the monitoring device was eventually much cheaper than existing commercial alternatives

The initial prototype was implemented on a breadboard. The block diagram of the design is shown in Figure 3.1

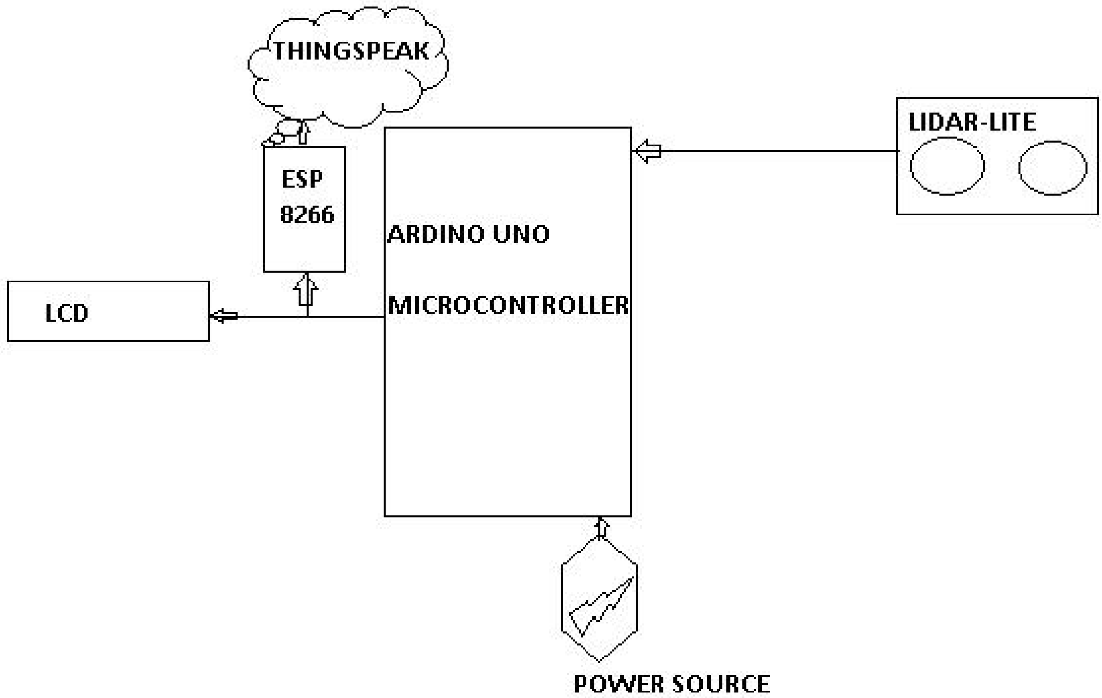

Figure 3.1: Block diagram of the prototype

The system consisted of an Arduino Uno microcontroller, a LiDAR-lite v3hp sensor by Garmin, an ESP 8266 WIFI module (with adapter), a 10K potentiometer, 1000uF capacitor and a power bank as power source. The device can be powered from the USB or barrel jack.When powered, it takes about 30 second for the system to initialize and output its first reading on the LCD. This reading is also uploaded unto the ThingSpeak channel in near real-time. Table 3.6 shows the bill of material for the device.

Table 3.6: Bill of material for the device.

S/N	COMPONENT	PRICE (Naira)
1.	Arduino Uno Microcontroller	8,500
2.	Lidar-lite v3hp	260,000
3.	ESP8266 (with Adapter)	4,000
4.	Casing	4,000
5.	Vero Board	500
6.	16 X 2 Liquid crystal display	3000
7.	1000uF capacitor	450
8.	1k resistor	150
9.	Connecting wires and soldering lead	700
10.	10k Potentiometer	200
	TOTAL	281,500

3.4.2 Circuit Schematic and Wiring Protocol

The circuit diagram was sketched using Fritzing app. Figure 3.2 shows the circuit diagram of the constructed prototype.

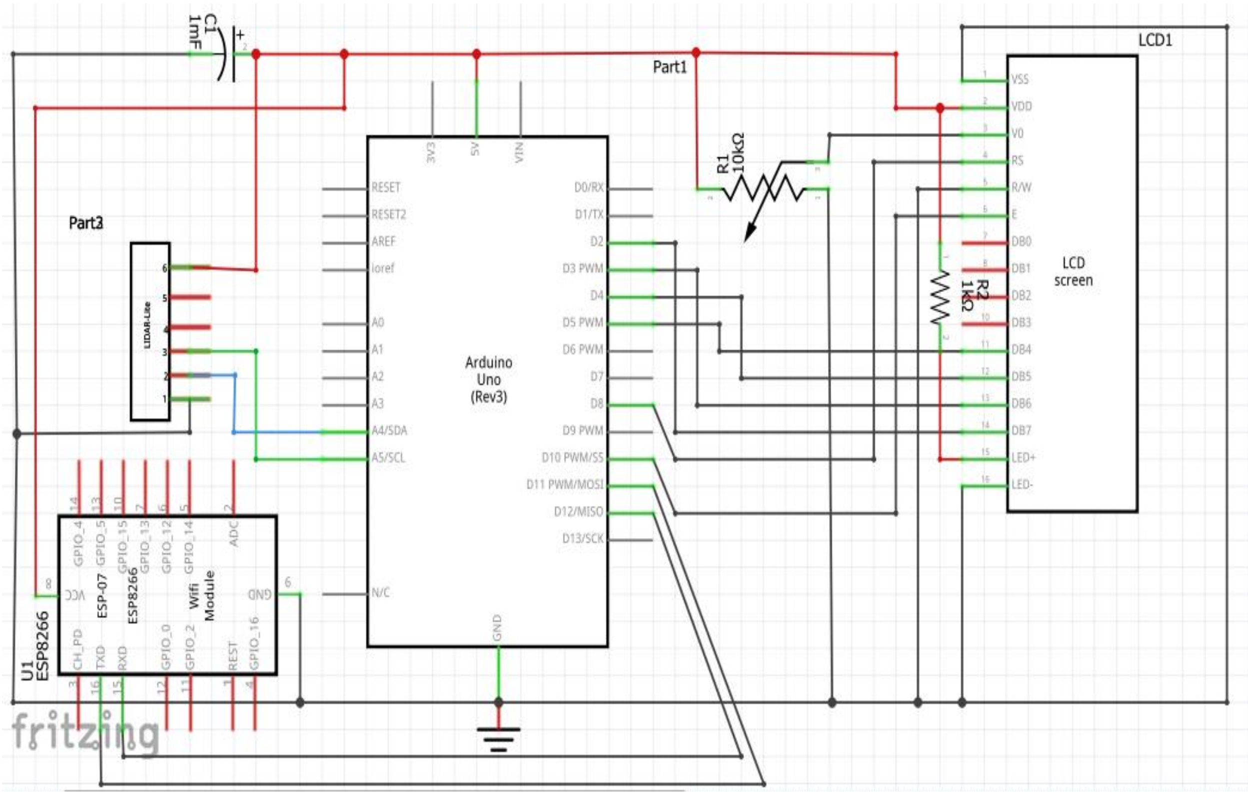

Figure 3.2 Circuit diagram of the prototype

3.4.2.1 Lidar-Lite v3HP to Arduino Uno (I²C Interface)

1. Using a male- male connector, connect the 5V pin in the Arduino to the positive voltage line (positive terminal) on the breadboard.

2. Connect the ground pin on the Arduino to the negative voltage line (negative terminal) on the breadboard.

3. On the breadboard, connect the positive terminal to column a on row 1; and the negative terminal to column a on row 5.

4. The LiDAR's Serial Clock Line (SCL) wire (green wire) is connected to the SCL pin(A5) on the Arduino. The LiDAR's Serial Data Line (SDA) wire (blue wire) is connected to the SDA pin (A4) on the Arduino board.
5. The positive voltage wire of the LiDAR (red wire) is connected to the 5V terminal of the Arduino, while the ground wire of the LiDAR (black wire) is connected to the ground of the Uno. It is recommended that an electrolytic capacitor (680 µF/1000 µF) is connected across the power and ground wire of the LiDAR-lite v3hp sensor. The role of the capacitor is to normalize fluctuations in voltage that arise from voltage drops due to current surges during the operation of the LiDAR sensor (Garmin, 2018).

The connection between the v3hp and the uno is summarized in Table 3.6:

Table 3.7: Connection for LiDAR-lite v3hp with Arduino uno

Lidar Wire	Color	Arduino Pin	Function
Power	Red	5 V	VCC (4.75–5.5 V)
Ground	Black	GND	Ground reference
SDA	Blue	A4	I²C data line

I²C pull-up resistors. The Lidar-Lite v3HP includes internal 1.8 kΩ pull-up resistors on SDA and SCL lines. External pull-ups are unnecessary and would create excessive current draw if the bus voltage exceeds the Lidar's internal logic level (3.3 V). The Arduino Uno's I²C pins (A4, A5) operate at 5 V, but the Lidar's 1.8 kΩ pull-ups limit current to safe levels (~1.4 mA) for the 3.3 V-tolerant I²C interface (Garmin, 2018).

3.4.2.2 ESP8266 ESP-01 to Arduino Uno (UART Interface)

The Esp8266 was socketed unto the esp-01 module. The Vcc and ground terminals of the module was connected to the +5v supply from the Arduino and ground respectively. It should be noted that although the Esp8266 requires 3.3V, this cannot be reliably provided by the 3.3v pin on the Arduino board. However, the voltage regulator present on the Adapter is able to provide the required 3.3v from the 5v supply it receives. The Tx and Rx of the adapter are connected to pin 11 and 12 of the Arduino. Table 3.7 gives a summary of the connection between the WiFi module and the Uno.

Table 3.8: Connection between ESP8266 and Arduino uno

ESP-01 Pin	Adapter Pin	Arduino Pin	Function
VCC	3.3 V (regulated)	—	3.3 V power supply
GND	GND	GND	Ground reference
TX	TX	11 (RX)	ESP transmit → Arduino receive
RX	RX	12 (TX)	ESP receive ← Arduino transmit
CH_PD	VCC (pulled high)	—	Chip enable
RST	VCC (pulled high)	—	Reset (inactive)

Voltage level shifting. The Arduino's 12 (TX) outputs 5 V logic HIGH, while the ESP8266's RX pin accepts maximum 3.6 V. A resistive voltage divider (1 kΩ series, 2 kΩ to GND) reduces 5 V to 3.3 V at the ESP RX pin:

$$V_X = 5 \times \frac{2}{1+2} = 3.3$$

Where V_X is the voltage at the WiFi module's RX pin.

The ESP's TX pin (3.3 V logic HIGH) is directly compatible with Arduino's 5 V-tolerant input threshold ($V_{IH(min)} = 3.0V$), so no level shifting is required in this direction. Where ($V_{IH(min)}$ is the minimum input voltage the Arduino digital pin needs to read "high" or "1".

3.4.2.3 16×2 LCD to Arduino Uno (4-Bit Parallel Interface)

1. VSS of LCD is connected to ground of Arduino
2. VDD of LCD is connected to +5v pin of Arduino)
3. VO of LCD is connected is connected to potentiometer center pin. The other les of the potentiometer are connected to the +5V power rail and ground (both from Uno) respectively.
4. RS of LCD is connected to Arduino's digital pin 8
5. RW of LCD is connected to Arduino's GND
6. E (enable) of LCD is connected to Arduino's digital pin 2
7. D4 of LCD is connected to Arduino's digital pin 5
8. D5 of LCD is connected to Arduino's digital pin 4
9. D6 of LCD Arduino's digital pin 3
10. D7 of LCD Arduino's digital pin 2
11. The A+ pin of LCD is connected through a 1k resistor to positive power rail (basically +5v supplied from Arduino)
12. The K- pin of the LCD is connected to the ground of the Arduino

Note that the connection to A+ and K- is for backlight display. A tabular description of this connection is presented in Table 3.7:

Table 3.9: Connection summary for LCD to Uno

LCD Pin	Symbol	Arduino Pin	Connection Detail
1	VSS	GND	Ground
2	VDD	5 V	Power supply
3	V0	Potentiometer wiper	Contrast adjustment (0–5 V)
4	RS	D8	Register select: 0=command, 1=data
5	R/W	GND	Write-only mode (tied low)
6	E	D10	Enable strobe (HIGH→LOW latches data)
7–10	D0–D3	—	Unused in 4-bit mode
11	D4	D5	Data bit 4 (MSB of nibble)
12	D5	D4	Data bit 5
13	D6	D3	Data bit 6
14	D7	D2	Data bit 7 (LSB of nibble; also busy

			flag)
15	A (LED+)	5 V via 220 Ω	Backlight anode
16	K (LED−)	GND	Backlight cathode

3.4.3 Physical Implementation

Prototype phase. Initial circuit assembly employed a solderless breadboard for rapid iteration and debugging. This phase verified:

i. correct I²C communication with Lidar;

ii. stable ESP8266 Wi-Fi connection;

iii. LCD functionality; and

iv. power supply adequacy.

Production phase. The verified circuit was transferred to a 7×9 cm veroboard (stripboard) with copper tracks cut using a track cutter at component junctions. Soldered connections replaced jumper wires to improve mechanical reliability. The veroboard assembly was housed in a 10×6×4 cm ABS plastic enclosure.

3.5.2 Software Architecture

The Arduino Integrated Development (IDE) software was downloaded from www.arduino.cc , a ThingSpeak account was registered on www.thingspeak.mathworks.com . The account had a single channel and was configured for public viewing. On the channel, real-time groundwater levels could be observed by anyone with the web link. The complete software code for this work can be found in the Appendix A. Figure 3.3 is a flow chart of the operational software code for the implemented device.

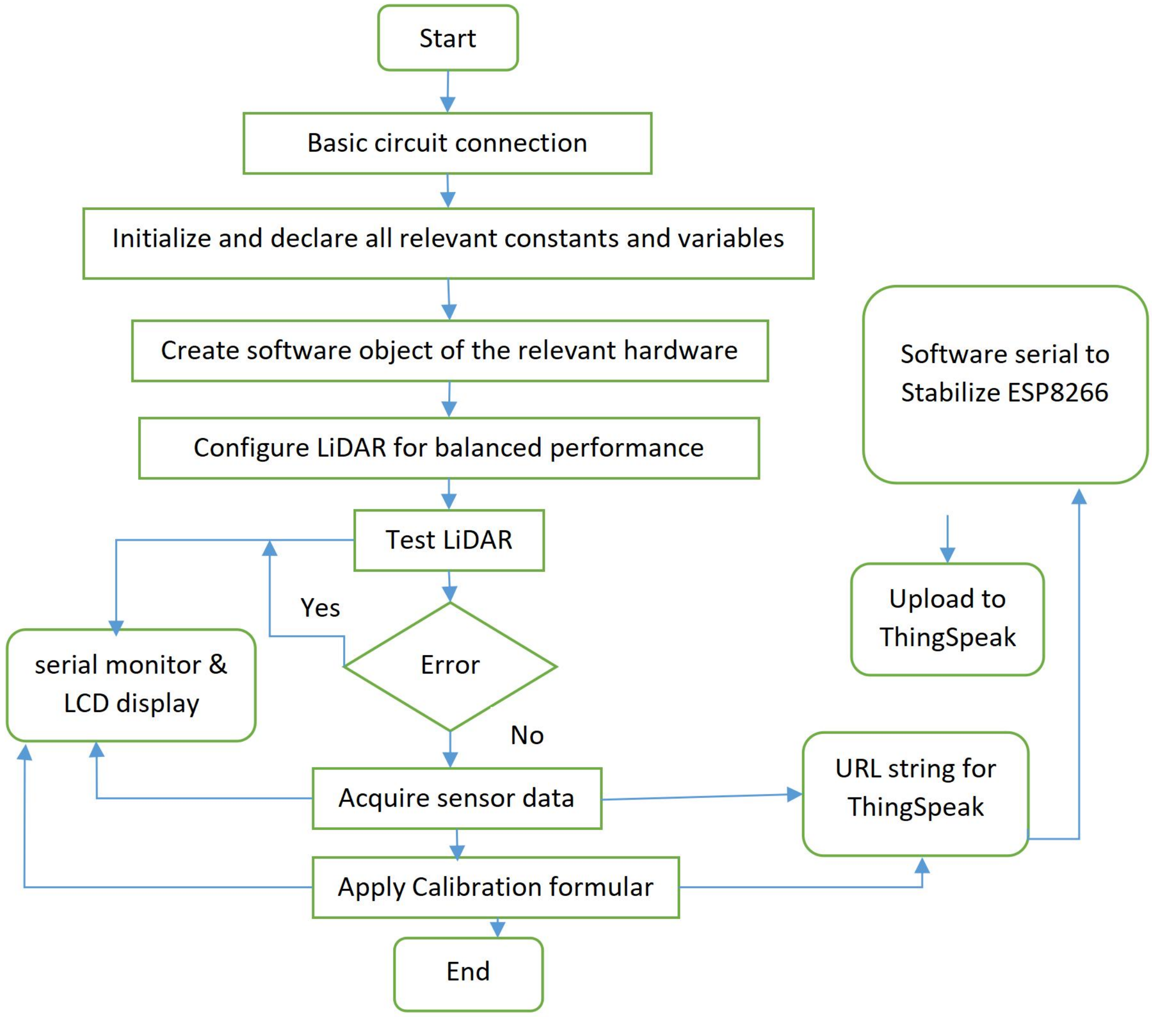

Figure 3.3: Flow chart for programming code of the devices

A summary of the operational flow is :

START - CONNECT - LOOP - REPEAT

Starting the device initializes the Arduino uno, The Lidar, the LCD, the wifi module . The connecting phase ensures the device joins an available wifi network. In the looping phase, Lidar measurement is triggered, Correction is applied ,Serial monitor and LCD are updated, HTTP GET request is initiated, measurement is uploaded on ThingSpeak and the Loop is repeated.

3.5.3.2 Telemetry Protocol

The HTTP GET request conforms to ThingSpeak API specification, the line of code is written as shown:

```
GET/update?api_key=<WRITE_API_KEY>&field1=<RAW_VALUE>&field2=<CORREC
TED_VALUE> HTTP/1.1
Host: api.thingspeak.com
Connection: close
```

This section of the code appends and displays the raw and corrected LiDAR measurement to the field1 and field2 columns on the ThingSpeak platform. The free tier permits maximum 1 update per 15 seconds. The firmware enforces this via delay(15000) after successful transmission. Attempted faster updates return HTTP 429 (Too Many Requests) and are logged as failed uploads.

Error handling. The sendCommand() function implements timeout and retry logic:

- Maximum response wait: maxTime × 100 ms iterations
- Expected response string: "OK" for AT commands, ">" for CIPSEND prompt
- Failure action: Log to serial monitor, display "Upload Failed" on LCD, continue operation.

3.6 Calibration Protocol

Calibration transforms the sensor output from "raw measurement" to "corrected measurement" traceable to a reference standard (steel measuring tape).

3.6.2 Reference Standard

Instrument: steel measuring tape, 10 m length, metric graduation

- **Resolution:** 1 mm

- **Reading procedure:** Lower a graduated steel tape to water surface; read at air-water meniscus; repeat 3 times; record mean

3.6.3 Calibration Procedure

The LiDAR-based groundwater level monitoring system was calibrated to ensure that distance values obtained from the LiDAR-lite v3hp was as close as possible to the values obtained from manual measurements from the observation well. The Calibration process involved a zero-point (offset) calibration and a span check for linearity across various ranges within the measurement range stated in the operational manual. For the zero-point calibration, the sensor was mounted in a fixed position above the well opening and a manual reference distance from the sensor to the water surface was obtained using a calibrated tape. The difference between the LiDAR reading and the reference measurement was computed and recorded. This offset bias was subsequently reduced by appropriately incorporating it in the software code as a constant offset (Garmin, 2018). For span linearity calibration, measurements were repeated at multiple water levels; the variation in groundwater levels were achieved through controlled evacuations or natural fluctuations. This span test was carried out to verify if the offset was linear for different groundwater level within the range limit of the sensor. Regression technique was carried out using Microsoft Excel to obtain a slope and intercept that were then applied as a correction or scaling factor by Equation (3.2) (Christakis *et al*.,2024) to improve the accuracy of the implemented device.

$$R_{corrected} = \frac{(R_{raw} - a)}{b} \qquad (3.2)$$

Where $R_{corrected}$, R_{raw}, a and b are the corrected LiDAR measurement, LiDAR measurement before applying correction, offset bias and a scaling factor representing the reciprocal of the slope respectively (Christakis *et al*.,2024). The calibration procedure is summarized below:

The tape is carefully lowered from the well head to the surface of the water and the depth to water surface is noted as D_{tape}.

The LiDAR unit was fastened to a plastic pipe which was securely positioned across the well head with the face of the sensor vertically facing down at the water surface.

The device was powered by the power bank and LiDAR readings ($L_{lidar\ i}$, i= 1,2,3….n) were obtained for about 30 mins.

The average LiDAR reading was then computed as $\bar{L}_{LiDAR}$ compared to the manual tape measurement D_{tape}. The offset bias was computed as the difference between the manual tape measurement and the average LiDAR reading.

Step 1: Zero-point offset determination

- Securely place Lidar at top of wellhead (measured with tape)
- Lower tape from sensor to water surface; record the average of three measurements depth as D_{tape}
- Power device and take consecutive Lidar readings ($L_{lidar,i}$,.. i=1,2,3…).
- Compute average LiDAR reading as $\bar{L}_{LiDAR}$
- Compute offset bias: offset bias = mean D_{tape} - $\bar{L}_{LiDAR}$

Step 2: Span linearity verification

- Vary water level via controlled pumping (evacuation) or wait for natural fluctuation
- At each of measured depth levels (five initially),record tape measurement and average LiDAR readings
- verify and confirmed that offset bias roughly increased with increased depth

Step 3: Regression and correction factor derivation

Plot the correlation graph of the LiDAR values versus tape measurement to determine the Linear fit model. From the trendline equation on the correlation plot of tape measurement vs average LiDAR readings the offset a and the reciprocal of the slope b were obtained as 12.40 and 1.01.

- a and b were then applied to the correction formula used in Christakis *et al.*,(2024).Thus corrected LiDAR reading was derived as $R_{corrected} = (R_{raw} - a) / b$

  The part of the software code used to achieve this s given below:

```
const float OFFSET = -12.40;    // Intercept bias [cm]
const float SLOPE = 1.01;       // Reciprocal of regression slope [dimensionless]
// Measurement acquisition
float acquireDistance() {
   uint16_t distance_raw = lidar.distance();  // I²C read, returns cm
   if (distance_raw == 1) {                  // Sensor error code
      return ERROR_CODE;                     // Flag invalid measurement
   }
   float distance_corrected = (distance_raw - OFFSET) / SLOPE;
   return distance_corrected;
```

Step 4: Validation

- Apply correction to code to adjust subsequent LiDAR measurements.
- Compute validation metrics: RMSE, bias, precision (CV)

Details of correction factors applied:

Well	Offset (cm)	Scaling Factor (1/b)	Formula
1	−12.40	1.01	$R_{corr} = (R_{raw} + 12.40) / 1.01$
2	−12.40	1.01	$R_{corr} = (R_{raw} + 12.40) / 1.0$

Note: Unified correction factor derived for well 1 was applied to Well 2 to confirm transferability.

3.7 Field Deployment and Measurement Acquisition

3.7.1 Study Site Characterization

Study location is Oghara, Ethiope West Local Government Area of Delta State, Nigeria falls within the Niger Delta Basin. Oghara is located within Longitudes 005° 39' 18" E - 005° 39' 25" E, Latitudes 5° 56' 38" N - 5° 56' 45" N and elevation of 87 - 90 m. (Igben and Eregare, 2022)

Table 3.10: Well Characteristics and depths investigated

Well	Characteristics	Depth Range Tested	Dimension
Well 1	Hand-dug artesian, unconfined aquifer	167.4–583.2 cm	Diameter- 80cm Depth - 10 m
Well 2	Hand-dug artesian, unconfined aquifer	193.6–739.2 cm	Diameter- 82cm Depth - 12 m

3.7.2 Deployment Protocol

Pre-deployment:

The following preliminary steps were carried out before installing the device on site;

1. Verify sensor functionality by measuring target at known distances
2. Confirm Wi-Fi connectivity at wellhead
3. Adjust LCD contrast for ambient lighting conditions

Installation:

The installation process involved the following :

1. Secure mounting arrangement at the wellhead to position the sensor
2. Ensure sensor optical axis vertically aligned
3. Measure and record sensor-to-wellhead distance (H) with tape, if setup does not ensure that sensor is placed to measure from wellhead position.
4. Connect power bank; verify system initialization (LCD displays "Init WiFi...")
5. Confirm first successful upload to ThingSpeak (verify timestamp and values)

Measurement sequence:

Measurements were obtained on intermittently spanning October 2024 to February 2026 across the two wells. The procedure adopted is outlined below;

1. Obtaining manual tape measurement by lowering tape to water surface and noting the reading D_{tape}
2. Record device readings: extract last N uploaded values from ThingSpeak
3. Repeat at varying depths (variation obtained by natural fluctuation and controlled evacuation)

3.8 Statistical Validation Framework

3.8.1 Statistical Methods

Descriptive statistics: Mean and standard deviation: the mean and standard deviation for each depth range was computed. Computation of bias: bias = D_{tape} - mean(L_{lidar})

Accuracy metrics: The Root mean square error (RMSE), is a performance metric that quantified the average error between Lidar and tape measurement, $RMSE = \sqrt{\left(mean(L_{Tape} - \bar{L}_{lidar})^2\right)}$. It is an accuracy metric.

Precision metrics: The Coefficient of variation(CV) measured of the strength of the linear relationship between the tape measurement and the mean LiDAR readings: $CV = \frac{SD}{mean} \times 100$, where SD is the standard deviation.

Agreement analysis (Bland-Altman):

The Bland Altman plot measured the limit of agreement between the two methods-tape and LiDAR measurement. $upper\ limit\ of\ agreement = Bias + 1.96std$; $lower\ limit\ of\ agreement = Bias - 1.96std$. Where bias is equivalent to the mean difference between the $L_{Tape}$and $\bar{L}_{lidar}$. The bias also quantified accuracy. std is the standard deviation of differences.

The difference between the upper and lower limit of agreement represents the 95% limits of agreement, ie the interval in which 95% of the data existed. This interval quantified precision.

Correlation analysis:

The raw and corrected LiDAR readings were plotted against the manual tape measurement. In addition to the strong linear relation that was established between the LiDAR and tape readings, the intercept in both the pre and post correction readings gave an indication of the bias that existed and how much the correction impacted on it.

3.8.2 Validation Dataset

The dataset was obtained from a total of 21 depth point with a combines total reading of about 630. The monitored depth ranged from 167.4 – 583.2cm for well 1 and 193.6 – 739.2cm for well 2.

Well	Depth Points	Readings per Point	Total Readings	Depth Range (cm)

1	10	30	300	167.4–583.2
2	11	30	330	193.6–739.2
Total	**21**	—	**630**	**167.4–739.2**

3.9 Scope Boundaries and Limitations

3.9.1 Explicit Inclusions

The implementation was carried out first on a breadboard. after preliminary tests that he device as working well it was transferred to a veroboard where the components were soldered on the board as dictated by the circuit diagram. The device was designed to communicate via WiFi only. Power was supplied to the device by an external 20,000 mAH power bank. The prototype was deployed in two artesian wells located in Oghara Delta state which has a relatively shallow aquifer. Readings obtained from the device was compared against manual tape measurement. The test spanned several days on the two wells observing natural and induced variations.

3.9.2 Explicit Exclusions

Printed circuit board (PCB) was not implemented, as the work was a proof of concept. Building and autonomous power unit for the system was not considered as focus was on measurement for validation. Future work could incorporate a solar based power supply. Gsm communication was not employed as Wi-Fi was chosen to demonstrate that low-cost IoT telemetry is achievable, with the recognition that operational deployment requires communication redundancy. Just one device was validated in two well and not a multi-well network which is the expected scenario in a regional monitoring scheme.

CHAPTER FOUR

RESULTS AND DISCUSSION

4.1 Introduction

This chapter discusses the results realized in this project. The implementation of this work was based on the Aim and Objectives stated earlier in Chapter One of this thesis, which was basically the construction and implementation of a home-grown LiDAR-based real-time remote monitoring groundwater level monitoring device capable of capturing short-term variations in groundwater level and reporting same in real-time on the ThingSpeak internet of things- IoT platform to be viewed by stakeholders.

This thesis, conceptualized since 2021, appears to be an extension of the works of Dementria *et al*., (2023) which we became aware of only in 2025. A significant difference of this study from that of the 2023 work is that this present study utilizes an ESP8266 Wi-Fi module instead of a SIM800C GSM/GPRS module used by Demetria and his team. Another difference is that the current effort deployed and tested the device on a real monitoring well instead of the PVC based simulated enclosure previously used. Lastly, the programming code used in this research was independently put together for our specific design that incorporated further calibration suggested by Demetria and his team to improve the accuracy.

4.2 Discussion of Results

The results of the project are discussed according to the different aspects of the work under the following sub-headings:

4.2.1 The Groundwater Level Monitoring Device

The groundwater level monitoring device was implemented to frequently measure depth to water surface from the point of installation at the top of an observation well. These readings are displayed on a screen- a 16 x 2 LCD integrated on the device, and also uploaded to the

ThingSpeak platform thereby ensuring remote access to the measured readings through an ESP8266 Wi-Fi module enabled telemetry system. The ESP8266 gives the Arduino Uno microcontroller the ability to connect to the internet to access, and visualize groundwater level data in such IoT platforms as ThingSpeak. Measured values took about 33 seconds to be uploaded unto the platform with a success rate of about 75%. The upload rate is strongly dependent on the reliability of the available network. The frequency of measurements could be reconfigured to cover longer time span, however it cannot be made lower than 15 seconds due to the inherent latency involved in measuring, processing and uploading the data on a free ThingSpeak account (Viegas *et al*., 2021). The stored measured data can be downloaded as a csv, jason or xml files from the cloud and are timestamped. A snapshot of the implemented device in breadboard and encased vero board is shown in Plate 4.1 and 4.2 respectively:

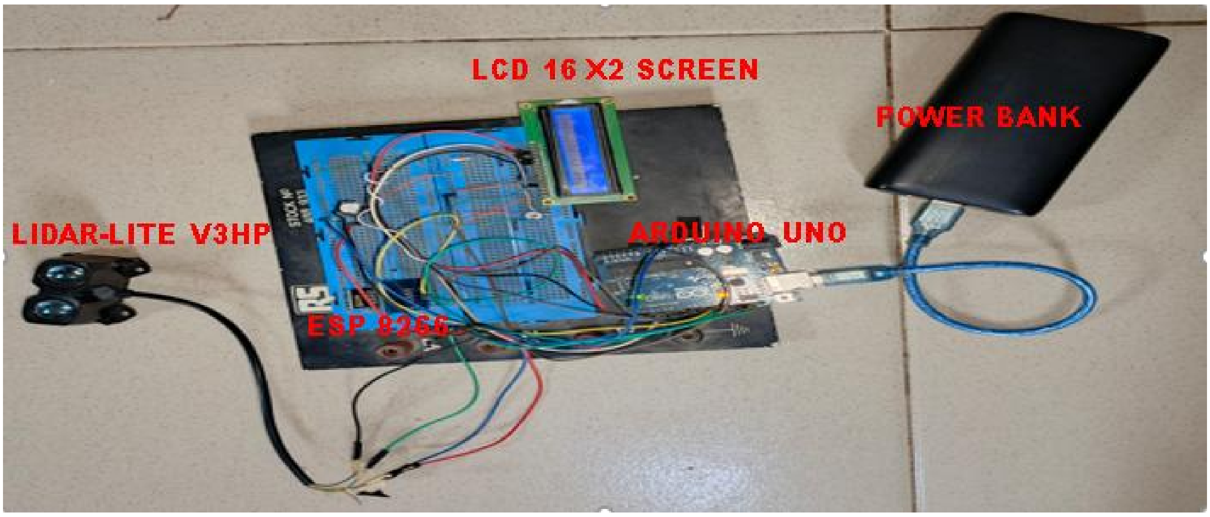

Plate 4.1: Implemented prototype in breadboard.

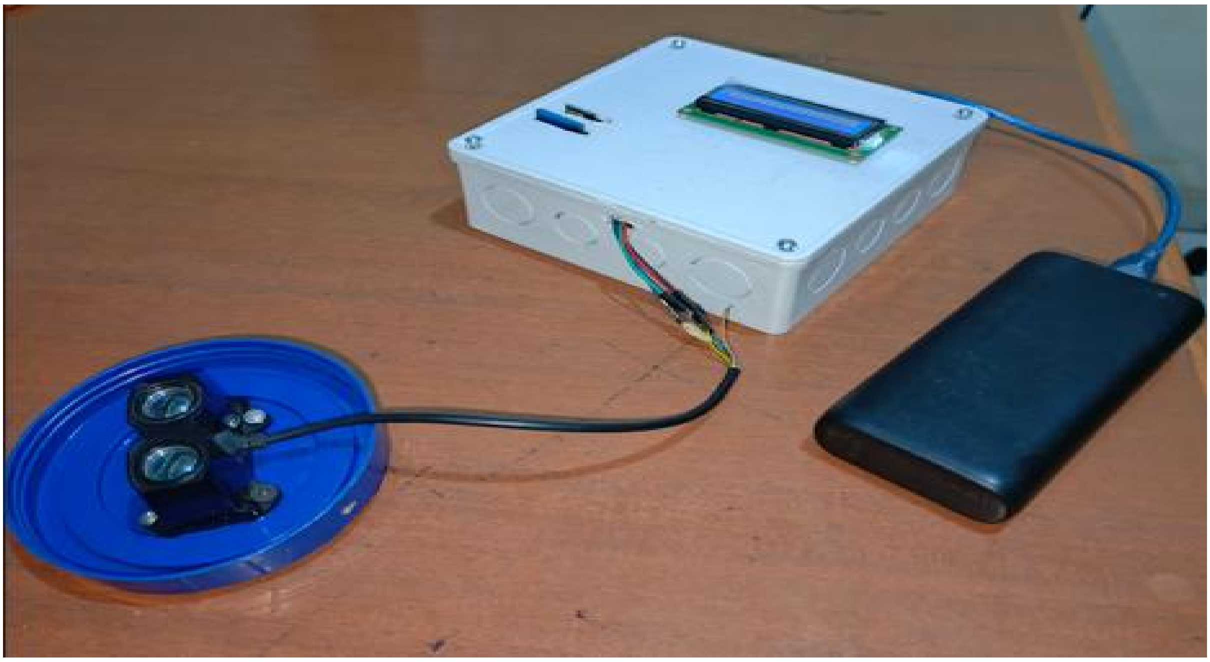

Plate 4.2: Prototype Implemented on vero board and encased.

4.2.2 Tabulated Results

Time stamped readings were obtained from the constructed device and from manual measurements at different times from two artesian wells in Oghara Delta state, spanning distances of up to 583cm and 739cm for well1 and well 2 respectively. Four of the Tables are shown in Table 4.1 to 4.4. It should be noted that the range of measurement observed in the work is within the 1m to 40m operational range of the LiDAR-Lite v3hp sensor (Garmin, 2018). The variation in groundwater levels were achieved through controlled evacuations/replenishing and natural fluctuations.

Table 4.1 LiDAR readings recorded for a tape measurement of 481 cm (well 1)

created_at	entry_id	RAW LIDAR MEASUREMENT (cm)	CORRECTED LIDAR MEASUREMENT (cm)
2025-01-28T07:10:10+01:00	495	471	478.67
2025-01-28T07:10:32+01:00	496	480	487.58
2025-01-28T07:11:19+01:00	497	474	481.64
2025-01-28T07:11:36+01:00	498	472	479.66
2025-01-28T07:12:11+01:00	499	473	480.65
2025-01-28T07:13:40+01:00	500	473	480.65
2025-01-28T07:14:14+01:00	501	471	478.67
2025-01-28T07:15:37+01:00	502	473	480.65
2025-01-28T07:16:56+01:00	503	473	480.65
…..	…..	…..	…..
…..	…..	…..	…..
2025-01-28T11:20:57+01:00	537	476	483.62
AVERAGE		**476**	**483.16**
STANDARD DEVIATION		**2.46**	**2.44**
COEFFICIENT OF VARIATION		**0.52 %**	**0.50%**
RMSE		**5.98**	**3.34**
TAPE MEASUREMENT			**481.00**

Table 4.2 : LiDAR readings recorded for a tape measurement of 583.2 cm (well 1)

created_at	entry_id	RAW LIDAR MEASUREMENT (cm)	CORRECTED LIDAR MEASUREMENT (cm)
2025-02-17T11:21:22+01:00	538	576	582.63
2025-02-17T11:22:56+01:00	539	576	582.63
2025-02-17T11:23:22+01:00	540	577	583.62
2025-02-17T11:23:42+01:00	541	578	584.61
2025-02-17T11:24:19+01:00	542	577	583.62
2025-02-17T11:24:55+01:00	543	572	578.67
2025-02-17T11:25:19+01:00	544	576	582.63
2025-02-17T11:25:38+01:00	545	577	583.62
2025-02-17T16:53:37+02:00	546	577	583.62
…..	…..	…..	…..
…..	…..	…..	…..
2025-02-17T17:06:56+02:00	561	561	567.78
AVERAGE		**576.00**	**582.18**
STANDARD DEVIATION		**4.57**	**4.52**
COEFFICIENT OF VARIATION		**0.79 %**	**0.77 %**
RMSE		**8.87**	**4.54**
TAPE MEASUREMENT			**583.20 cm**

Table 4.3: LiDAR readings recorded for a tape measurement of 234.1 cm (well 2)

created_at	entry_id	RAW LIDAR MEASUREMENT (cm)	CORRECTED LIDAR MEASUREMENT (cm)
2026-02-08T15:16:35+00:00	128	216	226.2
2026-02-08T15:16:54+00:00	129	216	226.2
2026-02-08T15:17:13+00:00	130	215	225.21
2026-02-08T15:18:28+00:00	131	216	226.2
2026-02-08T15:18:46+00:00	132	217	227.19
2026-02-08T15:19:03+00:00	133	217	227.19
2026-02-08T15:19:22+00:00	134	217	227.19
2026-02-08T15:19:42+00:00	135	217	227.19
2026-02-08T15:20:00+00:00	136	217	227.19
…..	…..	…..	…..
2026-02-08T17:23:59+00:00	249	227	237.09
2026-02-08T17:24:17+00:00	250	222	232.14
AVERAGE		**222**	**232.19**
STANDARD DEVIATION		**2.28**	**2.25**
COEFFICIENT OF VARIATION		**1.03%**	**0.97 %**
RMSE		**12.25**	**2.94**
TAPE MEASUREMENT			**234.1 cm**

Table 4.4 LiDAR readings recorded for a tape measurement of 739.2 cm (well 2)

created_at	entry_id	RAW LIDAR MEASUREMENT (cm)	CORRECTED LIDAR MEASUREMENT (cm)
2026-02-10T10:28:37+01:00	550	723	728.18
2026-02-10T10:28:56+01:00	551	719	724.22
2026-02-10T10:29:14+01:00	552	725	730.16
2026-02-10T10:29:33+01:00	553	723	728.18
2026-02-10T10:29:52+01:00	554	723	728.18
2026-02-10T10:30:10+01:00	555	727	732.14
2026-02-10T10:30:29+01:00	556	724	729.17
2026-02-10T10:30:47+01:00	557	720	725.21
2026-02-10T10:31:07+01:00	558	723	728.18
2026-02-10T10:32:40+01:00	559	724	729.17
…..	…..	…..	…..
…..	…..	…..	…..
2026-02-10T12:12:55+01:00	661	723	728.18
AVERAGE		**727.46**	**732.60**
STANDARD DEVIATION		**4.00**	**3.96**
COEFFICIENT OF VARIATION		**0.48 %**	**0.47 %**
RMSE		**11.79**	**7.04**
TAPE MEASUREMENT			**739.2 cm**

The complete Tables can be found in Appendix B and C respectively for both wells. It can be observed from the tables displayed that, the standard deviations for the measurements have marginal improvements for the corrected LiDAR measurements. However, further statistical analysis described in the subsections that follow reveal significant improvement for the corrected measurements over the raw LiDAR values when compared with tape measurements.

Plate 4.3 is a screenshot of the LiDAR measurements as displayed on the ThingSpeak dashboard.

Plate 4.3: Screenshot of measurement chart and numeric display on Thingspeak dashboard

In the chart display, Field 1 Chart shows the graph for raw LiDAR measurement data points automatically plotted against time. Clicking or hovering over any of the data points with a mouse will reveal the time-stamped measured value of the particular data point. Field 1 Numeric Display is directly beneath the Field 1 chart; it shows a raw LiDAR reading of 718.00 cm which corresponds to the last data point at the extreme right of Field 1 chart. Similarly, Field 2 chart displays the uploaded corrected LiDAR readings plotted against time.

Consequently, the Field 2 Numeric Display reveals the latest uploaded corrected LiDAR measurement of 723.23 cm, and it represents with the reading of last data point at the extreme right of Field 2 chart.

4.2.3 Correlation Plot and Analysis

The correlation coefficient r, is a measure of the strength of the linear relationship between two variables (Giavarina , 2015; Kalra , 2017). Figure 4.1 shows the correlation graph for the average raw LiDAR measurement plotted against the tape measurement for well 1. The correlation coefficient r, for this plot is computed as 0.99995. It is seen that there is a near perfect (r = 0.9999) linear relationship between the tape and LiDAR readings.

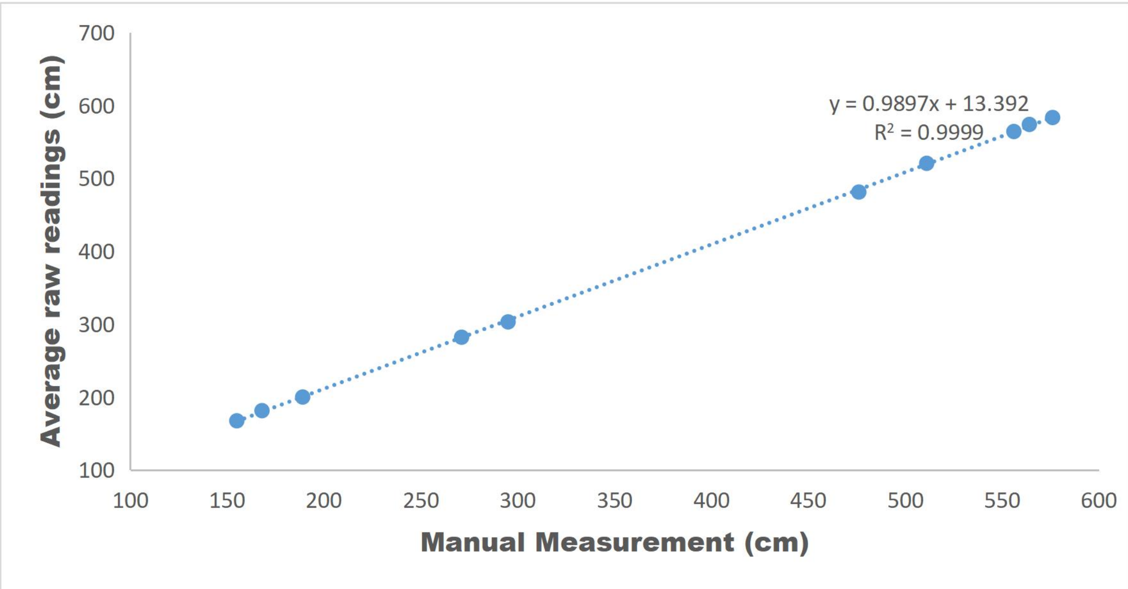

Figure 4.1 Pre- correction correlation plot for well 1

The trendline equation has an intercept of 13.392. The intercept is an indication of the magnitude of the disparity in between the two compared measurements (Chen and Chen, 2022). The Root Mean Square Error (RMSE) when the tape measurement was compared with raw LiDAR readings for well 1 was 10.28 cm.

Likewise, Figure 4.2 shows the correlation graph for the average corrected LiDAR measurement plotted against the tape measurement for well 1. This plot can be seen to have an identical r value with that of Figure 4.1. However, the trend line equation has an intercept of 0.8187. This lower intercept value confirms an improvement in the corrected LiDAR measurement over the raw measurements. The RMSE for comparison between the tape and corrected LiDAR readings for well 1 was 3.91 cm.

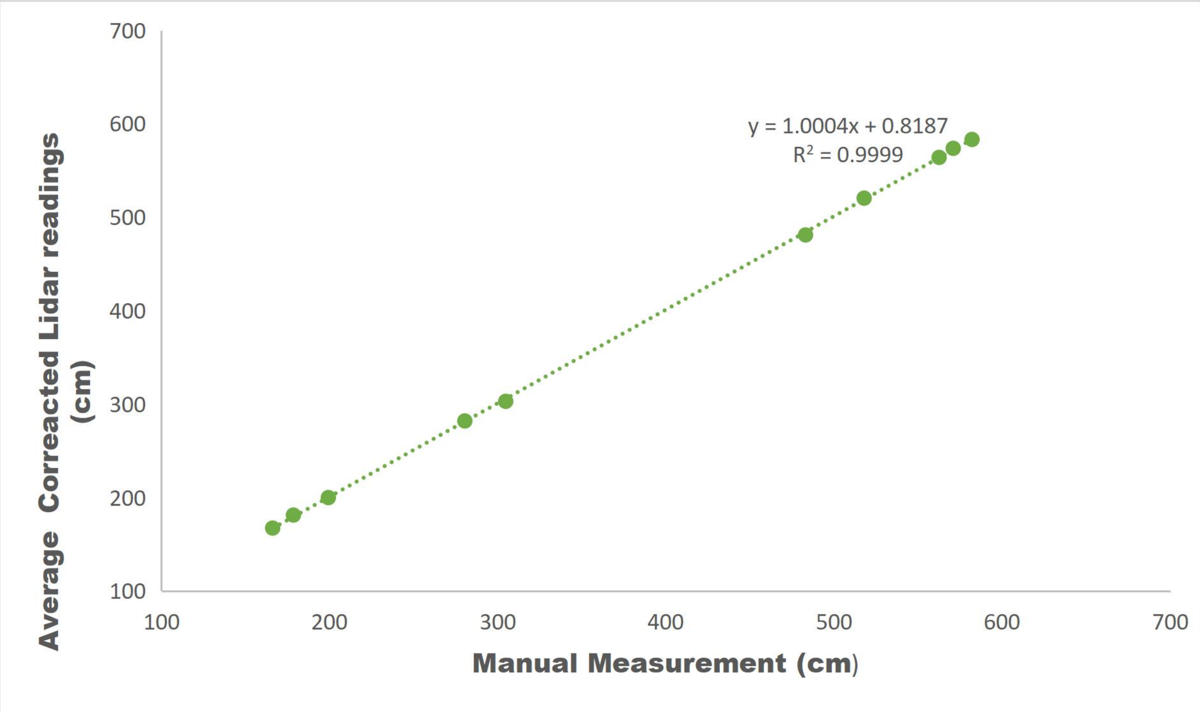

Figure 4.2: Post-correction correlation plot for well 1.

The corresponding plots for well 2 are presented in Figures 4.3 and 4.4. The graph for the average raw LiDAR measurement versus the tape measurement shown in Figure 4.3 reveal that the correlation coefficient was also near perfect when the tape measurements were compared with the raw LiDAR readings. The trendline equation has an intercept of 12.866.

The RMSE for comparison between the tape and raw LiDAR readings for well 2 was computed as 13.91 cm.

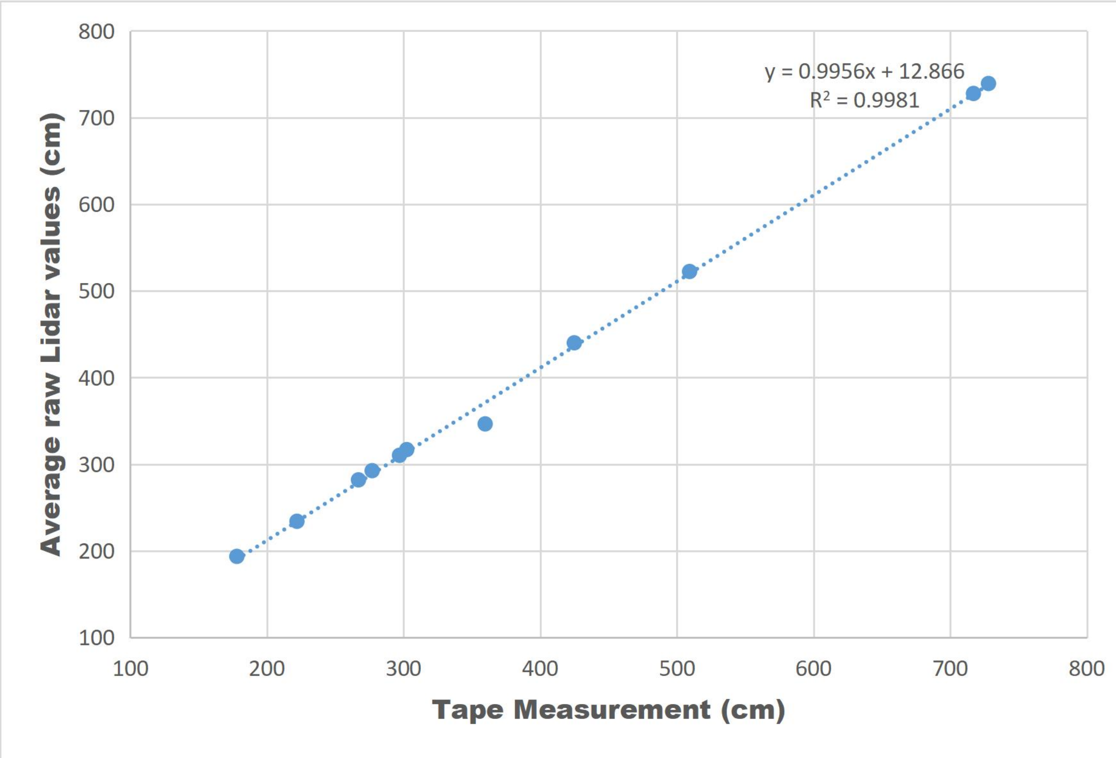

Figure 4.3 Pre- correction correlation plot for well 2.

Similarly, the correlation plot for the average corrected LiDAR measurement versus the tape measurement is displayed in Figure 4.4. This graph also shows an r- value of approximately unity when the corrected LiDAR readings were compared with tape measurements. The trendline equation is seen to have an intercept of 2.3296 which indicates that the corrected LiDAR measurement is a more accurate reading. The RMSE when the tape measurements were compared with corrected LiDAR readings for well 2 was 5.36 cm.

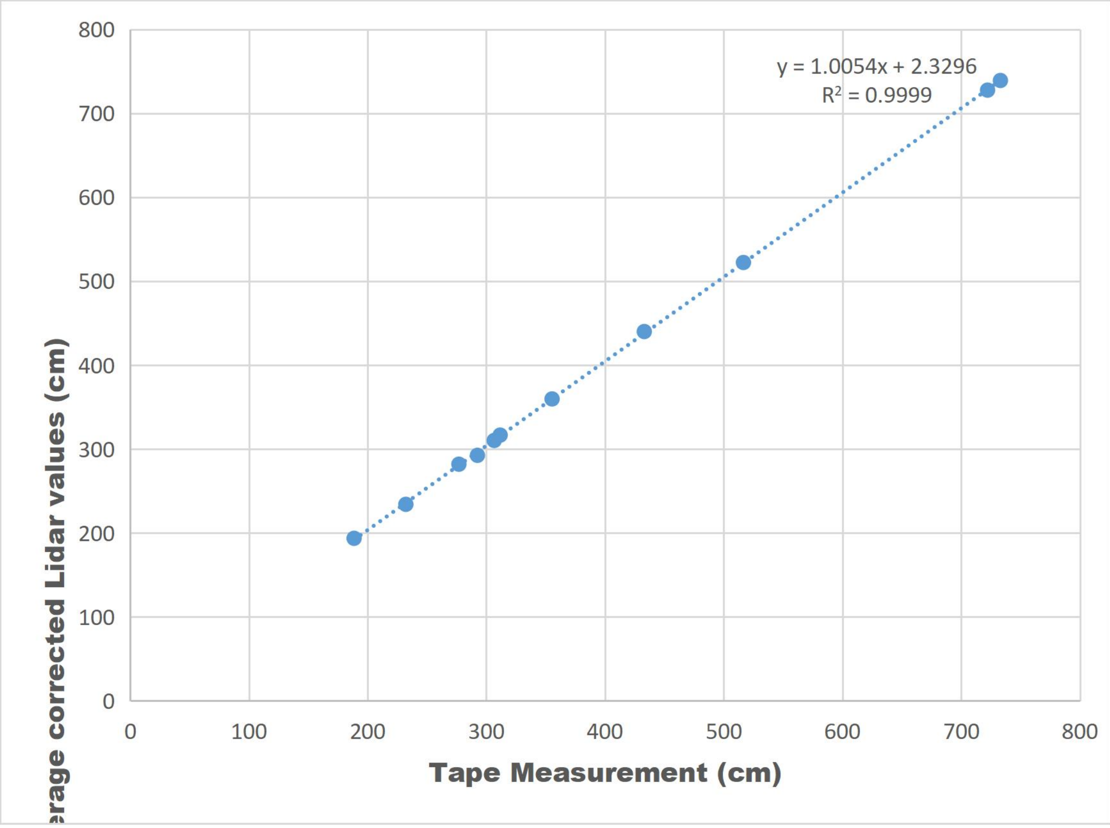

Figure 4.4. Post- correction correlation plot for well 2

The near perfect values for the correlation coefficient for measurements obtained for both wells, confirms that the constructed device is highly sensitive to changes in groundwater level across the observed ranges- linearly varying with the corresponding tape measurements taken at various instances.

The Root Mean Square Error (RMSE) is a performance evaluation metric that quantifies the average error between LiDAR and tape measurement. The value of this metric for comparison between the tape and LiDAR readings for both well1 and well 2 reduced in magnitude by a factor of about 2.6. This confirmed that the magnitude of the error decreased after application of the correction factor.

4.2.4 Bland Altman (BA) Plot and Analysis

The Bland Altman plot is a statistical technique that plots the difference between two measurement methods against their mean; it is an approach that measures the limit of agreement between the two methods using the averages and standard deviations of differences between two measurements (Altman and Bland, 1983). The upper and lower limits of agreement are computed with Equations 4.1 and 4.2 (Altman and Bland, 1983; Giavarina, 2015; Kalra , 2017).

$$upper\ limit\ of\ agreement = Bias + 1.96std \qquad (4.1)$$

$$lower\ limit\ of\ agreement = Bias - 1.96std \qquad (4.2)$$

Where Bias is the mean difference or the average of the differences between the tape and LiDAR measurement and std is the standard deviation of these differences. The bias for well 1obtained with raw LiDAR readings was computed as 9.5. However, the post correction value of the bias for this well was computed as 0.96. This implies that on average, the LiDAR device before the correction was applied, measured 9.5 cm less than the tape measurement for well 1, however this value reduced by an order of magnitude to 0.96cm after the correction was applied. Similarly, for well 2, the bias was computed as 13.50 for raw LiDAR readings while post-correction LiDAR readings have a bias of 4.73. This also implies the device measured on average 13.50cm less than the tape measurement before application of correction factor; however, application of the correction factor reduced this disparity to 4.73 cm. The implication is an almost three-fold reduction in the value by which both measurements compared after correction. This confirms that for measurement obtained from both wells, the correction factor increased overall accuracy. Figure 4.5 shows the Bland Altman plot for the average value of raw LiDAR measurements compared with values obtained from the tape measurements across the various ranges considered for well 1. The limit of agreement is seen to range between 14.45 to 4.55 cm for uncorrected LiDAR measurements.

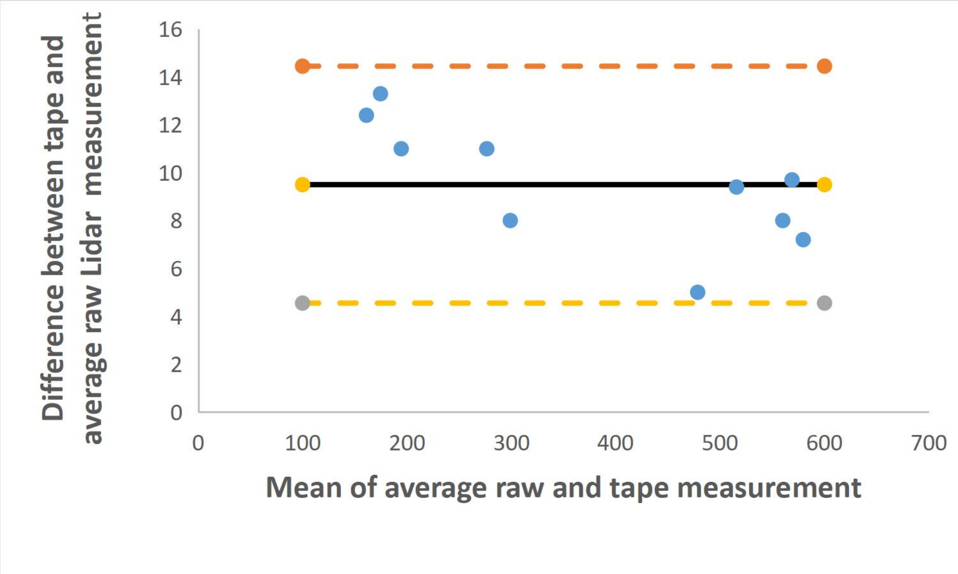

Figure 4.5: Pre-correction Bland Altman plot for measurements taken from well 1

Correspondingly, Figure 4.6 shows the BA plot for the average value of corrected LiDAR measurements compared with values obtained from the tape measurements across the various ranges considered for same well. The limit of agreement is observed to be between 4.32 to -2.40cm.

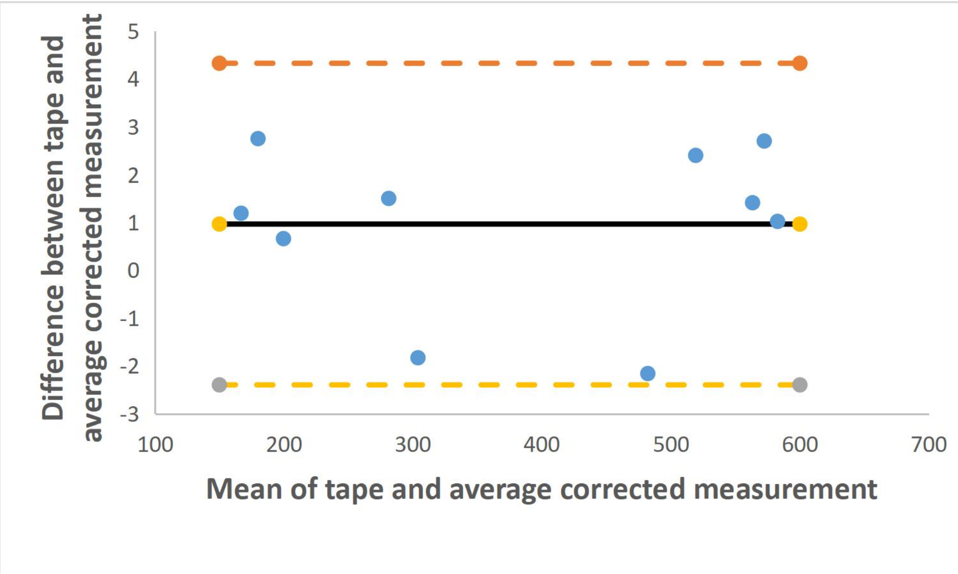

Figure 4.6: Post-correction Bland Altman plot for well 1

Comparing both plots it is obvious that the limit of agreement was narrower in post-correlation plot than that for pre-correlation. This is an indication that the precision of the constructed device increased for corrected LiDAR readings from well 1. Similarly, Figure 4.7 shows the BA plot for the average value of raw LiDAR measurements contrasted with values acquired from the tape measurements across the various ranges considered for well 2. The limit of agreement is observed to between 16.81 to 10.19 cm for uncorrected LiDAR measurements.

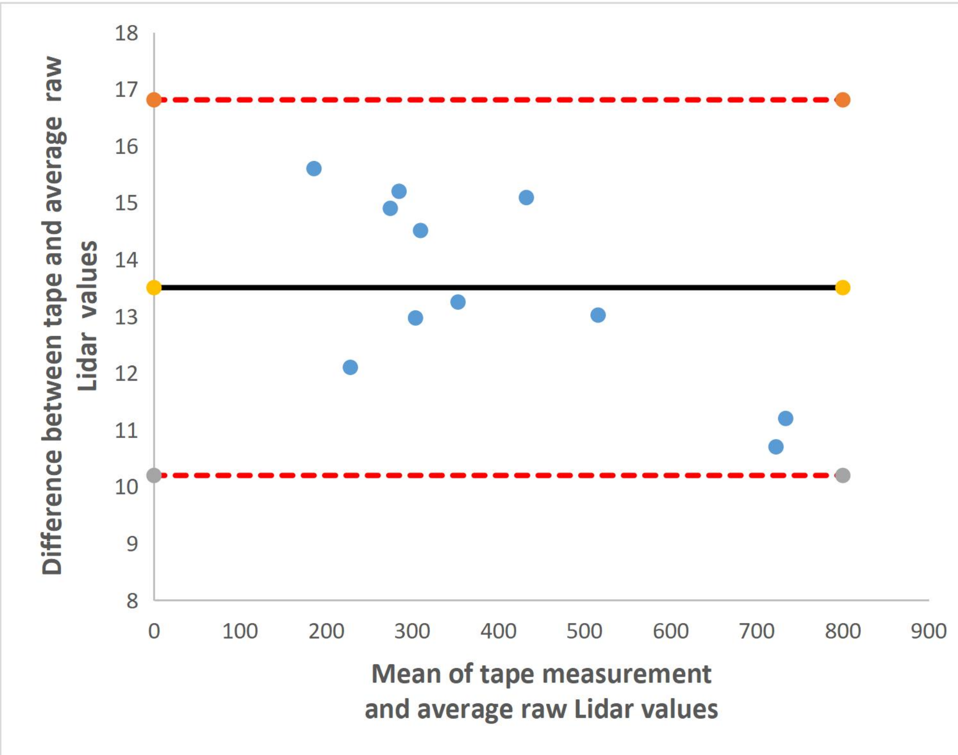

Figure 4.7: Pre-correction Bland Altman plot for well 2

Figure 4.8 presents thee BA plot for the average value of corrected LiDAR measurements contrasted against values obtained from the tape measurements for the same well. The limit of agreement is observed to be between 6.98 and 2.49cm. As was the case with well 1, a comparison of figure 4.7 and figure 4.8 clearly reveal that the limit of agreement was narrower in Figure 4.8 which utilized corrected LiDAR readings, than in Figure 4.7 where raw uncorrected LiDAR values was employed. Again, this is a clear indication that the precision and accuracy of the implemented device improved after corrected for readings from well 2.

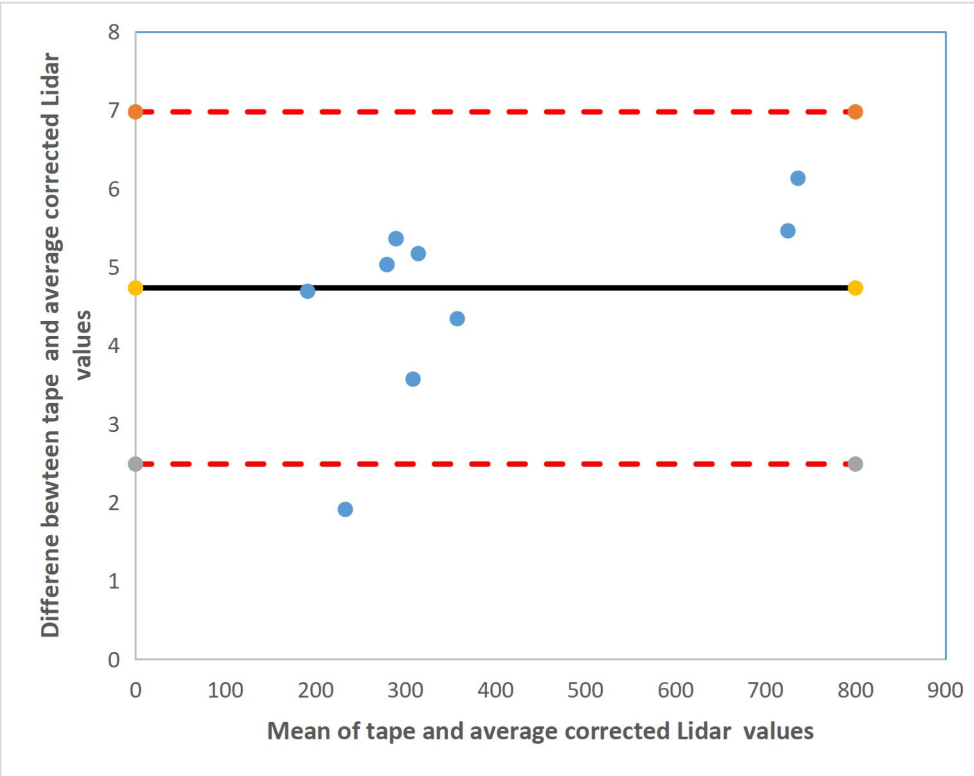

Figure 4.8: Post-correction Bland Altman plot for well 2

The BA graph presented in figure 4.9 and 4.10 is plotted with continuous measurements from the device for a specific single tape reading. This is different from the BA plots in Figure 4.5 - Figure 4.8 where measurements from the device at different groundwater level depths were compared with corresponding tape measurements across the measuring range observed. Plots for other individual measurement for both wells can be found in Appendix E.

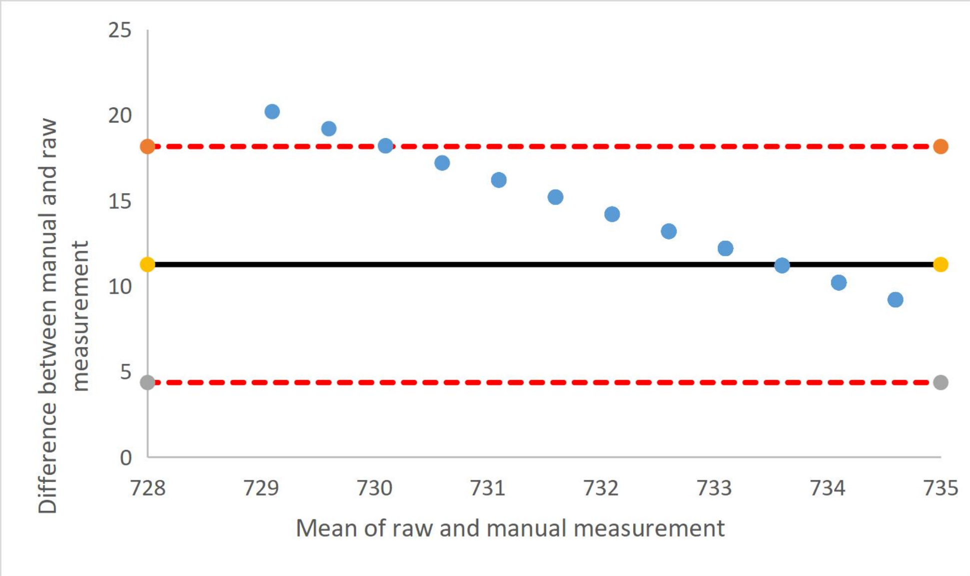

Figure 4.9: Pre-correction Bland Altman plot for individual measurement showing convergence

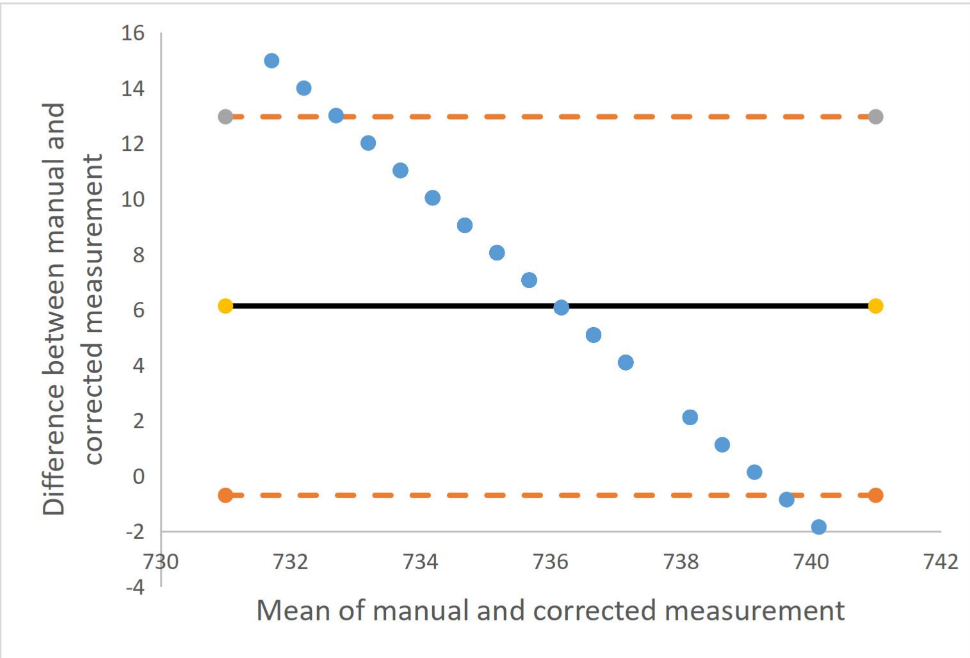

Figure 4.10: Post-correction Bland Altman plot for individual measurement showing convergence towards tape reading

The plots indicate that LiDAR readings converged toward the tape measurement after several measurements. This is consistent with the observation of Dementria *et al.,* (2023) that upon initiating a measurement session, the LiDAR readings were below the actual depth but gradually approached the manual measurement after several successive measurements. However, Dementria and his team suggested further calibration as a solution to reduce observed measurement residuals and improve accuracy

4.2.5 Coefficient of Variation and Analysis

The standard deviation computed from each set of measurement taken from both wells together with the mean was used to determine the coefficient of variation (CV) also known as the relative standard deviation. It is a measure of the variability of measured values from their mean (Santos and Dias, 2021). Pre-corrected and post-corrected values for well 1 was 1.21% and 1.15 %, while these values for well 2 was 0.56 % and 0.54 % respectively. The marginal difference in these values notwithstanding is a confirmation of improvement in accuracy of the constructed device. The small value of the CV is an indication that comparative error in measurements is mainly due to systematic error contribution (Jimenez-Olmedo *et al*, 2024). Some of the possible sources of the systematic error are:

i. The reflectivity properties of water surface within the well

ii. Atmospheric conditions within the well column, particularly relative humidity and temperature gradients

iii. Difference in property of target surface used during factory calibration, from that of well water surface in actual field deployment

Water surface exhibit complex reflective properties that is dependent on angle of incidence and the condition of the surface. Specular reflections are the ideal returns that is envisaged in a LiDAR system. However, if the LiDAR is not properly positioned, the return can completely miss the detector and would not be recorded/registered hence no distance would be computed. Surface rogosity-which defines the roughness of the water surface, can arise from disturbances like wind or gentle breeze. This can result in diffuse reflection which may cause reflected signal to traverse longer paths thereby spending more time and introducing error in computation of distance in the LiDAR.

LiDAR units utilize velocity of laser light in the computation of range of interest. Atmospheric conditions in the well such as relative humidity and temperature gradient can affect the refractive index of air and consequently the propagation velocity of the light; thus variations in these atmospheric properties can introduce systematic errors (Ruttner *et al*., 2025).

The water surface in the well may present different optical properties from that used in during calibration of the instrument in the factory, this can potentially induce a constant systematic offset during field measurement (Behzadian *et al*., 2025).

CHAPTER FIVE

SUMMARY AND CONCLUSION

5.1 Summary

This research was motivated by the critical need to strengthen groundwater monitoring infrastructure in developing regions, particularly Nigeria, where existing networks are sparse, data accessibility is limited, and conventional contact-based sensors suffer from degradation due to corrosion and biofouling. The study set out to design, construct, and validate a low-cost, non-contact, real-time groundwater level monitoring device that leverages advances in laser-based distance sensing and Internet of Things (IoT) connectivity.

The thesis is organized into five chapters. Chapter One established the context for the research, highlighting that groundwater constitutes over 95% of global fresh liquid water and serves as the primary drinking water source for 85% of urban and 75% of rural populations in Nigeria. It identified three core problems: the absence of home-grown monitoring solutions, insufficient temporal resolution in existing programmes (currently limited to 12-hourly measurements by the Nigerian Hydrological Service Agency), and the centralization of data in Abuja, which limits local and regional access. The chapter articulated the aim of constructing a Lidar-based real-time groundwater monitoring system and outlined three specific objectives: integrating a Lidar-lite v3HP sensor with an Arduino Uno microcontroller, implementing Wi-Fi-based data transmission to an IoT platform, and evaluating the accuracy and reliability of the prototype through field validation.

Chapter Two provided a comprehensive literature review, examining both manual and automatic groundwater measurement techniques. Manual methods—including steel tapes, airline submergence, electrical probes, and piezometers—were reviewed alongside automatic techniques such as pressure transducers, ultrasonic sensors, radar systems, and laser-based methods. The theoretical foundations of Lidar reflection were examined in detail, covering specular and diffuse reflection, Lambert's cosine law, Fresnel reflection coefficients, and the Lidar radar equation. A critical survey of related studies revealed that while Lidar-based water level monitoring has shown promise for surface water and flood applications, its deployment for groundwater monitoring in real artesian wells remained underexplored, particularly in the context of low-cost IoT-enabled systems in sub-Saharan Africa.

Chapter Three detailed the materials and methods employed in the research. The hardware implementation involved interfacing a Garmin Lidar-lite v3HP sensor (operating at 905 nm with a 1.3 W peak power and effective range of 1–40 m) with an Arduino Uno Rev 3 microcontroller, an ESP8266 Wi-Fi module with an adapter, and a 16×2 LCD display. The I^2C communication protocol was employed for digital accuracy between the Lidar and Arduino. The software implementation utilized the Arduino IDE for firmware development and the ThingSpeak IoT platform for cloud-based data visualization and remote access. The prototype was initially assembled on a breadboard and subsequently transferred to a Vero board and encased for field deployment. A two-stage calibration procedure was implemented: a zero-point offset calibration to correct systematic bias, followed by a span linearity check using regression analysis to derive a scaling correction factor applied to improve the reliability of the system

Chapter Four presented the results and discussion. The device was deployed on two artesian wells in Oghara, Delta State, Nigeria, with manual tape measurements serving as ground truth. Time-stamped Lidar readings were collected at various depths ranging from 167.4 cm to 739.2 cm across both wells. Statistical validation employed correlation analysis, Bland-Altman plots, and coefficient of variation metrics to compare raw and corrected Lidar measurements against manual tape readings. The results demonstrated that the implemented system successfully transmitted data to the ThingSpeak platform with an average upload latency of approximately 33 seconds, achieving a success rate of about 75% dependent on network reliability.

This chapter now concludes the thesis by synthesizing the principal findings, articulating the contributions to knowledge, and proposing directions for future research.

5.2 Findings

The following findings emerged from the implementation, calibration, and field validation of the Lidar-based ESP8266-enabled real-time groundwater monitoring device:

1. the Lidar-lite v3HP sensor was successfully interfaced with the Arduino Uno microcontroller via the I²C protocol, with both raw and corrected measurements obtained.
2. the device achieved near real-time data upload to the ThingSpeak platform with an average latency of 33 seconds per measurement cycle. The upload success rate was approximately 75%, with failures attributable primarily to network reliability rather than hardware malfunction.
3. raw LiDAR measurements consistently underestimated the actual groundwater depth relative to manual tape measurements. For Well 1, the raw readings exhibited a bias of 9.5 cm, while for Well 2, the bias was 13.50 cm. Application of the two-parameter linear correction factor substantially improved measurement accuracy. The correction reduced the bias from 9.5 cm to 0.96 cm for Well 1 (a nearly tenfold improvement) and from 13.50 cm to 4.73 cm for Well 2 (an approximately 3-fold improvement). The Root Mean Square Error (RMSE) decreased from 10.28 cm to 3.91 cm for Well 1, and from 13.91 cm to 5.36 cm for Well 2.
4. LiDAR based measurement and ground truth manual measurement values are close, having an accuracy of $\pm$ 2.75 cm, a correlation coefficient of 0.9995 and a coefficient

of variation (CV) ranging from 0.54% to 1.21%; validating the accuracy, precision and reliability of the system

5. the device represents a novel low-cost solution for groundwater level monitoring in Nigeria; the production cost of the device is at least 60% less than the prevailing pressure-based equipment used in Nigeria, which lacks automated telemetry.

5.3 Conclusion

This research demonstrates that a low-cost real-time laser based accurate groundwater monitoring system is technically achievable, economically viable and can strengthen monitoring infrastructure in developing countries and resource-constrained environments where conventional monitoring systems are unaffordable or unavailable. Analysis of the correlation and Bland Altman's plots, reveal improved measurements from the implemented device. While the correlation coefficient for both corrected and uncorrected readings where same, the regression relation indicated greater error bias for the raw LiDAR values, which was evident through a larger intercept. This is confirmed by the coefficient of variation and the root mean square error (RMSE) which improved from 10.28 and13.91 for uncorrected measurements taken from well 1 and well 2 respectively, to 5.36 and 3.91 for corrected values.

The research represents a necessary but insufficient step toward addressing global groundwater challenges. The success of the device in strengthening groundwater management will require cooperative engagement with water resource agencies and integration into policy frameworks that support sustainable groundwater management.

5.4 Contributions to Knowledge

This study makes the following original contributions to the body of knowledge in environmental monitoring, hydrogeological instrumentation, and IoT-enabled sensing systems:

1. A home grown LiDAR based ESP8266 enabled groundwater monitoring device that can remotely monitor groundwater level in real-time has been implemented.
2. Established a groundwater level monitoring device that is reconfigurable and can achieve continuous sub-minute monitoring with average RMSE of as low as 3.91
3. a rigorously validated, field-derived linear correction methodology specifically tailored for LiDAR-based groundwater depth measurement

5.5 Suggestions for Further Studies

The following are the suggestions for further studies:

1. integrating other sensors like water quality sensor, to expand functionality of the system.
2. incorporating a 3G module to the system to complement the wifi module and increase redundancy and reliability.
3. incorporate a GPS module to equip the unit with geolocation capability and facilitate its deployment for regional remote groundwater level monitoring.
4. access the effect of environmental factors like temperature and humidity on the performance of the device
5. incorporate solar power unit to eliminate dependence on external power banks and enable autonomous, long-term deployment.

REFERENCE

Ali, M., Akbar, A., Waqar, M., Zhang, X. and Ahmed, A. (2024) An overview of deep learning applications in groundwater level modelling: bridging the gap between academic research and industry applications, Applied Computational Intelligence and Soft Computing, 2024, pp. 1–21. https://doi.org/10.1155/2024/9480522.

Altman D.G. and Bland J.M.(1983). Measurement in medicine: the analysis of method comparison studies. *Statistician* , 32, 307–317. http://dx.doi.org/10.2307/2987937

Arab Center for the studies of Arid Zones and Dry Lands (ACSAD) and German federal Institutes for Geosciences and Natural Resources (BGR), (2003). Management, protection and sustainable use of groundwater and soil resources in the Arab region (vol. 6). ACSAD/BGR. https://www.bgr.bund.de/EN/Themen/Grundwasser/Downloads/guideline_acsad-bgr_vol6_pdf.pdf [Accessed 17/10/2024]

Arduino.cc. (2023). *Overview of the Arduino UNO Components*. Retrieved from https://docs.arduino.cc/tutorials/uno-rev3/intro-to-board/ (accessed 30/07/2025)

Bacour, C., Bréon, F.-M., Gonzalez, L., Price, I., Muller, J.-P. and Straume, A. G. (2020). Simulating multi- directional narrowband reflectance of the Earth's surface using ADAM (a surface reflectance database for ESA's Earth Observation Missions). *Remote Sensing, 12*(10), 1679. https://doi.org/10.3390/rs12101679

Baker,E.(2014). Open source data logger for low-cost environmental monitoring. *Biodiversity Data Journal*, 2, e1059. https://doi.org/10.3897/BDJ.2.e1059

Behzadian, A., Zhang, L., Adu-Gyamfi, Y. and Buttlar, W. (2025). Feasibility and reliability assessment of inexpensive solid-state LiDAR for rutting measurement in asphalt pavement, *Transportation Research Record*, 2679(1), pp. 12-25.

Benjamin, J., and Kaplan, D. (2017). Development of a laser-based water level sensor for fine-scale ecohydrological measurements. In *2017 IEEE Conference on Technologies for Sustainability (SusTech)* (pp. 1-8). IEEE. https://doi.org/10.1109/SusTech.2017.8333522

Boon, J. D., Heitsenrether, R. M., and Hensley, W. M. (2012). Multi-sensor evaluation of microwave water level measurement error. In *Proceedings of OCEANS 2012* (pp. 1–8). IEEE. https://doi.org/10.1109/OCEANS.2012.6405079

Born, M., and Wolf, E. (2019). *Principles of optics: Electromagnetic theory of propagation, interference and diffraction of light* (7th expanded ed.). Cambridge University Press. https://doi.org/10.1017/9781108769914

Bulusu, S., Prieto García, C., Dahlke, H. E. and Levintal, E. (2024). Technical note: An open-source, low-cost system for continuous monitoring of low nitrate concentrations in soil and open water. *Biogeosciences, 21*, 3007–3013. https://doi.org/10.5194/bg-21-3007-2024

Cain, S.F., David, G. A., Loheide, S. P. and Butler, J. J. (2004) 'Noise in pressure transducer readings produce by variations in solar radiation', *Ground Water*, 42(6), pp. 939 – 944. https://doi.org/10.1111/j.1745-6584.2004.t01-12-.x

Calderwood , A. J., Pauloo, R. A., Yoder , M. A., & Fogg, G. E., (2020). Low-Cost, Open Source Wireless Sensor Network for Real-Time, Scalable Groundwater Monitoring. *Water,* 12, 1066; 1 – 17. https://doi.org/10.3390/w12041066

Ceccarini, C. (2022). Designing interfaces to display sensor data: A case study on occupants' context-awareness. *Sensors, 22*(9), 1–17. https://doi.org/10.3390/s22093364

Chen J., Wu H., Qian H., and Li X. (2016). *Challenges and prospects of sustainable groundwater management in an agricultural plain along the Silk Road Economic Belt, north-west China*. International Journal of Water resources Development, vol. 34, no. 3, 354– 368 https://doi.org/10.1080/07900627.2016.1238348

Chen, H.Y., and Chen, C(2022). Evaluation of calibration equations by using regression analysis: An example of chemical analysis. *Sensors*, 22(2), 447. 368 https://doi.org/10.3390/s22020447

Chooruang,K.,Kulna,W. and Sonard, N. (2023). Development of IoT Underground Water Level Monitoring Based on LiDAR. IEEE (2023) *Proceedings of the 20th International Conference on Electrical Engineering/Electronics, Computer, Telecommunications and Information Technology (ECTI-CON 2023)*. Nakhon Phanom, Thailand, 9–12 May. Available at: https://doi.org/10.1109/ECTI-CON58255.2023.10153386

Christakis, I., Tsakiridis, O., Sarri, E., Triantis, D. and Stavrakas, I. (2024). *Nonlinear regression approach as a correction factor of measurements of low-cost electrochemical air quality sensors. Applied Sciences, 14*(8), 3282. https://doi.org/10.3390/app14083282

Cobbing , J., Roy, K., Islam, H.M.N.,Singh, G. &WaterAid (2021). Analysis of the groundwater resource and governance in Bangladesh, Ghana, India, Nepal and Nigeria [Report]. WaterAid. https://www.researchgate.net/publication/355576124 [Accessed 19/10/2024]

Cunningham, W. L., and Schalk, C. W. (Comps.). (2011). *Groundwater technical procedures of the U.S. Geological Survey* (Techniques and Methods 1–A1). U.S. Geological Survey. https://pubs.usgs.gov/tm/1a1/pdf/tm1-a1.pdf

Dementria D.D.A.,Medina, G.A.V.A., Guico, M.L.C., Kwong, J.C.T., Galicia, J.K.A., and Retirado, M. G. F.(2023). Fully Automated Telemetry System for Underground Water LIDAR Sensor. 2023 IEEE International Conference on Internet of Things and Intelligence Systems (IoTaIS), pp 72 – 78 . https://doi.org/10.1109/IoTaIS60147.2023.10346073

Ding, N., Zhu, Q., Cherqui, F., Walcker, N., Bertrand-Krajewski, J.-L. and Hamel, P.(2024). Laboratory performance assessment of low-cost water level sensor for field monitoring in the tropics. *Water Research X, 27*, 100298. https://doi.org/10.1016/j.wroa.2024.100298

Drage, J. and Kennedy, G. (2020). Building a low-cost, Internet-of-Things, real-time groundwater level monitoring network. *Groundwater Monitoring & Remediation, 40*(2), 67–73. https://doi.org/10.1111/gwmr.12408

Driverless Global. (2018). *LIDAR-Lite Garmin v3HP laser-based sensor*. Driverless.global. https://www.driverless.global/articles/36-products-solutions/LiDAR-radar-and-sensors/331-LiDAR-lite-garmin-v3hp-laser-based-sensor

Feng, F., Ghorbani, H. and Radwan, A.E. (2024) 'Predicting groundwater level using traditional and deep machine learning algorithms', Frontiers in Environmental Science, 12, p. 1291327. https://doi.org/10.3389/fenvs.2024.1291327

Gao, W., Liu, W., Li, F., and Hu, Y. (2021). Analysis and Validation of Ultrasonic Probes in Liquid Level Monitoring Systems. *Sensors*, 21(4), 1320. https://doi.org/10.3390/s21041320

García-López, S., Vélez-Nicolás, M., Zarandona-Palacio, P., Curcio, A. C., Ruiz-Ortiz, V., Barbero, L. (2023). UAV-borne LiDAR revolutionizing groundwater level mapping. Science of the Total Environment, 859(1), 160272. https://doi.org/10.1016/j.scitotenv.2022.160272

Garmin. (2018). *LIDAR-Lite v3HP operation manual*. Garmin Ltd. https://static.garmin.com/pumac/LIDAR-Lite_v3HP_Instructions_EN.pdf [accessed 30/10/2024]

Giavarina , D. (2015). Understanding Bland Altman analysis. *Biochemia Medica* ;25(2):141–51. http://dx.doi.org/10.11613/BM.2015.015

Gleick, P. (1993). Water in Crisis:Chapter 2 A guide to the World's Fresh water resources.*Oxford university press. https://www.academia.edu/902661/Water_in_Crisis_Chapter_2_Oxford_university_Press_1993*

Green, T. R., Taniguchi, M., Kooi H., Gurdak J. J.,Allen, D.M., Hiscoc, K.M., Treidel H. and Aureli, A.(2011). Beneath the surface of global change: Impacts of climate change on groundwater. *Journal of Hydrology*, 405(3–4), 532-560. https://doi.org/10.1016/j.jhydrol.2011.05.002

Hampton, S.E., Jones, M.B., Wasser, L.A., Schildhauer, M.P., Supp, S.R., Brun, J., Hernandez, R.R., Boettiger, C., Collins, S.L., Gross, L.J., Fernández, D.S., Budden, A., White, E.P., Teal, T.K., Labou, S.G. and Aukema, J.E. (2013) 'Skills and knowledge for data-intensive environmental research', *BioScience*, 67(6), pp. 546–557. https://10.1093/biosci/bix042.

Healy, R.W., and Cook, P.G. Using groundwater levels to estimate recharge. *Hydrogeology Journal* 10, 91–109 (2002). https://doi.org/10.1007/s10040-001-0178-0

Hecht, E. (2017). *Optics* (5th ed.). Pearson Education.

Henley, C., Ragan, C., and Raskar, R. (2025). Detection and mapping of specular surfaces using multibounce LiDAR returns. *IEEE Transactions on Computational Imaging, 11*, 166–178. https://doi.org/10.1364/OE.479900

Hernández-Rodríguez, E., González-Rivero, R. A., Schalm, O., Martínez, A., Hernández, L., Alejo-Sánchez, D., Janssens, T. and Jacobs, W. (2023). Reliability testing of a low-cost, multi-purpose Arduino-based data logger deployed in several applications such as outdoor air quality, human activity, motion, and exhaust gas monitoring. *Sensors, 23*(17), 7412. https://doi.org/10.3390/s23177412

Hitachi. (n.d.). *HD44780U (LCD-II) dot matrix liquid crystal display controller/driver* [Datasheet]. Retrieved from https://cdn.sparkfun.com/assets/9/5/f/7/b/HD44780.pdf [accessed 28/08/2025]

Hong, W. J., Shamsuddin, N., Abas, E., Apong, R. A., Masri, Z., Suhaimi, H., Gödeke, S. H., and Noh, M. N. A. (2021). Water quality monitoring with Arduino based sensors. *Environments, 8*(1), 6. https://doi.org/10.3390/environments8010006

IGRAC, 2020. Groundwater monitoring programmes: A global overview of quantitative groundwater monitoring networks. https://un-igrac.org/wp-content/uploads/2024/12/National-groundwater-monitoring-programmes-A-global-overview-of-quantitative-groundwater-monitoring-networks-2021-update_0-1.pdf (accessed 14/10/2024)

Igwebuike, N., Ajayi, M., Okolie, C. and Anike, L. (2025) 'Application of machine learning and deep learning for predicting groundwater levels in the West Coast Aquifer System, South Africa', Earth Science Informatics, 18, p. 6. https://doi.org/10.1007/s12145-024-01623-w

Jijingi, H. E., Simeon, P. O., and Emerson, K. U., (2019). Development and Management of Groundwater for Appropriate Water Supply in Nigeria: Problems and Actualisation Strategies. *American Journal of Engineering Research (AJER*), 8(8), pp. 01-06

Jimenez-Olmedo, J. M., Tortosa-Martínez, J., Cortell-Tormo, J. M., and Pueo, B. (2024). Assessing the Validity of the Ergotex IMU in Joint Angle Measurement: A Comparative Study with Optical Tracking Systems. *Sensors*, *24*(6), 1903. https://doi.org/10.3390/s24061903

Kalra ,A.(2017). Decoding the Bland–Altman plot: Basic review. Journal of the Practice of Cardiovascular Sciences ,3 (1),36 – 38. https://doi.org/10.4103/jpcs.jpcs_11_17

Kalu, N. N. (2018). Groundwater management protection program for Nigeria. *RUDN Journal of Ecology and Life Safety, 26*(3), 367–378. https://doi.org/10.22363/2313-2310-2018-26-3-367-378

Kashani, A. G., Olsen, M. J., Parrish, C. E., and Wilson, N. (2015). A review of LIDAR radiometric processing: From ad hoc intensity correction to rigorous radiometric calibration. *Sensors, 15*(11), 28099–28128. https://doi.org/10.3390/s151128099

Kondapuram, A. R., Treytl, A., Bigler, T., and Sauter, T. (2024, January). *Design and evaluation of an IoT-based real-time underground water-level sensor system*. In *Proceedings of the 2024 IEEE Applied Sensing Conference (APSCON)* (pp. 1–4). IEEE. https://doi.org/10.1109/APSCON60364.2024.10466069

Kondaveeti, H. K., Kumaravelu, N. K., Vanambathina, S. D., Mathe, S. E., & Vappangi, S. (2021). A systematic literature review on prototyping with Arduino: Applications, challenges, advantages, and limitations. *Computer Science Review, 40,* 100364. https://doi.org/10.1016/j.cosrev.2021.100364

Ma, H., Luo, Y., He, Y., Pan, S.,Ren, L. and Shang, J.(2022). The Short-Range, High-Accuracy Compact Pulsed Laser Ranging System. *Sensors* ,2146. https://doi.org/10.3390/s22062146

Mary, X. A., Rose, L., & Rajasekaran, K. (2018). Continuous and remote monitoring of ground water level measurement in a well. *International Journal of Water, 12*(4), 356–369. https://doi.org/10.1504/IJW.2018.095397

Masood, A.,Tariq, M.A.U.R., Hashmi, M.Z.U.R., Waseem, M., Sarwar, M.K., Ali, W., Farooq, R., Almazroui, M.,& Ng, A.W.M., (2022). An Overview of Groundwater

Monitoring through Point-to Satellite-Based Techniques. *Water*, 14, 565. https://doi.org/10.3390/w14040565

Mesquita, J., Guimarães, D., Pereira, C., Santos, F. M., Almeida, L. M. and Sá, J. (2018). Assessing the ESP8266 WiFi module for the Internet of Things. In *Proceedings of the 2018 IEEE 23rd International Conference on Emerging Technologies and Factory Automation (ETFA)* (pp. 784-791). IEEE. https://doi.org/10.1109/ETFA.2018.8502562

Miry, A. H. and Aramice, G. A. (2020). Water monitoring and analytic based ThingSpeak. *International Journal of Electrical and Computer Engineering (IJECE), 10*(4), 3588–3595. https://doi.org/10.11591/ijece.v10i4.pp3588-3595

Mobley, C. D. (1994). Light and water: Radiative transfer in natural waters. Academic Press.

Mobley, C. D. (2021). The LiDAR equation. *In* Ocean optics web book. OceanOpticsBook.info. https://www.oceanopticsbook.info/view/radiative-transfer-theory/level-2/the-LiDAR-equation [Accessed 3/10/2025]

Mobley, C. D., Sundman, L. K., and Boss, E. (2003). Phase function effects on oceanic light fields. *Applied Optics*, 42(15), 2788-2804. https://doi.org/10.1364/AO.42.002788

Nejad, S. M., and Haji Mirsaeidi, M. H. (2005). Altitude measurement using laser beam reflected from water surface. *Iranian Journal of Electrical & Electronic Engineering, 1*(1), 36–40. https://ijeee.iust.ac.ir/article-1-42-en.pdf

Nejad, S. M., and Olyaee, S. (2006). Comparison of TOF, FMCW and Phase-Shift Laser Range-Finding Methods by Simulation and Measurement.*Quartarly Journal of Technology & Education*, *1*(Special issue), 51 – 58. https://jte.sru.ac.ir/article_1236_8910e236af4d861b8719d0db6228525d.pdf

NerdShed .(n.d). ESP8266 ESP-01 Serial wifi wireless adapter module. https://nerdshed.com.ng/product/essp8266-esp-01-serial-wifi-wireless-adapter-module [accessed 22/10/2023]

Nicodemus, F. E. (1970). Reflectance Nomenclature and Scene Parameters. *Applied Optics*, *9*(8), 1840-1845.https://opg.optica.org/ao/abstract.cfm?URI=ao-9-6-1474

Nielsen, D.M. and Nielsen,G.L.,(2007). The essential handbook of ground-water sampling. CRC Press. http://www.taylorandfrancis.com

Njoku , L (2022) 'Why implementation of National water resources master plan has been poor', Guardian newspaper [Online],29 April. Available from: **https://guardian.ng/news/why-implementation-of-national-water-resources-master-plan-has-been-poor-by-minister/** [Accessed 19 October, 2024]

Padmanabhan, P., Hughes, L., Van Dijk, M., Hancock, J, and Moghaddam, M. (2019). Modeling and analysis of a direct time-of-flight sensor architecture for LiDAR applications. *Sensors, 19*(5464). https://doi.org/10.3390/s19245464

Panagopoulos, Y., Papadopoulos, A., Poulis, G., Nikiforakis, E.and Dimitriou, E.(2021) Assessment of an Ultrasonic Water Stage Monitoring Sensor Operating in an Urban Stream. *Sensors*. 21, 4689. https://doi.org/10.3390/s21144689

Parida, D., Behera, A., and Naik, J. K. (2019). Real-time environment monitoring system using ESP8266 and ThingSpeak on Internet of Things platform. *2019 International Conference on Intelligent Computing and Control Systems (ICCS)*. IEEE. https://doi.org/10.1109/ICCS45141.2019.9065451

Paul, J. D., Buytaert, W., Allen, S., and Harrison, R. (2020). Technical evaluation of LiDAR-based river water level measurements. *Water Resources Research, 56*(9), e2019WR026810. https://doi.org/10.1029/2019WR026810

Pereira, T. S. R., de Carvalho, T. P., Mendes, T. A., and Formiga, K. T. M. (2022). Evaluation of water level in flowing channels using ultrasonic sensors. Sustainability, 14(9), 5512. https://doi.org/10.3390/su14095512

Ranieri, C. M., Foletto, A. V. K., Garcia, R. D., Matos, S. N., Medina, M. M. G., Marcolino, L. S., and Ueyama, J. (2024). Water level identification with laser sensors, inertial units, and machine learning. *Engineering Applications of Artificial Intelligence, 127*, 107235. https://doi.org/10.1016/j.engappai.2023.107235

Ross, J.H., (2001). Evaluation of Non-Contact Measurement Instrumentation for Ground Water Wells. Presentation made at the AGWSE Annual Meeting and Conference, Nashville, TN, December, 2001.

Rudavskyi, I., Klym, H., Kostiv, Y., Karbovnyk, I., Zhydenko, I., Popov, A. I. and Konuhova, M. (2024). Utilizing an Arduino Uno-based system with integrated sensor data fusion and filtration techniques for enhanced air quality monitoring in residential spaces. *Applied Sciences, 14*(19), 9012. https://doi.org/10.3390/app14199012

Ruttner, P., Voordendag, A., Hartmann, T., Glaus, J., Wieser, A. and Bhler, Y. (2025) 'Monitoring snow depth variations in an avalanche release area using low-cost LiDAR and optical sensors', *Natural Hazards and Earth System Sciences*, 25(6), pp. 1315-1331. doi: 10.5194/nhess-25-1315-2025.

Santos, C.,and Dias, C.,(2021).Notes on coefficient of variation properties. *Brazillian Electronic Journal of Mathematics,* 2(4), 101 – 111. https://doi.org/10.14393/BEJOM-v2-n4-2021-58062

Saputri, F. R., Rahmad, R. and Pratama, A. R. (2025). Design and development of an irrigation monitoring and control system. *PLOS ONE, 20*(3), e0298765. https://doi.org/10.1371/journal.pone.0298765

Shahrul, N., Jabarullah, N. H., Hannan, M. A. and Rahman, M. S. A. (2021). A review on the use of the ESP8266 microcontroller for IoT applications**.** *Indonesian Journal of Electrical Engineering and Computer Science, 23*(3), 1650–1660. https://doi.org/10.11591/ijeecs.v23.i3.pp1650-1660

SparkFun Electronics. (n.d.). *LIDAR-Lite v3HP (SEN-14599) [Product page]*. SparkFun. Retrieved October 23, 2024, from https://www.sparkfun.com/LiDAR-lite-v3hp.html

Suemori, K., Komatsu ,Y., and Nobeshima, T. (2023). Flange-type liquid-level sensor based on laser light reflection. *Sensor International*, 4 , 100230. https://doi.org/10.1016/j.sintl.2023.100230

Tamari, S., and Guerrero-Meza, V. (2016). Flash flood monitoring with an inclined LiDAR installed at a river bank: Proof of concept. *Remote Sensing, 8*(10), 834. https://doi.org/10.3390/rs8100834

Tamari, S., Guerrero-Meza, V., Rifad, Y., Bravo-Inclán, L.,and Sánchez-Chávez, J.J. (2016). Stage monitoring in turbid reservoirs with an inclined terrestrial near-infrared LiDAR. Remote Sens. 8 (12), 999. http://dx.doi.org/10.3390/rs8120999

Tatoglu, A., and Pochiraju , K. (2012). Point cloud segmentation with LIDAR reflection intensity behavior. *IEEE International Conference on Robotics and Automation*, pp. 786-790. doi: 10.1109/ICRA.2012.6225224.

Taylor, C. J.and Alley W. M., (2001). Ground-water-level monitoring and the importance of long-term water-level data. U.S. Geological Survey circular , 1217, page 42. https://pubs.usgs.gov/circ/circ1217/html/pdf.html

Tonval, D., (2020). Study of reflective and polarization properties of objects found in automotive LiDAR applications. *Master's Thesis in Engineering Physics Department of Physics Umeå University*. Availble on http://www.diva-portal.org/smash/get/diva2:1453642/FULLTEXT01.pdf Accessed 03/07/2025

Viegas, V., Dias Pereira, J.M., Girão, P.M. and Postolache, O. (2021) Study of latencies in ThingSpeak', *Advances in Science, Technology and Engineering Systems Journal*, 6(1), pp. 342–348. doi: https://doi.org/10.25046/aj060139

Vishay Intertechnology. (n.d.). *LCD-016N002M-TTI-ET 16×2 character LCD module* [Datasheet]. Retrieved from https://www.vishay.com/docs/37481/lcd016n002mttiet.pdf [accessed 28/08/2025]

Weitkamp, C. (Ed.). (2005). *LiDAR: Range-resolved optical remote sensing of the atmosphere* (Vol. 102). Springer Science & Business Media.

Wu, Z., Huang, Y., Huang, K., Yan, K., and Chen, H., (2023). A Review of Non-Contact Water Level Measurement Based on Computer Vision and Radar Technology. Water, 15(3233), 1-20. https://doi.org/10.3390/w15183233

APPENDICES

Appendix A: The software program code.

```
#include <LIDARLite.h>
#include <Wire.h>
#include <SoftwareSerial.h>
#include <LiquidCrystal.h>

// Initialize LCD with specific pins: (rs, enable, d4, d5, d6, d7)
LiquidCrystal lcd(8, 10, 5, 4, 3, 2);
```

```
// Define pins for the ESP8266 "Software Serial" communication
#define RX 11                    // Pin 11 on Arduino connects to TX on ESP8266
#define TX 12                    // Pin 12 on Arduino connects to RX on ESP8266 (via voltage
divider)
SoftwareSerial esp8266(RX, TX);   // Create the serial object named 'esp8266'

float offset = -12.40;            // Fixed error value to subtract/add (intercept)
float slope = 1.01;              // Scaling factor for the distance (gradient)

// --- Global Variables for Data Storage ---
float rawVal = 0;
float corrVal = 0;
int cal_cnt = 0;

// --- WiFi & ThingSpeak Credentials ---
String AP = "TECNO SPARK 30 Pro"; // WiFi network name
String PASS = "bbcc63747044";     // WiFi password
String API = "O0Q14CIMRJE5QLS9";  // ThingSpeak Write API Key for channel
String HOST = "api.thingspeak.com";// ThingSpeak server address
String PORT = "80";

// Create the LiDAR object
LIDARLite LiDARLite;

// Variables for the command tracking logic
int countTrueCommand;
int countTimeCommand;
boolean found = false;

void setup() {
  lcd.begin(16, 2);              // Start the LCD and set its dimensions
  Serial.begin(9600);            // Start the PC Serial monitor for debugging

  LiDARLite.begin(0, true);       // Start the LiDAR sensor (default I2C address)
  LiDARLite.configure(4);         // Set LiDAR to balanced performance mode

  // Start ESP8266 serial at 9600 baud (Essential for SoftwareSerial stability)
  esp8266.begin(115200);

  lcd.print("Init WiFi...");      // Show status message on LCD
  sendCommand("AT", 5, "OK");     // Check if ESP8266 is responding
  sendCommand("AT+CWMODE=1", 5, "OK"); // Set ESP8266 to "Station Mode" (WiFi
client)

  // Connect ESP8266 to your phone's hotspot
  sendCommand("AT+CWJAP=\"" + AP + "\",\"" + PASS + "\"", 20, "OK");

  lcd.clear();                   // Clear screen once connected
}
```

```
void loop() {

  getSensorData();

  // 2. Build the URL string for ThingSpeak
  // field1 = Raw data | field2 = Corrected data
  String getData = "GET /update?api_key=" + API + "&field1=" + String(rawVal) +
"&field2=" + String(corrVal);

  // 3. Begin the HTTP upload sequence
  sendCommand("AT+CIPMUX=1", 5, "OK");

  // Start a TCP connection to the ThingSpeak server on port 80
  sendCommand("AT+CIPSTART=0,\"TCP\",\"" + HOST + "\"," + PORT, 15, "OK");

  sendCommand("AT+CIPSEND=0," + String(getData.length() + 4), 4, ">");

  esp8266.println(getData);
  delay(1500);                    // Wait for the ESP8266 to transmit to the web

  countTrueCommand++;
  sendCommand("AT+CIPCLOSE=0", 5, "OK");

  // ThingSpeak Free Tier requires a 15-second delay between updates
  delay(15000);
}

void getSensorData() {
  float tempRaw;

  if (cal_cnt == 0) {
    tempRaw = LiDARLite.distance();
  } else {
    tempRaw = LiDARLite.distance(false);
  }

  // Apply the linear calibration formula: y = (x - c) / m
  float tempCorr = (tempRaw - offset) / scaling factor;

  // Save the calculated values into global variables for use in the loop()
  rawVal = tempRaw;
  corrVal = tempCorr;

  cal_cnt++;                     // Increment the bias counter
  cal_cnt = cal_cnt % 100;       // Reset counter once it hits 100

  // Display results on the LCD screen
  lcd.setCursor(0, 0);
  if (tempCorr >= 4000 || tempCorr <= 1) {
```

```
    Serial.println("OUT OF RANGE");
    lcd.clear();
    lcd.print("OUT OF RANGE");
  } else {
    lcd.clear();
    // Print to PC Serial Monitor
    Serial.print("Raw: "); Serial.print(rawVal);
    Serial.print(" | Corrected: "); Serial.println(corrVal);

    // Print to LCD (R for Raw, C for Corrected)
    lcd.print("R:"); lcd.print((int)rawVal);
    lcd.print(" C:"); lcd.print(corrVal, 1);
    lcd.setCursor(0, 1);
    lcd.print("Uploading...");
  }
}

void sendCommand(String command, int maxTime, char readReplay[]) {
  found = false;
  countTimeCommand = 0;

  Serial.print("Sending: ");
  Serial.println(command);

    while (countTimeCommand < (maxTime * 10)) {
    esp8266.println(command);
    if (esp8266.find(readReplay)) {
      found = true;
      break;
    }
    delay(100);
    countTimeCommand++;
  }

  if (found) {
    Serial.println("Response: OK");
  } else {
    Serial.println("Response: Fail");
  }
}
```

APPENDIX B. Complete Table for Time stamped LiDAR readings for well 1

Table B1. Complete Table for Time stamped LiDAR readings recorded for a tape measurement of 481 cm (well 1)

created_at	entry_id	RAW LIDAR MEASUREMENT (cm)	CORRECTED LIDAR MEASUREMENT (cm)
2025-01-28T07:10:10+01:00	495	471	478.67

2025-01-28T07:10:32+01:00	496	480	487.58
2025-01-28T07:11:19+01:00	497	474	481.64
2025-01-28T07:11:36+01:00	498	472	479.66
2025-01-28T07:12:11+01:00	499	473	480.65
2025-01-28T07:13:40+01:00	500	473	480.65
2025-01-28T07:14:14+01:00	501	471	478.67
2025-01-28T07:15:37+01:00	502	473	480.65
2025-01-28T07:16:56+01:00	503	473	480.65
2025-01-28T07:17:12+01:00	504	482	489.56
2025-01-28T07:17:57+01:00	505	473	480.65
2025-01-28T07:30:37+01:00	506	474	481.64
2025-01-28T07:31:30+01:00	507	473	480.65
2025-01-28T07:31:56+01:00	508	476	483.62
2025-01-28T07:33:02+01:00	509	475	482.63
2025-01-28T07:33:57+01:00	510	474	481.64
2025-01-28T07:34:15+01:00	511	474	481.64
2025-01-28T07:35:40+01:00	512	476	483.62
2025-01-28T07:38:02+01:00	513	476	483.62
2025-01-28T07:38:23+01:00	514	476	483.62
2025-01-28T07:39:18+01:00	515	481	488.57
2025-01-28T07:39:39+01:00	516	475	482.63
2025-01-28T07:40:27+01:00	517	477	484.61
2025-01-28T07:41:42+01:00	518	476	483.62
2025-01-28T07:42:02+01:00	519	476	483.62
2025-01-28T07:42:26+01:00	520	477	484.61
2025-01-28T11:07:36+01:00	521	472	479.66
2025-01-28T11:08:44+01:00	522	477	484.61
2025-01-28T11:10:10+01:00	523	478	485.60
2025-01-28T11:11:17+01:00	524	476	483.62
2025-01-28T11:11:42+01:00	525	478	485.60
2025-01-28T11:12:13+01:00	526	476	483.62
2025-01-28T11:15:09+01:00	527	477	484.61
2025-01-28T11:15:33+01:00	528	475	482.63
2025-01-28T11:15:59+01:00	529	477	484.61
2025-01-28T11:16:17+01:00	530	479	486.59
2025-01-28T11:17:15+01:00	531	475	482.63
2025-01-28T11:17:34+01:00	532	476	483.62
2025-01-28T11:18:14+01:00	533	478	485.60
2025-01-28T11:19:17+01:00	534	474	481.64
2025-01-28T11:19:48+01:00	535	477	484.61
2025-01-28T11:20:37+01:00	536	476	483.62
2025-01-28T11:20:57+01:00	537	476	483.62
AVERAGE		**476**	**483.1632512**
STANDARD DEVIATION		**2.462566**	**2.438183965**

COEFFICIENT OF VARIATION		**0.52 %**	**0.50%**
RMSE		**5.98**	**3.34**
MANUAL MEASUREMENT			**481.00**

Table B2. Complete Table for Time stamped LiDAR readings recorded for a tape measurement of 583.2 cm (well 1)

created_at	entry_id	RAW LIDAR MEASUREMENT (cm)	CORRECTED LIDAR MEASUREMENT (cm)
2025-02-17T11:21:22+01:00	538	576	582.63
2025-02-17T11:22:56+01:00	539	576	582.63
2025-02-17T11:23:22+01:00	540	577	583.62
2025-02-17T11:23:42+01:00	541	578	584.61
2025-02-17T11:24:19+01:00	542	577	583.62
2025-02-17T11:24:55+01:00	543	572	578.67
2025-02-17T11:25:19+01:00	544	576	582.63
2025-02-17T11:25:38+01:00	545	577	583.62
2025-02-17T16:53:37+02:00	546	577	583.62
2025-02-17T16:54:57+02:00	547	578	584.61
2025-02-17T16:55:45+02:00	548	579	585.60
2025-02-17T16:56:32+02:00	549	580	586.59
2025-02-17T16:58:02+02:00	550	578	584.61
2025-02-17T16:58:33+02:00	551	576	582.63
2025-02-17T16:59:12+02:00	552	579	585.60
2025-02-17T17:01:30+02:00	553	577	583.62
2025-02-17T17:02:07+02:00	554	577	583.62
2025-02-17T17:02:50+02:00	555	573	579.66
2025-02-17T17:03:31+02:00	556	574	580.65
2025-02-17T17:04:00+02:00	557	579	585.60
2025-02-17T17:04:26+02:00	558	577	583.62
2025-02-17T17:04:48+02:00	559	576	582.63
2025-02-17T17:06:16+02:00	560	563	569.76
2025-02-17T17:06:56+02:00	561	561	567.78
AVERAGE		**576.00**	**582.18**
STANDARD DEVIATION		**4.57**	**4.52**
COEFFICIENT OF VARIATION		**0.79 %**	**0.77 %**
RMSE		**8.87**	**4.54**
TAPE MEASUREMENT			**583.20**

APPENDIX C: Complete Table for Time stamped LiDAR readings for well 2

Table C1. Complete Table for Time stamped LiDAR readings recorded for a tape measurement of 234.1 cm (well 2)

created_at	entry_id	RAW LIDAR MEASUREMENT (cm)	CORRECTED LIDAR MEASUREMENT (cm)
2026-02-08T15:16:35+00:00	128	216	226.2
2026-02-08T15:16:54+00:00	129	216	226.2
2026-02-08T15:17:13+00:00	130	215	225.21
2026-02-08T15:18:28+00:00	131	216	226.2
2026-02-08T15:18:46+00:00	132	217	227.19
2026-02-08T15:19:03+00:00	133	217	227.19
2026-02-08T15:19:22+00:00	134	217	227.19
2026-02-08T15:19:42+00:00	135	217	227.19
2026-02-08T15:20:00+00:00	136	217	227.19
2026-02-08T15:20:18+00:00	137	217	227.19
2026-02-08T15:20:36+00:00	138	219	229.17
2026-02-08T15:20:54+00:00	139	217	227.19
2026-02-08T15:21:13+00:00	140	219	229.17
2026-02-08T15:21:31+00:00	141	219	229.17
2026-02-08T15:21:49+00:00	142	219	229.17
2026-02-08T15:22:07+00:00	143	222	232.14
2026-02-08T15:22:26+00:00	144	219	229.17
2026-02-08T15:24:44+00:00	145	221	231.15
2026-02-08T15:26:30+00:00	146	217	227.19
2026-02-08T15:26:49+00:00	147	221	231.15
2026-02-08T15:27:07+00:00	148	222	232.14
2026-02-08T15:28:43+00:00	149	221	231.15
2026-02-08T15:29:01+00:00	150	221	231.15
2026-02-08T15:29:21+00:00	151	223	233.13
2026-02-08T15:29:39+00:00	152	223	233.13
2026-02-08T15:30:04+00:00	153	221	231.15
2026-02-08T15:30:23+00:00	154	221	231.15
2026-02-08T15:32:00+00:00	155	223	233.13

2026-02-08T15:32:19+00:00	156	224	234.12
2026-02-08T15:32:37+00:00	157	223	233.13
2026-02-08T15:32:55+00:00	158	222	232.14
2026-02-08T15:36:19+00:00	159	222	232.14
2026-02-08T15:38:53+00:00	160	221	231.15
2026-02-08T15:39:11+00:00	161	222	232.14
2026-02-08T15:39:29+00:00	162	221	231.15
2026-02-08T15:39:47+00:00	163	222	232.14
2026-02-08T15:40:07+00:00	164	221	231.15
2026-02-08T15:40:26+00:00	165	222	232.14
2026-02-08T15:42:03+00:00	166	222	232.14
2026-02-08T15:42:21+00:00	167	221	231.15
2026-02-08T15:42:41+00:00	168	223	233.13
2026-02-08T15:42:58+00:00	169	221	231.15
2026-02-08T15:43:17+00:00	170	223	233.13
2026-02-08T15:43:34+00:00	171	221	231.15
2026-02-08T15:43:53+00:00	172	223	233.13
2026-02-08T15:46:49+00:00	173	222	232.14
2026-02-08T15:52:23+00:00	174	227	237.09
2026-02-08T15:54:01+00:00	175	222	232.14
2026-02-08T15:56:34+00:00	176	223	233.13
2026-02-08T15:56:52+00:00	177	222	232.14
2026-02-08T15:58:29+00:00	178	222	232.14
2026-02-08T15:58:48+00:00	179	223	233.13
2026-02-08T16:01:43+00:00	180	222	232.14
2026-02-08T16:34:54+00:00	181	222	232.14
2026-02-08T16:36:08+00:00	182	222	232.14
2026-02-08T16:36:27+00:00	183	224	234.12
2026-02-08T16:38:35+00:00	184	223	233.13
2026-02-08T16:38:54+00:00	185	223	233.13
2026-02-08T16:40:31+00:00	186	223	233.13
2026-02-08T16:40:48+00:00	187	224	234.12
2026-02-08T16:41:06+00:00	188	224	234.12
2026-02-08T16:41:25+00:00	189	223	233.13
2026-02-08T16:41:43+00:00	190	223	233.13
2026-02-08T16:42:02+00:00	191	224	234.12
2026-02-08T16:43:39+00:00	192	223	233.13
2026-02-08T16:43:57+00:00	193	223	233.13
2026-02-08T16:45:34+00:00	194	224	234.12
2026-02-08T16:47:13+00:00	195	223	233.13
2026-02-08T16:49:06+00:00	196	223	233.13
2026-02-08T16:50:20+00:00	197	223	233.13
2026-02-08T16:51:57+00:00	198	224	234.12
2026-02-08T16:52:16+00:00	199	223	233.13

2026-02-08T16:54:55+00:00	200	223	233.13
2026-02-08T16:55:13+00:00	201	221	231.15
2026-02-08T16:56:49+00:00	202	222	232.14
2026-02-08T16:58:27+00:00	203	222	232.14
2026-02-08T16:58:45+00:00	204	222	232.14
2026-02-08T16:59:04+00:00	205	223	233.13
2026-02-08T17:00:24+00:00	206	222	232.14
2026-02-08T17:00:42+00:00	207	225	235.11
2026-02-08T17:01:01+00:00	208	225	235.11
2026-02-08T17:01:19+00:00	209	222	232.14
2026-02-08T17:01:38+00:00	210	223	233.13
2026-02-08T17:01:56+00:00	211	224	234.12
2026-02-08T17:02:14+00:00	212	222	232.14
2026-02-08T17:02:33+00:00	213	223	233.13
2026-02-08T17:05:28+00:00	214	221	231.15
2026-02-08T17:07:05+00:00	215	222	232.14
2026-02-08T17:07:23+00:00	216	224	234.12
2026-02-08T17:07:41+00:00	217	223	233.13
2026-02-08T17:08:00+00:00	218	222	232.14
2026-02-08T17:08:18+00:00	219	223	233.13
2026-02-08T17:08:37+00:00	220	223	233.13
2026-02-08T17:08:54+00:00	221	223	233.13
2026-02-08T17:09:13+00:00	222	224	234.12
2026-02-08T17:09:31+00:00	223	223	233.13
2026-02-08T17:09:50+00:00	224	222	232.14
2026-02-08T17:10:07+00:00	225	224	234.12
2026-02-08T17:10:25+00:00	226	223	233.13
2026-02-08T17:10:44+00:00	227	224	234.12
2026-02-08T17:11:02+00:00	228	224	234.12
2026-02-08T17:11:23+00:00	229	223	233.13
2026-02-08T17:13:00+00:00	230	226	236.1
2026-02-08T17:13:19+00:00	231	225	235.11
2026-02-08T17:13:37+00:00	232	224	234.12
2026-02-08T17:13:56+00:00	233	222	232.14
2026-02-08T17:14:14+00:00	234	223	233.13
2026-02-08T17:14:31+00:00	235	223	233.13
2026-02-08T17:14:50+00:00	236	224	234.12
2026-02-08T17:15:08+00:00	237	222	232.14
2026-02-08T17:15:27+00:00	238	226	236.1
2026-02-08T17:15:45+00:00	239	223	233.13
2026-02-08T17:18:39+00:00	240	223	233.13
2026-02-08T17:18:57+00:00	241	223	233.13
2026-02-08T17:19:15+00:00	242	223	233.13
2026-02-08T17:20:52+00:00	243	223	233.13
2026-02-08T17:21:09+00:00	244	223	233.13

2026-02-08T17:21:28+00:00	245	223	233.13
2026-02-08T17:21:46+00:00	246	224	234.12
2026-02-08T17:22:05+00:00	247	224	234.12
2026-02-08T17:23:40+00:00	248	222	232.14
2026-02-08T17:23:59+00:00	249	227	237.09
2026-02-08T17:24:17+00:00	250	222	232.14
AVERAGE		**222**	**232.19**
STANDARD DEVIATION		**2.28**	**2.25**
COEFFICIENT OF VARIATION		**1.03%**	**0.97 %**
RMSE		**12.25**	**2.94**
TAPE MEASUREMENT			**234.1**

Table C2. Complete Table for stamped LiDAR readings recorded for a Tape measurement of 739.2 cm (well 2)

created_at	entry_id	RAW LIDAR MEASUREMENT (cm)	CORRECTED LIDAR MEASUREMENT (cm)
2026-02-10T10:28:37+01:00	550	723	728.18
2026-02-10T10:28:56+01:00	551	719	724.22
2026-02-10T10:29:14+01:00	552	725	730.16
2026-02-10T10:29:33+01:00	553	723	728.18
2026-02-10T10:29:52+01:00	554	723	728.18
2026-02-10T10:30:10+01:00	555	727	732.14
2026-02-10T10:30:29+01:00	556	724	729.17
2026-02-10T10:30:47+01:00	557	720	725.21
2026-02-10T10:31:07+01:00	558	723	728.18
2026-02-10T10:32:40+01:00	559	724	729.17
2026-02-10T10:32:57+01:00	560	727	732.14
2026-02-10T10:33:18+01:00	561	727	732.14
2026-02-10T10:33:36+01:00	562	726	731.15
2026-02-10T10:34:51+01:00	563	728	733.13
2026-02-10T10:36:25+01:00	564	729	734.12
2026-02-10T10:36:42+01:00	565	729	734.12
2026-02-10T10:37:01+01:00	566	727	732.14
2026-02-10T10:38:25+01:00	567	730	735.11
2026-02-10T10:38:42+01:00	568	728	733.13
2026-02-10T10:39:05+01:00	569	729	734.12

2026-02-10T10:39:22+01:00	570	724	729.17
2026-02-10T10:39:41+01:00	571	722	727.19
2026-02-10T10:40:00+01:00	572	730	735.11
2026-02-10T10:40:29+01:00	573	732	737.09
2026-02-10T10:40:47+01:00	574	729	734.12
2026-02-10T10:41:06+01:00	575	726	731.15
2026-02-10T10:41:24+01:00	576	730	735.11
2026-02-10T10:41:41+01:00	577	732	737.09
2026-02-10T10:42:00+01:00	578	727	732.14
2026-02-10T10:43:13+01:00	579	729	734.12
2026-02-10T10:43:32+01:00	580	723	728.18
2026-02-10T10:43:50+01:00	581	729	734.12
2026-02-10T10:44:09+01:00	582	728	733.13
2026-02-10T10:44:28+01:00	583	727	732.14
2026-02-10T10:44:46+01:00	584	729	734.12
2026-02-10T10:45:03+01:00	585	729	734.12
2026-02-10T10:45:22+01:00	586	723	728.18
2026-02-10T10:46:59+01:00	587	729	734.12
2026-02-10T10:47:16+01:00	588	729	734.12
2026-02-10T10:47:35+01:00	589	727	732.14
2026-02-10T10:48:02+01:00	590	727	732.14
2026-02-10T10:48:20+01:00	591	732	737.09
2026-02-10T10:48:39+01:00	592	726	731.15
2026-02-10T10:49:00+01:00	593	728	733.13
2026-02-10T10:50:14+01:00	594	722	727.19
2026-02-10T10:51:52+01:00	595	730	735.11
2026-02-10T10:52:13+01:00	596	730	735.11
2026-02-10T10:52:31+01:00	597	730	735.11
2026-02-10T10:52:53+01:00	598	727	732.14
2026-02-10T10:53:13+01:00	599	726	731.15
2026-02-10T10:54:49+01:00	600	732	737.09
2026-02-10T10:55:11+01:00	601	730	735.11
2026-02-10T10:55:29+01:00	602	732	737.09
2026-02-10T10:55:48+01:00	603	730	735.11
2026-02-10T10:58:05+01:00	604	730	735.11
2026-02-10T10:58:29+01:00	605	729	734.12
2026-02-10T10:58:46+01:00	606	734	739.07
2026-02-10T11:00:23+01:00	607	725	730.16
2026-02-10T11:00:42+01:00	608	727	732.14
2026-02-10T11:01:03+01:00	609	728	733.13
2026-02-10T11:01:21+01:00	610	728	733.13
2026-02-10T11:03:41+01:00	611	729	734.12
2026-02-10T11:04:12+01:00	612	733	738.08
2026-02-10T11:04:32+01:00	613	729	734.12

2026-02-10T11:04:50+01:00	614	723	728.18
2026-02-10T11:05:09+01:00	615	732	737.09
2026-02-10T11:06:30+01:00	616	735	740.06
2026-02-10T11:06:48+01:00	617	727	732.14
2026-02-10T11:07:05+01:00	618	727	732.14
2026-02-10T11:07:24+01:00	619	729	734.12
2026-02-10T11:08:43+01:00	620	729	734.12
2026-02-10T11:10:24+01:00	621	732	737.09
2026-02-10T11:10:43+01:00	622	734	739.07
2026-02-10T11:11:59+01:00	623	726	731.15
2026-02-10T11:12:18+01:00	624	727	732.14
2026-02-10T11:12:35+01:00	625	727	732.14
2026-02-10T11:12:54+01:00	626	729	734.12
2026-02-10T11:15:12+01:00	627	736	741.05
2026-02-10T11:15:30+01:00	628	732	737.09
2026-02-10T11:15:49+01:00	629	733	738.08
2026-02-10T11:18:52+01:00	630	732	737.09
2026-02-10T11:19:11+01:00	631	735	740.06
2026-02-10T11:22:09+01:00	632	726	731.15
2026-02-10T11:22:28+01:00	633	725	730.16
2026-02-10T11:23:42+01:00	634	727	732.14
2026-02-10T11:26:23+01:00	635	727	732.14
2026-02-10T11:26:41+01:00	636	727	732.14
2026-02-10T11:27:56+01:00	637	732	737.09
2026-02-10T11:29:34+01:00	638	729	734.12
2026-02-10T11:29:51+01:00	639	725	730.16
2026-02-10T11:31:26+01:00	640	730	735.11
2026-02-10T11:31:45+01:00	641	730	735.11
2026-02-10T11:35:22+01:00	642	727	732.14
2026-02-10T11:39:02+01:00	643	725	730.16
2026-02-10T11:39:19+01:00	644	729	734.12
2026-02-10T11:39:36+01:00	645	735	740.06
2026-02-10T11:41:22+01:00	646	727	732.14
2026-02-10T11:41:43+01:00	647	726	731.15
2026-02-10T11:42:01+01:00	648	732	737.09
2026-02-10T11:42:21+01:00	649	736	741.05
2026-02-10T11:46:45+01:00	650	727	732.14
2026-02-10T12:00:20+01:00	651	721	726.2
2026-02-10T12:00:47+01:00	652	726	731.15
2026-02-10T12:02:35+01:00	653	724	729.17
2026-02-10T12:02:56+01:00	654	721	726.2
2026-02-10T12:03:18+01:00	655	724	729.17
2026-02-10T12:04:29+01:00	656	716	721.25
2026-02-10T12:04:53+01:00	657	720	725.21

2026-02-10T12:06:09+01:00	658	718	723.23
2026-02-10T12:07:52+01:00	659	718	723.23
2026-02-10T12:10:24+01:00	660	719	724.22
2026-02-10T12:12:55+01:00	661	723	728.18
AVERAGE		**727.4643**	**732.5996**
STANDARD DEVIATION		**4.004257**	**3.964214**
COEFFICIENT OF VARIATION		**0.48 %**	**0.47 %**
RMSE		**11.79**	**7.04**
TAPE MEASUREMENT			**739.2**

Appendix D. Bland Altman plots for individual measurements, showing convergence towards tape measurements.

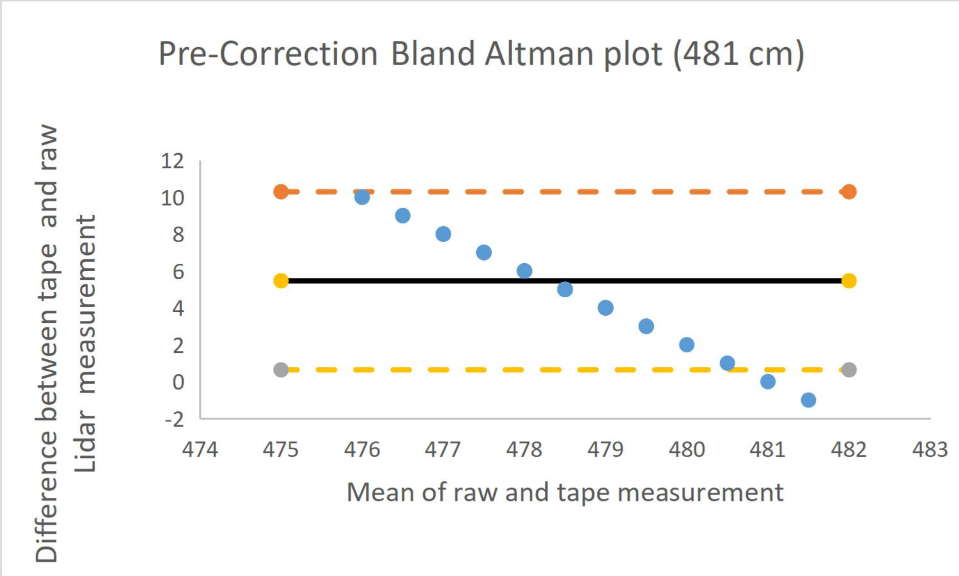

Figure D1. Bland Altman plot for raw LiDAR value and 481 cm tape measurement (well 1)

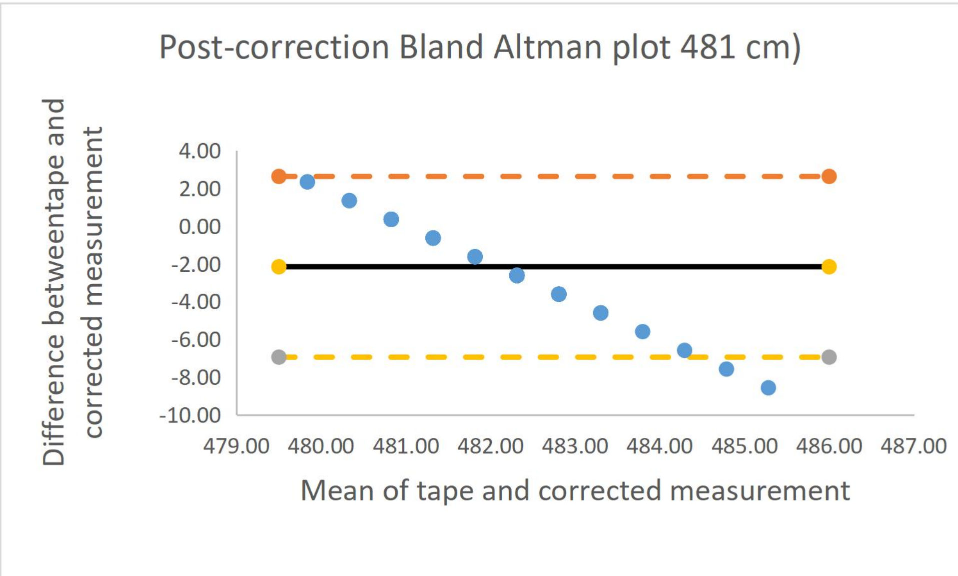

Figure D2. Bland Altman plot for corrected LiDAR value and 481 cm tape measurement (well 1)

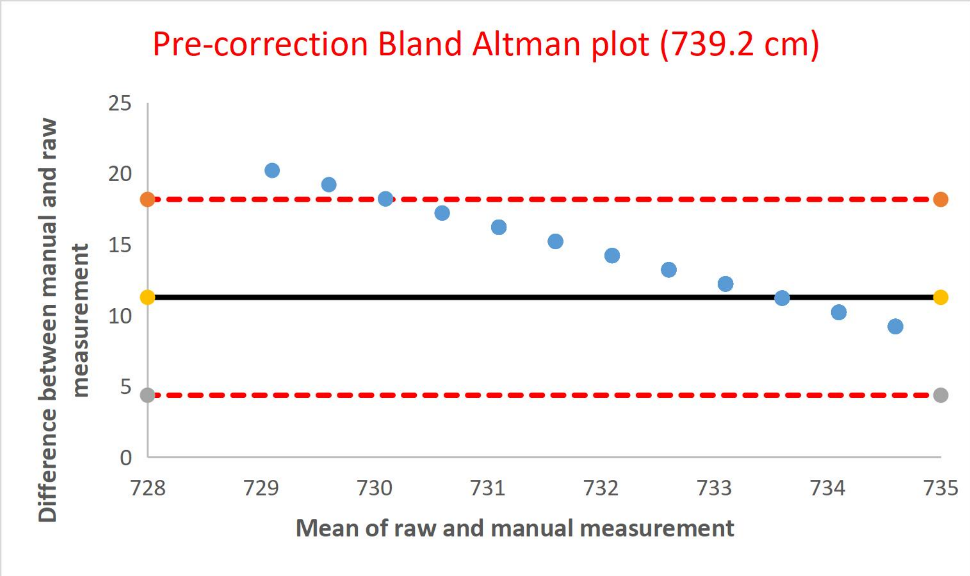

Figure D3. Bland Altman plot for raw LiDAR value and 739.2 cm tape measurement (well 2)

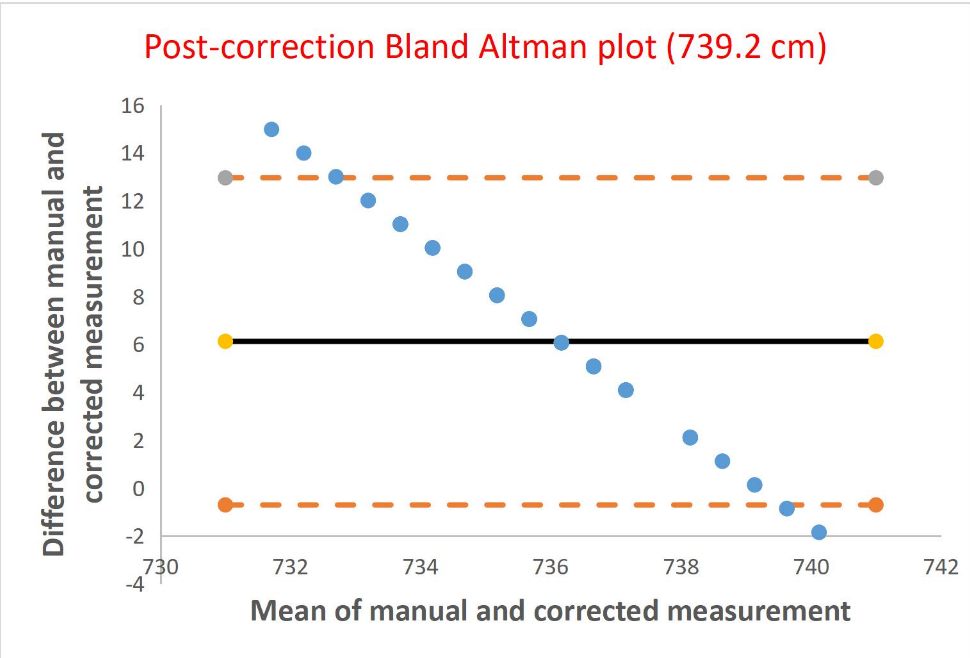

Figure D4. Bland Altman plot for corrected LiDAR value and tape measurement of 739.2 cm (well 2)

Appendix E. Parameters for Sketching Bland Altman Plot

Table E1. Parameters for plotting the pre-correction BA graph (Figure 4.5) for well 1.

Tape measurement (cm)	Average Raw LiDAR measurement (cm)		Difference (cm)	Mean (cm)
167.4	155		12.4	161.2
181.3	168		13.3	174.65
200	189		11	194.5
282	271		11	276.5
303	295		8	299
481	476		5	478.5
520.4	511		9.4	515.7
564	556		8	560
573.7	564		9.7	568.85
583.2	576		7.2	579.6
		Bias (mean difference)	9.5	
		Standard deviation (of difference-std)	2.526306	
Bias+1.96*std		upper limit of agreement	14.45156	
bias-1.96*std		lower limit of agreement	4.54844	

Table E2. Parameters for plotting the post-correction Bland Altman plot graph(Figure 4.6) for well 1.

Tape measurement (cm)	Average Corrected LiDAR measurement (cm)		Difference (cm)	Mean (cm)
167.4	166.21		1.19	166.81
181.3	178.55		2.75	179.93
200	199.34		0.66	199.67
282	280.50		1.5	281.25
303	304.83		-1.83	303.92
481	483.16		-2.16	482.08
520.4	518.00		2.4	519.2
564	562.59		1.41	563.3

573.7	571.00		2.7	572.35
583.2	582.18		1.02	582.69
		Bias (mean difference)	0.964	
		Standard deviation (of difference-std)	1.71478	
Bias+1.96*std		upper limit of agreement	4.324969	
bias-1.96*std		lower limit of agreement	-2.39697	

Table E3: Parameters for plotting the pre-correction BA graph(Figure 4.7) for well 2.

Tape measurement (cm)	Average Raw LiDAR measurement (cm)		Difference (cm)	Mean (cm)
193.6	178		15.6	185.8
234.1	222		12.1	228.05
281.9	267		14.9	274.45
292.2	277		15.2	284.6
310.2	297.23		12.97	303.715
316.8	302.29		14.51	309.545
359.7	346.45		13.25	353.075
440	424.91		15.09	432.455
522.3	509.28		13.02	515.79
727.7	717		10.7	722.35
739.2	728		11.2	733.6
		Bias (mean difference)	13.503636	
		Standard deviation (of difference-std)	1.6873605	
Bias+1.96*std		upper limit of agreement	16.810863	
bias-1.96*std		lower limit of agreement	10.19641	

Table E4. Parameters for plotting the post-correction Bland Altman plot (Figure 4.8) for well 2

Tape measurement (cm)	Average Corrected LiDAR measurement (cm)		Difference (cm)	Mean (cm)
193.60	188.91		4.69	191.26
234.10	232.19		1.91	233.15
281.90	276.87		5.03	279.39
292.20	286.84		5.36	289.52
310.20	306.63		3.57	308.42
316.80	311.63		5.17	314.22
359.70	355.36		4.34	357.53
440.00	433.05		5.03	279.39
522.30	516.58		5.36	289.52
727.70	722.24		5.46	724.97
739.20	733.07		6.13	736.14
		Bias (mean difference)	4.73	
		Standard deviation(std)	1.15	
		upper limit of agreement	6.98	
		lower limit of agreement	2.49	